Universidad del País Vasco / Euskal Herriko Unibertsitatea

Facultad de Medicina y Enfermería

Departamento de Neurociencias

Role of amyloid β oligomers in oligodendrocyte and myelin pathology in Alzheimer´s disease

Tesis doctoral para optar al grado de Doctor, presentada por:

Tania Quintela López

2018

Directora de tesis:

Dr. Elena Alberdi

Esta tesis doctoral ha sido realizada gracias al disfrute de una beca del Programa Predoctoral de Formación de Personal Investigador No Doctor del Departamento de Educación, Política Lingüística y Cultura del Gobierno Vasco durante el periodo 2014-2017.

El trabajo experimental ha sido financiado por el Centro de Investigación Biomédica en Red de Enfermedades Neurodegenerativas (CIBERNED), proyectos del Ministerio de Economía y Competitividad (SAF2013-45084-R y SAF2016-75292-R), proyectos de grupos consolidados del Gobierno Vasco (IT702-13).

Table of contents

Introduction

Introduction

1. Alzheimer's disease.

Alzheimer's disease (AD), the most common cause of dementia, is an irreversible neurodegenerative pathology characterized by a progressive neuron loss. This pathology was first reported by the German psychiatrist Aloysius "Alois" Alzheimer (1864-1915), who described for the first time a dementing condition which later became known as AD. Alzheimer studied in detail the progression of the peculiar disease of Auguste D, a 51-year-old woman whose symptoms included hallucinations and loss of several mental functions, as memory and language impairment. After Auguste's death in 1906 her case was published under the title "On an Unusual Illness of the Cerebral Cortex" (from the German "Über eine eigenartige Erkrankung der Hirnrinde") (Alzheimer, 1907). Post-mortem analyses showed the presence of intra- and extracellular aggregates being these features extensively used years later for AD diagnosis. Interestingly, it was later described that the extracellular aggregates that were observed by Alzheimer were insoluble aggregates of the amyloid β peptide (Aβ) called senile plaques, and those intracellular were neurofibrillar tangles composed by filamentous accumulations of hyperphosphorylated protein tau (**Figure 1**). After Alzheimer's report on the pathology, Kraepelin introduced for the first time the name of the disease in his text "Psychiatrie" (Kraepelin, 1910).

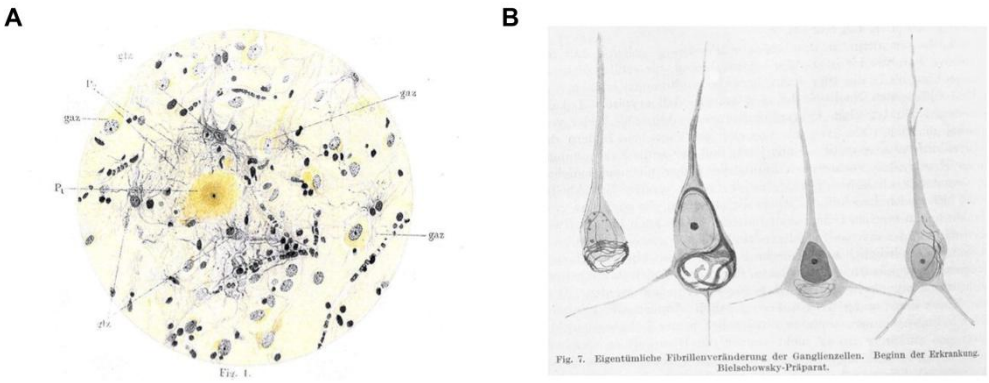

Figure 1. Pictures of original drawings of Alois Alzheimer showing pathological features of the disease. Drawings of senile plaques (A) and neurons with intracellular tangles (B) present in tissue samples from Alzheimer's disease patients.

As abovementioned, AD is a neurodegenerative disorder characterized by a profound cognitive decline occurring as a consequence of a progressive and irreversible neuronal loss. These neurodegenerative events developed in AD patients follow a well-established anatomical pattern, being the entorhinal cortex and hippocampus the first brain structures affected (Braak & Braak, 1995). The degeneration of these specific areas is related to deficits in learning and formation of new memories. The disease usually spreads to the neocortex, promoting alterations in several other cognitive functions. Reduction in the abundance of synapses is another important feature of this condition that, in addition to preceding neuronal degeneration, correlates better with observed cognitive deficits.

AD has been classified mainly in two different forms, the early-onset or familial AD and the late-onset or sporadic AD.

1.1. Early-onset or familial Alzheimer's disease.

The early-onset or familial AD is a subtype of this pathology that represents the 5-10% of the clinical cases, appearing the first symptoms at an early age, usually before 65. Familial AD is characterized by Mendelian inheritance, being shown that the presence of specific mutations is sufficient to provoke the clinical and pathological manifestations of the disease. Mutations associated with this form of AD mainly affect genes related to Aβ peptide formation and oligomerization processes. Among others, mutations in at least three genes have been described to be promoters of disease onset. Mutations in the gene located at the chromosome 21 which coding for the amyloid precursor protein (APP) (Goate et al., 1991), are associated with an autosomal dominant inheritance. The Swedish mutation is one of the most well known genetic variation that causes early onset familial AD. It produces a two aminoacid-change in the protein sequence immediately before the Aβ peptide sequence (lysine-methionine for asparagine-leucine). The presence of these mutations implies greater amyloidogenic processing of APP or increased oligomerization of the Aβ peptide. In addition, these mutations are associated with an earlier age of onset, which can be around 40 years. In addition to APP, genes encoding for presenilin 1 (PSN1) and presenilin 2 (PSN2) have been also associated with this subtype of AD (Cruts,

Hendriks, & Van Broeckhoven, 1996). PSN1 is located in the chromosome 14, and about 180 mutations in this gene have been described. On the other hand, PSN2 which locus is localized at the chromosome 1 has about 15 mutations related to triggering the disease. However, due to the variability in the mutation penetrance its age of appearance is also more variable.

1.2. Late-onset or sporadic Alzheimer's disease.

The second subtype of the disease, namely late-onset or sporadic AD, starts before 65 years old and encompasses the majority of clinical cases, around 90-95%. In these cases, AD etiology is much more diffuse and complex than familial AD, multiple risk factors being described to affect the predisposition to the disease. However, the presence of these risk factors is not enough to cause AD. In addition to ageing, the best characterized risk factor is apolipoprotein E (ApoE), which is the main cholesterol transporter in the brain and has been related to the transport and release of Aβ peptide (Bu, 2009). The gene encoding ApoE may present three different allelic variants, ApoEε2, ApoEε3 and ApoEε4, the latter being able to triple the probability of suffering AD in the case of heterozygotes, and multiply it by 15 in the case of homozygotes, with respect to ApoEε2 and ApoEε3 haplotypes (Huang, 2006). In addition, by using genetic association studies such as those carried out by Bertram and co-workers (2007), a database has been generated in recent years gathering information on those genes which mutations could be related to the predisposition to late AD can be consulted (http://www.alzgene.org).

1.3. Alzheimer's disease pathology. Amyloid β peptide.

Since the first description of presenile dementia by Alzheimer, senile plaques and neurofibrillar tangles (NFT) are considered the key pathological hallmarks of AD and have been traditionally used to the histological post-mortem diagnosis. While the formation of NFT follows well-established patterns, senile plaques appear and distribute in a more random manner. Interestingly, the density of these plaques is lower in clinically relevant regions of the brain, as the hippocampus (Braak & Braak, 1995). In addition to plaques distribution, the detection of Aβ as a main constituent of the plaques (Glenner & Wong,

1984b) and the identification of gene mutations related to Aβ synthesis in familial AD, lead to formulate the amyloid cascade hypothesis (J. A. Hardy & Higgins, 1992; D J Selkoe, 1991).

The amyloid cascade hypothesis postulates that the deposition of Aβ, which is due to the unbalance between the production and elimination, finally leads to neurodegeneration and subsequent dementia (Glenner & Wong, 1984a; J. Hardy & Allsop, 1991; J. Hardy & Selkoe, 2002). This hypothesis proposes Aβ peptide as a candidate for initiating the disease, appearing NFTs after Aβ-induced damage. Aβ peptide is synthesized as a 4.5 kDa monomer from the proteolytic processing of the amyloid precursor protein (APP). APP is a transmembrane protein with a large extracellular domain that carries out a wide range of biological functions in the CNS. Interestingly, it is implicated in the regulation of neurites growth during development (Herms et al., 2004), however in the adult brain its role is more related to cell adhesion, neuroprotection, synapse formation, and transcription modulation of several genes (reviewed in Raychaudhuri & Mukhopadhyay, 2007). In addition, several proteins have been shown to interact with APP, regulating their processing and intracellular signaling, which may be related to a role of APP as a cell surface receptor (Zheng y Koo, 2011).

The proteolytic sequential processing of APP mainly occurs by two different pathways, one non-amyloidogenic and one amyloidogenic (**Figure 2**). The first consists on the cleavage of APP by the enzyme α-secretase that generates the soluble protein APPsα (N-terminus) and a smaller fragment called APP-CTFα (C-terminus), which remains anchored to the cell membrane. Then, APP-CTFα fragment is cleaved by the γ-secretase producing two soluble peptides, p3 which biological function is yet to be understood, and AICD (APP intracytoplasmic domain), that can act as a transcriptional regulator of several genes as GSK-3β or p53, among others (Kimberly, Zheng, Guénette, & Selkoe, 2001; von Rotz et al., 2004). In contrast, in the amyloidogenic or toxic pathway the first cleavage is performed by β-secretase, which activity generates APPsβ (a fragment that is shorter than APPsα) and APP-CTFβ. Further processing of the last by γ-secretases produces AICD and Aβ peptide, the last being released to the extracellular medium. Remarkably, while the first pathway is predominant in physiological conditions, avoiding excessive production of

Aβ peptide, the equilibrium between the two pathways is lost in AD patients. In addition, there are several non-canonical pathways through which APP can be processed distinct from those two above mentioned, some of them also contributing to Aβ peptide generation (U. C. Müller, Deller, & Korte, 2017).

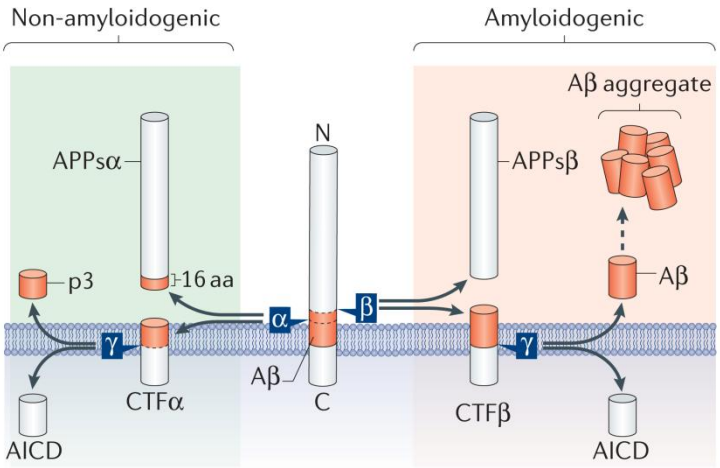

Figure 2. Schematic representation of canonical amyloid precursor protein (APP) processing. The non-amyloidogenic (green background) and amyloidogenic (red background) pathways are shown. The proteolytic cleavage of APP by α- or β-secretase, and subsequently by γ-secretase, generates APP intracellular domain (AICD), and p3 or amyloid β (Aβ) peptides, respectively. Adapted from Müller *et al*., 2017.

Since γ-secretases exhibit lack of specificity of the proteolytic cleavage of APP, Aβ peptide length may vary and can be formed by 37-49 aminoacids (Weidemann et al., 2002). Most of the circulating Aβ peptide consists of 40-aminoacid-long peptides, being also present in a less extent those formed by 42 or 43 aminoacids ($Aβ_{1-40}$, $Aβ_{1-42}$ and $Aβ_{1-43}$, respectively). In addition, shorter (38- or 39-aminoacid-long) and longer (46 to 49-aminoacid-long) peptides can be found (Takami et al., 2009). After APP processing, Aβ monomers, especially $Aβ_{1-42}$, tend to aggregate due to their structure, forming oligomers that will lead to protofibers and fibers, and eventually generating senile plaques. In this sense, *in vitro* and *in vivo* experiments have shown that the Aβ peptide monomer aggregation into high molecular weight species makes them toxic (Chromy et al., 2003; Pike, Walencewicz, Glabe, & Cotman, 1991; Walsh, Lomakin, Benedek, Condron, &

Teplow, 1997), oligomers representing the predominant neurotoxic Aβ peptide species (Glabe, 2005; W. L. Klein, 2002).

In addition to this, Aβ peptide oligomers have been isolated from animal models of AD (Oddo y cols., 2006; Tomiyama y cols., 2010) and from cerebrospinal fluid and brains from AD patients (Bao et al., 2012), in whom the presence of this peptide seem to correlate with disease progression (Santos et al., 2012). In fact, nanomolar concentrations of Aβ oligomers are able to induce neuronal death in hippocampal organotypic slices (Alberdi et al., 2010; Lambert et al., 1998), inhibit long-term potentiation (Lambert et al., 1998; Q. Wang, Walsh, Rowan, Selkoe, & Anwyl, 2004), and promote Ca^{2+} dysregulation and cell membrane disruption interfering with the optimal function of neurons (Alberdi et al., 2010; Demuro et al., 2005). Due to the complexity of Aβ peptide biochemistry (oligomerization, varying length, etc.), it is very promiscuous molecule able to signal through a repertoire of receptors, promoting a wide range of effects in neurons and other cell types (Viola & Klein, 2015) (**Figure 3**).

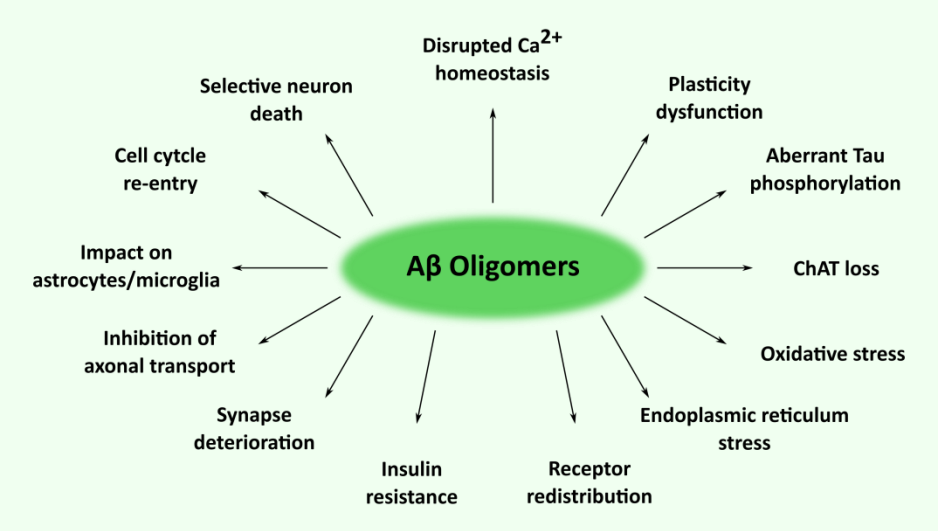

Figure 3. Scheme of the roles of Amyloid β peptide in Alzheimer's disease. Amyloid β peptide promotes a wide repertoire of alterations on both neurons and glial cells. Adapted from Viola & Klein, 2015.

1.4. Animal models of Alzheimer's disease.

The identification of mutations related to AD onset and progression has allowed generating animal models useful to increase the knowledge on the pathobiology of the disease. In fact, in the last decades a wide range of animal models has emerged and therefore, nowadays it is possible to independently study each pathological event occurring in the disease (**Table 1**). In this sense, it has been possible to successfully generate animal models that exhibit increased synthesis and/or deposition of Aβ peptide leading to senile plaque formation, as a result of APP overexpression or mutations in PSN1. Since the first of these models resembling AD pathology was created by producing a single mutation in APP (Games et al., 1995), many others carrying two or three genetic manipulations have been generated. Besides, after the identification of mutations in the protein tau gene observed in patients suffering from Parkinson's disease, it has been also possible to produce transgenic mice developing tauopathies (Götz et al., 1995; Higuchi et al., 2002; Hutton et al., 2000). However, although most of the models develop either tangles or senile plaques, the apparition of one of them do not promote the generation of the other. Therefore, more complicated models were necessary in order to completely understand AD pathology, including those carrying multiple transgenes, hybrids from crossbreeding independent transgenic mice strains, or by microinjection of pathological proteins in transgenic mice (Gotz y cols., 2001; Lewis y cols., 2001).

Table 1. Neuropathological characteristics of the main mouse models of Alzheimer's disease (Schaeffer, Figueiro, & Gattaz, 2011).

Mouse model	Gene (mutation)	Intraneuronal Aβ	Parenchymal Aβ plaques	Hyperphos-phorylated Tau	Neurofi-brillary tangles	Neuronal loss	Synaptic loss	CAA	Primary reference
PDAPP	APP (V717F)	-	Yes	Yes	No	No	Yes	-	Games et al. 1995
Tg2576	APP (K670N/M671L)	Yes	Yes	-	-	No	No	-	Hsiao et al. 1996
TgCRND8	APP (K670N/M671L, V717F)	-	Yes	-	No	No	-	-	Chishti et al. 2001
APP/PS1	APP (K670N/M671L), PS1 (M146L)	-	Yes	-	-	-	-	-	Holcomb et al. 1998
APP23	APP (K670N/M671L)	-	Yes	Yes	No	Little	Yes	Yes	Sturchler-Pierrat et al. 1997
Tg-SwDI	APP (E693Q, D694N)	-	Yes	-	-	-	-	Yes	Davis et al. 2004
APPDutch	APP (E693Q)	-	Little	-	-	-	-	Yes	Herzig et al. 2004
APPDutch/PS1	APP (E693Q), PS1 (G384A)	-	Yes	-	-	-	-	Little	Herzig et al. 2004
hAPP-Arc	APP (E693G, K670N/M671L, V717F)	-	Yes	-	-	-	-	Little	Cheng et al. 2004
Tg-ArcSwe	APP (E693G, K670N/M671L)	Yes	Yes	-	-	-	-	Yes	Lord et al. 2006 Knobloch et al. 2007
APPArc	APP (E693G)	-	Yes	-	-	-	-	Yes	Rönnbäck et al. 2011
TAPP	APP (K670N/M671L), Tau (P301L)	-	Yes	-	Yes	-	-	-	Lewis et al. 2001
3xTg-AD	APP (K670N/M671L), Tau (P301L), PS1 (M146V)	Yes	Yes	Yes	Yes	-	No	-	Oddo et al. 2003
APP_{SL}/PS1	APP (K670N/M671L, V717I), PS1 (M146L)	Yes	Yes	-	-	Yes	Yes	-	Wirths et al. 2002
APP/PS1KI	APP (K670N/M671L, V717I), PS1 (M233T/L235P)	Yes	Yes	-	-	Yes	Yes	-	Casas et al. 2004
5xFAD	APP (K670N/M671L, I716V, V717I), PS1 (M146L/L286V)	Yes	Yes	-	-	Yes	Yes	-	Oakley et al. 2006

CAA = cerebral amyloid angiopathy; Dash (-) = not reported.

Therefore, one of the most complete models of AD is the triple transgenic mouse (3xTg-AD) (Oddo et al., 2003) that was created by directly microinjecting two tansgenes, APPSwe and tauP301L, in a genetically-modified mouse germ line (PSIM146V). Thus, these mice carry three transgenes related to the development of AD: Swedish mutation of APP (APPSwe; K670N/M671L), a mutation in PSN1 (M146V), and a mutation in protein tau (P301L). This model was a pioneer since it develops both senile plaques and neurofibrillar tangles in AD-relevant brain regions, showing ageing-associated cognitive defects related to learning and memory that highly resemble those found in AD patients.

The first histopathological feature exhibited by 3xTg-AD mice is intraneuronal Aβ peptide, which is detectable from 3-4 months in the cortex and from 6 months in the hippocampus. Accumulation of intraneuronal Aβ peptide negatively correlated with levels of synaptic transmission observed in these animals, included in the long-term potentiation. From this age on, extracellular deposits of Aβ peptide start to appear mainly in the cortex at 6 months and the hippocampus at 12 months. Regarding soluble Aβ peptide oligomers, they can be detected intracellularly from the second month of life,

levels go down at 12 months probably due to the increase in fiber formation, and in 15-month-old mice these levels rise again (**Figure 4**). On the other hand, neurofibrillar tangles start to form at 12 months in the hippocampus then expanding to the cortex. This, in fact, support amyloid cascade hypothesis, since the initial event in these mice is the accumulation of Aβ peptide.

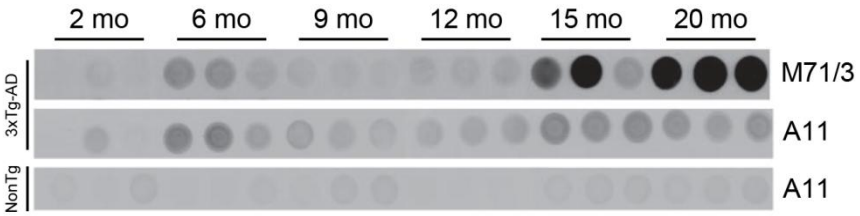

Figura 4. **Temporal profile of Aβ peptide oligomer formation in 3xTg-AD mice**. Dot blot showing the density of low (M71/3) and high (A11) molecular weight Aβ peptide oligomers in 2 to 20-month-old control and 3xTg-AD mice. Extracted from Oddo *et al*., 2006.

2. Oligodendrocytes.

Oligodendrocytes are the glial cells responsible for producing a multilamellar lipid structure highly specialized around the axons called myelin in the central nervous system (CNS). This cell type was described by Pío del Río-Hortega in 1921 as small cell bodies containing nuclei with large amounts of chromatin and exhibiting a highly complex network of cellular extensions without fibers but filled with cytoplasmic granules.

During late embryonic developmental stages, oligodendrocytes originate from multipotential neural progenitor cells (NPCs). Under specific signals, NPCs start to express Olig2 triggering the first embryonic wave of specification of oligodendrocyte progenitors cells (OPCs) (Naruse, Ishizaki, Ikenaka, Tanaka, & Hitoshi, 2017). Then, OPCs migrate from ventricular/subventricular zone of the brain to the developing white matter where they proliferate and form an evenly spaced network of cell processes. After OPCs migration and establishment at a suitable region, some of them remain in a precursor state while others differentiate into postmitotic myelin-forming oligodendrocytes (Simons & Nave, 2016).

2.1. Oligodendrocyte differentiation.

OPCs differentiation undergoes several stages of cell maturation which are extensively defined by morphological aspects and specific-marker proteins. The sequential expression of developmental markers divide the lineage into distinct phenotypic stages (Baumann & Pham-Dinh, 2001). Early progenitor cells are responsible for migration and proliferation, and are mainly characterized by expressing the platelet-derived growth factor receptor-α (PDGFR-α). These cells have a bipolar morphology and are able to differentiate into late progenitor cells, which acquire the marker O4 and develop a more complex shape. At this stage, cells keep their ability to proliferate, but they lose their motility almost completely. Following oligodendrocyte lineage progression, late progenitors give rise to immature cells that express the earliest myelin-related marker, 2',3'-Cyclic nucleotide-3'-phosphodiesterase (CNPase). Finally, these cells will differentiate into mature oligodendrocytes which exhibit the ability to synthesize myelin-related proteins as myelin basic protein (MBP) and myelin proteolipid protein (PLP).

After development, a population of OPCs remain in the adult brain preserving their ability to proliferate and generate new mature oligodendrocytes, which will be needed to maintain myelination processes both in healthy or diseased adult brain (Young et al., 2013).

Oligodendrocyte differentiation require a series of well-coordinated events that orchestrate all stages, from OPCs proliferation to myelin synthesis regulation, following an intrinsic program of maturation controlled by extracellular and intracellular signals (Almeida, Czopka, ffrench-Constant, & Lyons, 2011). Therefore, differentiation and myelination are properly controlled a wide repertoire of both negative and positive regulators.

Regarding extracellular signals, the Leucine-rich repeat and immunoglobulin domain-containing-1 (LINGO1) is a transmembrane protein expressed in axons and oligodendrocytes is one of the main negative regulators. LINGO-mediated signaling pathways repress oligodendrocyte differentiation by decreasing Fyn kinase activity and

subsequent RhoA signaling (Mi et al., 2005). The G-protein-coupled receptor 17 (GRP17), exclusively expressed in oligodendrocyte and the Notch-1 receptor also act as negative regulators of this process. While, GRP17 is transiently expressed in late OPCs to inhibit oligodendrocyte differentiation (Chen et al., 2009), Notch-1 have a double role in cell maturation depending on the axonal proteins it interacts with. The binding between axonal Jagged-1, Delta-1, and Notch-1 generates an intracellular domain which enters in the nucleus and increase expression of inhibitors transcription factor (S. Wang et al., 1998). In contrast, axonal F3/contractin-Notch-1 binding promotes OPC differentiation by expressing myelin proteins (Hu et al., 2003). In turn, a variety of diffusible factors positively influence in oligodendrocyte differentiation. In addition to being involved in OPC survival and proliferation, insulin-like growth factor 1 (IGF-1) signaling is required for oligodendrocyte differentiation and myelin formation (Zeger et al., 2007) via PI3K/Akt/mTOR signaling pathway (Flores et al., 2008; Tyler et al., 2009). In addition, thyroid hormone 3 (T3) also regulates oligodendrocyte differentiation, observing a reduction in myelin gene expression in human hypothyroidism patients and rodents (S. Mitew et al., 2014).

Concerning the intracellular regulators of oligodendrocyte differentiation, there are several transcription factors regulating all the stages of this process. Among the differentiation inhibitors, bHLH transcription factors acts as negative regulators binding directly to pro-differentiation factors as Olig1 and Sox10 to inhibit their function (Liu et al., 2006; Samanta & Kessler, 2004). The transcription factor Tcf12 also is involved in differentiation blockade being recruited by β-catenin via Wnt signaling pathway. As positive regulators, Olig2 is constantly expressed through all oligodendrocyte lineage, being its levels progressively decreased at mature stages (Kitada & Rowitch, 2006). Ablation of Olig2 in OPCs causes a sustained decrease in oligodendrocyte differentiation, while ablation in mature cells have no detrimental effect, suggesting that Olig2 mediates cell differentiation but has no role on mature oligodendrocyte functions, as myelination (Mei et al., 2013). In contrast, the transcription factor Myrf is specifically induced during oligodendrocyte differentiation and is also required for maintenance of myelin. Inducible conditional ablation of Myrf in mature cells results in a severe reduction in myelin genes and a subsequent demyelination (Emery et al., 2009; Koenning et al., 2012).

2.2. Oligodendrocyte functions.

The main function of mature oligodendrocytes is the formation of the myelin sheath around the axon. Myelin provides the structural basis for rapid impulse propagation required to properly develop of motor, sensory and cognitive functions in CNS. Axonal insulation by myelin membrane restricts their energy requirements and accelerates nerve conduction 20-100-fold in comparison with non-myelinated axons. Moreover, oligodendrocytes are able to myelinate a varying number of axonal areas (internode), between 20 and 80, depending on several factors as axon caliber and length (Snaidero & Simons, 2014a). In this sense, most of oligodendrocytes myelinating large caliber axons develop less number of internodal areas, but these are longer and thicker.

In addition to electrical insulation of axons, oligodendrocytes provide them with trophic and metabolic support (**Figure 5**). In this process, glutamate plays relevant roles as its neuronal activity-dependent release regulates oligodendrocyte metabolic supportive function (Saab et al., 2016). After glutamate binding to NMDA receptor in oligodendrocytes, these cells uptake glucose to generate lactate that is transported to and released into periaxonal space. Then, lactate is taken up by neurons which catabolize it to generate ATP. Other metabolites, proteins, mRNA and neuronal trophic factors are transported from oligodendrocyte soma towards axons likely through myelin cytoplasmic channels in order to support their activity (Nave & Werner, 2014). These cytoplasmic channels are non-compacted areas in which microtubules and multivesicular bodies are present, that preserve functional axon integrity by permitting oligodendrocyte-axon support. In fact, cytoplasmic channels loss observed in CNPase null-mice results in axonal degeneration, in spite of the absence of myelin defects (Snaidero et al., 2017). In turn, MBP-deficient mice that develop a severe dysmyelination conserve an intact axonal function, likely due to the maintenance of the glia-driven metabolic support. Indeed, evidences observed in different myelin models suggest that absence of myelin is better than the presence of defective one for sustaining proper axonal functions, as this defective myelin is associated with an uncoupling of oligodendrocyte support of axons (Simons & Nave, 2015).

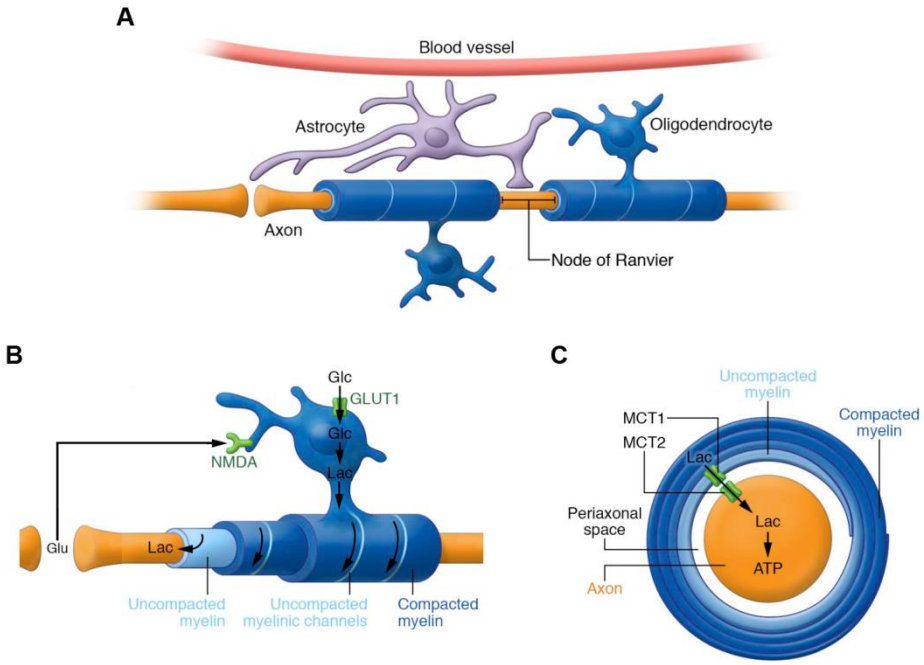

Figura 5. **Oligodendrocyte provides metabolic support to neurons**. **(A)** Oligodendrocytes and astrocytes contribute to neuronal metabolic support. **(B)** Oligodendrocyte metabolic supportive function is regulated by glutamate release from electrically active neurons. Glutamate binds to oligodendrocytes NMDA receptors, leading an enhanced glucose uptake to be finally transformed to lactate. **(C)** Lactate is transported through oligodendrocyte uncompacted myelinic channels to periaxonal space where is imported by axon and processed for ATP synthesis. Adapted from Philips & Rothstein 2017.

a. Oligodendrocyte myelination.

The precise and coordinated production of myelin by mature oligodendrocytes supports the smooth functioning and development of CNS. In order to ensure the optimal function of this process, myelination is tightly regulated by several signals that control both initial formation and maintenance of myelin sheaths. Oligodendrocytes must integrate all these regulatory signals which are determined not only by axonal factors, but by electrical activity (Gibson et al., 2014; Wake, Lee, & Fields, 2011a), spatial density of OPCs (Rosenberg, Kelland, Tokar, De La Torre, & Chan, 2008), and cues from astrocytes (Back et al., 2005; Hammond et al., 2014) and microglia/macrophages (Miron et al., 2013; Ruckh et al., 2012).

Mature oligodendrocytes extend their processes to make contact with axons and then, initiate wrapping around them. Oligodendrocytes rapidly reorganize their

cytoskeleton morphology, and increase microfilament polymerization and branching in response to axon-oligodendrocyte recognition (Bauer, Richter-Landsberg, & Ffrench-Constant, 2009; Simons & Trotter, 2007). Most of the axonal signals that participate in this regulation act as negative regulators, as occurs during differentiation stages. Axonal proteins, as Jagged-1 and Lingo1 that interact with Notch-1 and Nogo receptor, inhibit myelination and oligodendrocyte process outgrowth, besides their role as regulators of oligodendrocyte differentiation (Mi et al., 2005; S. Wang et al., 1998). In addition, the expression of polysialylated-neural cell adhesion molecule (PSA-NCAM) regulate myelin formation, being necessary to be downregulated before myelination onset (Charles et al., 2000; Fewou, Ramakrishnan, Büssow, Gieselmann, & Eckhardt, 2007). These inhibitory signals regulate the initiation steps of myelination and prevent over-myelination.

Oligodendrocytes also receive neuronal pro-myelinating signals which have to be integrated by them to control their responses. An essential neuronal signal integrator is Fyn (Krämer-Albers & White, 2011), a member of the Src non-receptor tyrosine kinase family which expression is predominant and upregulated during oligodendrocyte differentiation (Osterhout, Wolven, Wolf, Resh, & Chao, 1999). It has been described that Fyn activation is essential for myelination and MBP translation (Krämer-Albers & White, 2011). Moreover, *in vivo* studies have demonstrated the importance of Fyn as mediator of myelin formation process, since knock-out Fyn mice present severely reduced levels of myelin and oligodendrocyte loss in corpus callosum and optic nerve (B R Sperber et al., 2001). In addition, analysis in the zebrafish model have confirmed the important role of Fyn in myelination process showing that it regulates over the number of myelin sheaths per oligodendrocyte (Czopka, ffrench-Constant, & Lyons, 2013).

During oligodendrocyte maturation, Fyn kinase activity is compartmentalized and recruited into lipid raft membrane domains with another specific proteins, as integrin α6β1, to promote their interaction (White & Krämer-Albers, 2014). Fyn is activated by axonal-glia contact in which axonal cell adhesion molecule L1 and extracellular matrix-derived laminin-2 interact with an oligodendroglial complex of integrin β1 and contactin-1 (Lisbeth Schmidt Laursen, Chan, & ffrench-Constant, 2009; White et al., 2008). Furthermore, it has been shown that neuronal activity stimulates Fyn kinase, which may

be mediated by increased axonal surface expression of L1 (Wake, Lee, & Fields, 2011b). Fyn activation also interferes in oligodendrocyte maturation and in particular process outgrowth (C. Klein et al., 2002; Brian R. Sperber & McMorris, 2001). In addition to regulating the cytoskeleton recruitment and local MBP synthesis, Fyn kinase in involved in regulating morphological differentiation of oligodendrocytes triggered by integrin receptor activation (Liang, Draghi, & Resh, 2004) (**Figure 6**).

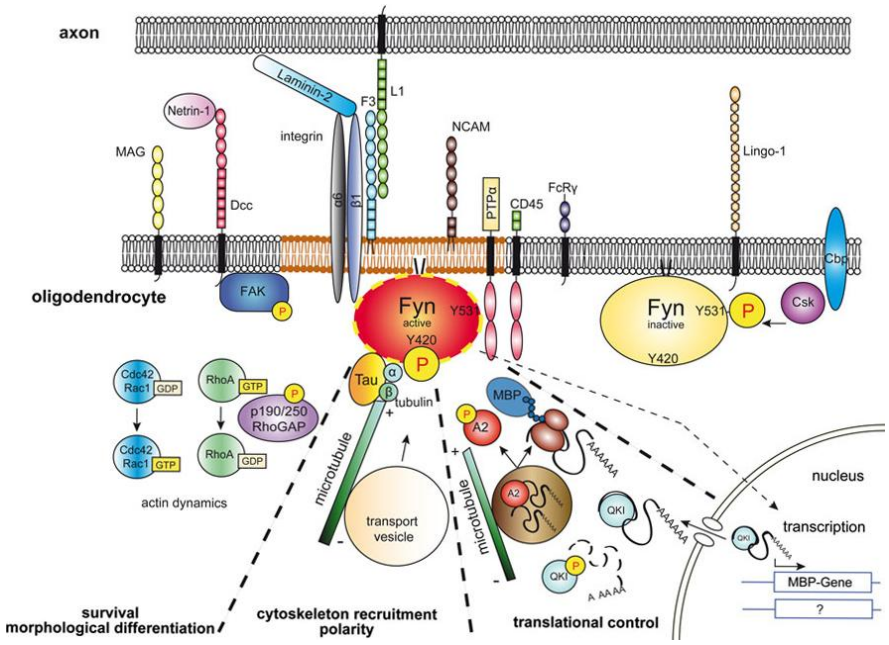

Figure 6. The role of Fyn kinase during oligodendrocyte-axon interactions. Fyn activation induced by axon-derived signaling modulates oligodendrocyte survival and differentiation, and MBP mRNA transport and translation (Adapted from Krämer-Albers & White, 2011).

One of the main receptors implicated in Fyn activation is integrin β1 (Holly Colognato, Ramachandrappa, Olsen, & ffrench-Constant, 2004; L. S. Laursen, Chan, & ffrench-Constant, 2009). Integrins are a major family of extracellular matrix receptor formed by two subunits, α and β, and are widely expressed in neurons and glial cells. During oligodendrocyte development, the expression of this heterodimeric receptor vary depending on the differentiation stage, being integrin α6β1 and αvβ1 strongly expressed in newly formed oligodendrocytes (Malek-Hedayat & Rome, 1994; Milner & Ffrench-Constant, 1994) (**Figure 7**). Interestingly, environmental cues also change the expression pattern of integrin receptors suggesting an involvement in diverse cellular function. It has been described that integrins, specifically integrin β1, mediate oligodendrocyte survival

(Benninger et al., 2006; Corley, Ladiwala, Besson, & Yong, 2001) and differentiation (Buttery & ffrench-Constant, 1999), and participate in the initiation of myelination. Indeed, using a dominant negative integrin β1 mouse model it has been demonstrated a reduction in the density of internodes and myelinated axons, as well as a higher axonal diameter threshold required for myelination (Câmara et al., 2009; K. K. Lee et al., 2006). However, conditional ablation of integrin β1 in oligodendrocytes showed strong effects on oligodendrocyte survival but little effects on myelination (Benninger et al., 2006). These contradictory results may be due the presence of other receptors implicated in Fyn-mediated myelination which likely compensate for lack of integrin β1 expression. One proposed candidate involved in this compensatory effect is the dystroglycan receptor (H. Colognato et al., 2007). Moreover, integrin β1 is also required in myelin thickness determination, since no functional integrin β1 mice exhibit thinner myelin sheaths at later stages (Barros et al., 2009; K. K. Lee et al., 2006).

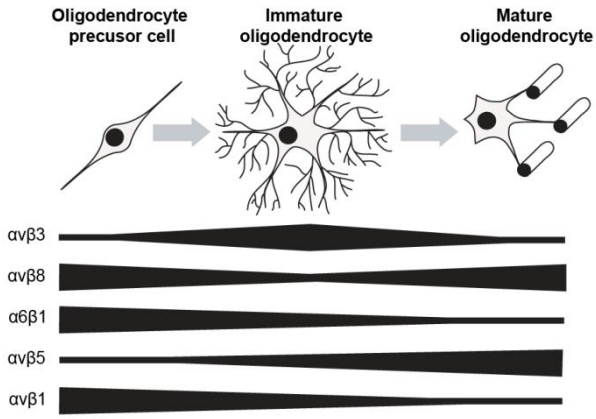

Figure 7. Integrin receptor expression during oligodendrocyte differentiation. Integrin receptors are differentially expressed during oligodendrocyte development. The expression of αvβ3 is strongly increased in immature oligodendrocytes, while αvβ5 is markedly expressed at mature stages. α6β1 and αvβ1 are mainly expressed at early stages, whereas the expression of αvβ8 is increased both in precursor and mature oligodendrocytes (Adapted from O'Meara, Michalski, & Kothary, 2011).

Myelin formation is also regulated by the molecular signaling triggered by neuregulins (NRG), which act through ErbB tyrosine kinase receptor. NRG expression is restricted mainly to neurons where is cleaved by β- (BACE) and γ-secretases to mediate ErbB receptor activation. Although it is described that NRG mediate oligodendrocyte

survival and differentiation, its role in myelination process is still under debate. Both NRG and ErbB receptor knockout mice exhibit normal myelination (Brinkmann et al., 2008), while the expression of dominant negative of ErbB4 result in reduced myelin thickness and oligodendrocyte density (Roy et al., 2007). Moreover, overexpression of NRG induces CNS hypermyelination (Brinkmann et al., 2008) and in turn, NRG and ErbB reduced expression observed in schizophrenia causes hypomyelination (Makinodan, Rosen, Ito, & Corfas, 2012). Thus, these data suggest that NRG/ERbB signaling have an impact in oligodendrocyte myelination, although this process is yet to be fully understood.

After oligodendrocyte stimulation by extracellular mediators, several intracellular signaling pathways have been shown to be implicated in the molecular events which lead oligodendrocytes to myelination. Among them, PI3-Kinase/Akt/mTOR and ERK1/2-MAPK pathways as well as the Ca^{2+}/CaMKII act as important mediators of myelin formation (Gaesser & Fyffe-Maricich, 2016; White & Krämer-Albers, 2014).

In addition to axonal extracellular cues, myelination is also regulated by oligodendrocyte transcription factors such as Olig1, Sox10, and Myrf. *In vivo* ablation or blocking of these factors results in myelin loss (Dai, Bercury, Ahrendsen, & Macklin, 2015; Hornig et al., 2013; Koenning et al., 2012), revealing their contribution in myelin synthesis process. Moreover, it has been described that transcriptional factor activities are associated with regulatory network intrinsic to oligodendrocytes as chromatin remodeling, histone and DNA modifications, micro-RNAs and non-coding RNA that regulate oligodendrocyte myelination (Emery & Lu, 2015). Importantly, integration of myelination-mediated signals and subsequently, crosstalk between activated molecular pathways allow oligodendrocyte controlling and supplying myelination failures to ensure a robust myelination.

3. Myelin.

The myelin sheath is an extension of the oligodendrocyte plasma membrane that wraps axons in the central nervous system. Myelin was considered a neuronal secretion until Pío del Río Hortega described this membrane as part of oligodendroglial cells by

using of silver carbonate staining. The main function of the myelin sheath is to insulate axons and restrict the generation of action potential to unmyelinated axonal segments, the nodes of Ranvier, which are essential for the fast saltatory conduction in the brain. The term myelin was coined by Rudolf Virchow in 1864 and comes from Greek word "myeloid" (marrow).

Myelin structure is composed of a multilayered stack of membranes organized in alternating electron-dense (major dense line) and electron-light layers (the intraperiod line), as observed using transmission electron microscopy. Major dense lines represent the adhesion zone between closely condensed cytoplasmic membranes, while intraperiod lines consist of extracellular apposed myelin membranes (Hartline, 2008) (Figure 8). This compacted area appears in repeating patterns of 12 nm and provides the high electrical resistance and low capacitance that is essential for propagation of axon potentials. The myelinated segments along axons are separated by the nodes of Ranvier, small areas lacking of myelin where the excitable axonal membrane is exposed to the extracellular space. The nodes are characterized by a high density (>1200/μm^2) of sodium channels which allow the generation of the action potential during saltatory conduction (Stephen G. Waxman & Ritchie, 1993). At both sides of them, myelin lateral edges form the paranode, a non-compacted structure in which myelin is firmly attached to axon. This specialized contact area is maintained by the adhesion of contactin and Caspr proteins on the axonal surface and Neurofascin-155 on the glial side (Salzer, Brophy, & Peles, 2008).

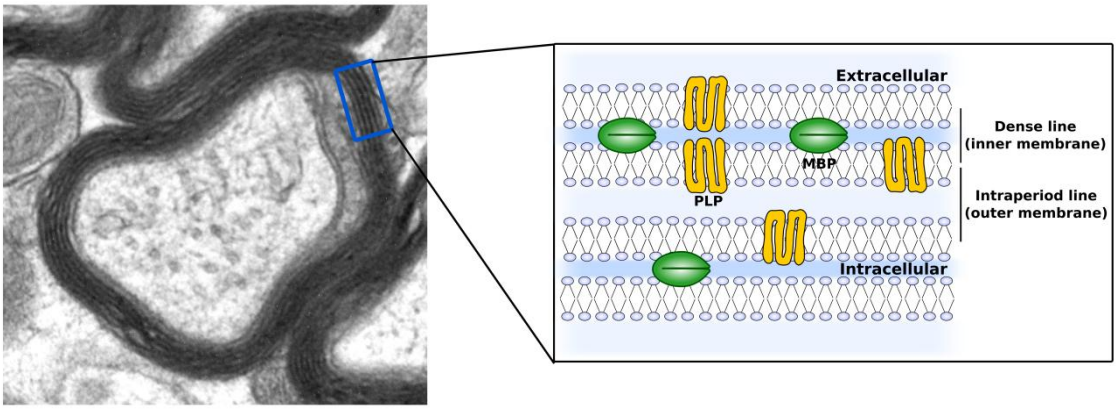

Figure 8. Myelin structure. Myelin is composed of stacked layers of oligodendrocyte cell membrane mainly packed by MBP. Due to the tight package, two alternating types of layers can be observed under the electron microscope, electron-dense (major dense line) and electron–light layers (the intraperiod line).

In addition to myelin membrane ultrastructure, its specialized molecular composition makes myelin a unique membrane in the CNS. Myelin sheath is a poor hydrated structure containing 70-80% lipids (by dry weight) and a low proportion of highly hydrophobic small proteins, MBP and PLP being the most abundant. This hydrophobic context exerts a repulsive force towards the extracellular fluid, which contribute to myelin stability and compaction. Moreover, the specific content of lipids, organized in lipids rafts, and their interaction with proteins, confers this membrane a solid molecular stability turning it into a highly stable system. In this sense, myelin membrane components, as myelin proteins and lipids, have half-lives on the order of several weeks to months. Interestingly, even when oligodendrocytes are ablated from inducible transgenic mice by using a diphtheria toxin, myelin remains stable for several weeks (Pohl et al., 2011; Traka et al., 2010).

3.1. Myelin biogenesis.

Myelin synthesis implies extensive changes in oligodendrocyte morphology and membrane architecture. Despite the complicated detection of oligodendrocyte structural changes due to technical limitations, several models of myelin biogenesis in the CNS have been proposed. First, it was proposed a peripheral nervous system model in which glial membrane extends along the axon towards the node of Ranvier and then, inner tongue begin to wrap the axon, known as jelly roll model (BUNGE, BUNGE, & RIS, 1961). However, the application of new techniques in electron microscopy and the use of high-pressure frozen samples and three-dimensional reconstructions has made possible to study myelin ultrastructure during optic nerve development and thus propose a new model (Snaidero et al., 2014). These analyses revealed that myelin is a single extension of membrane with a triangular shape where the outer layer is in direct contact with the oligodendrocyte cell body and the innermost layer with the axon. This model suggests that the wrapping occur by two different, but coordinated movements. First, the oligodendrocyte send out the process which makes contact with the axon and the inner tongue leads the wrapping around it, expanding the membrane underneath the previously generated layers. This motion is the responsible for creating new membrane layers. Second, there is a lateral extension of all layers towards the node of Ranvier to increase myelin length (**Figure 9**). Thus, oligodendrocyte has two direct contact zones

with axon surface, one at the innermost layer and the other one at the lateral edges of each myelin layer which form the complex paranode zone.

In order to progress with myelin development, it is necessary to transport newly synthesized myelin components from the soma of oligodendrocytes to the growing areas in the myelin sheath. For that, there is an elaborated system of cytoplasmic-rich channels containing microtubules and vesicular carriers that transport new membrane elements to the growing zones, both inner tongue and lateral edges. The trafficking pathways for radial and lateral growth are spatially separated. During myelin development, these cytoplasmic channels are largely present in the myelin sheath. However, when myelination is complete, their number is notably reduced (Snaidero et al., 2014), although many of them remain active in the adult brain. The presence of these channels may generate functional connections between oligodendrocyte soma to axon, creating communication and allowing the distribution of glial metabolites to axonal compartment, as previously described. Thus, myelin is a highly dynamic structure in which lipids and small proteins diffuse freely, enabling the active and plastic design of the developing myelin sheath (Snaidero & Simons, 2014b).

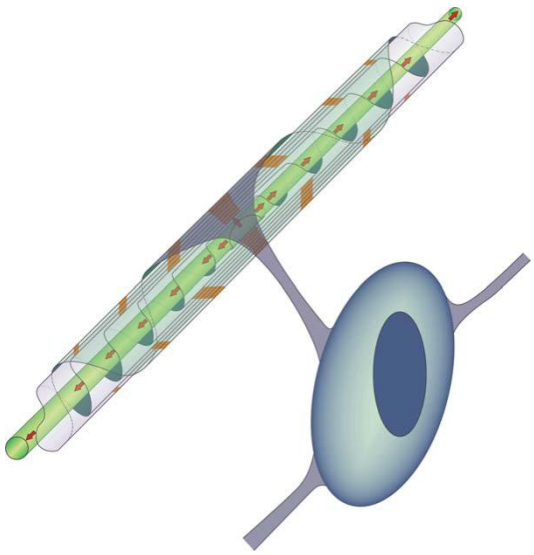

Figure 9. **Model of myelin wrapping around axons by oligodendrocytes**. There are two types of motion during myelin wrapping. After axon-oligodendrocyte contact, glial membrane wraps around the azon forming new layers. Second, layers expand laterally towards the node of Ranvier to increase myelin length.

3.2. Myelin compaction.

Myelin compaction is mainly carried out by MBP and occurs early in the development, after only few wraps (Readhead et al., 1987). The compaction starts in the outermost layers (closer to oligodendrocyte soma) and progresses inward both radially and longitudinally in parallel with membrane growth. However, it has been described that MBP mRNA is transported from the nucleus to the innermost layers and there, closed to axon, is translated to protein. Thus, to prevent premature compaction at inner tongue, the myelin membrane-associated enzyme CNPase acts as spacer between two adjacent cytoplasmic-membranes and regulate the compaction rate. In absence of CNPase, myelin compaction extends to inner tongue (Snaidero et al., 2014), while its overexpression lead to a lack of compaction (Gravel et al., 1996; Yin, Peterson, Gravel, Braun, & Trapp, 1997). Thereby, due to CNPase presence MBP protein can be transported from inner tongue to outer layers, and there begin myelin compaction (Snaidero & Simons, 2014b).

3.3. Myelin plasticity and remodeling.

Myelin is a dynamic structure with adaptive capacity in response to neuronal activity changes. This plasticity allow myelin to modulate information processing and network activity during adult life (Fields, 2008). In this sense, it has been observed that inhibition of new oligodendrocyte generation by tamoxifen-induced ablation of Myrf transcription factor in adult mice, results in a blockade of *de novo* myelination and a subsequent fail in motor task learning. This data suggest that myelination in adult mice is essential to learning (McKenzie et al., 2014). Supporting these data, a study of Young and co-workers (2013) demonstrated that myelination also occurs throughout adulthood. By using an inducible PDGFr-α knock-out mouse model, they observed the generation of adult-born OPCs that were able to proliferate and differentiate into mature oligodendrocyte engaged in myelin remodeling. However, these new adult-born mature cells form myelin with different properties, creating myelin sheaths with shorter, but more abundant internodes in comparison with oligodendrocytes generated during early development. More importantly, evidences of myelin plasticity also have been observed in human brain (Bengtsson et al., 2005; Scholz, Klein, Behrens, & Johansen-Berg, 2009).

Therefore, it has been proposed that subtle changes in myelin thickness or nodal length participate in the timing of conduction velocity. During evolution of nervous systems, most of myelinated fibers have acquired a specific myelin thickness and length adequate for obtaining the maximal conduction velocity. However, several areas of the mammalian brain exhibit different caliber axons which need to synchronize their conduction velocity. In this case, myelin is able to adapt its thickness and length to facilitate a coupled neuronal activity (Snaidero & Simons, 2014a).

In this sense, it has been described that myelin thickness is directly related to axon caliber, being the theoretical *g*-ratio index around 0.6 (Chomiak & Hu, 2009). This measurement is based on the ratio of the axonal diameter to the total fibers diameter and is commonly used as structural myelination index. When myelin thickness is deviated from this value, either higher or lower, conduction velocity drops (S G Waxman, 1997). In addition to myelin thickness, internodal length also influence speed conduction raising the optimal velocity when axons with large caliber have long internode lengths (Friede & Bischhausen, 1982). Moreover, a recent study proposed node of Ranvier length as another conduction velocity regulator (Arancibia-Cárcamo et al., 2017). This predictive model shows that node elongation is related to slow conduction by increasing the node capacitance. On the other hand, the density of Na^+ channels at the node has to remain unchanged in order to avoid loss of conduction velocity.

4. Myelin basic protein (MBP).

Myelin basic protein (MBP) is one of the most abundant proteins in myelin sheath membranes. MBP is a product of a large gene complex called Golli in which 7 exons give rise to classic MBP. In addition, due to alternative splicing several isoforms of MBP have been described (Boggs, 2006).

In general, the process of myelination is remarkably resistant to genetic ablation of its structural components. While most of major myelin proteins, including PLP, are not essential, the absence of MBP leads to severe myelination deficits as it was observed in

shiverer mice. Thus, MBP has a unique and essential role in myelin formation and maintenance (Krämer-Albers & White, 2011).

4.1. MBP function: Myelin compaction.

The main function of MBP is related to myelin compaction by membrane association. MBP regulates the protein/lipid ratio in myelin sheath membranes to form a proper lipid-rich insulating membrane. For that, MBP carries positive electrostatic charges that interact with the negatively-charged headgroups of phospholipids in the inner leaflet, leading to the compaction of the two opposing cytoplasmic membrane layers (Fitzner et al., 2006; Musse, Gao, Homchaudhuri, Boggs, & Harauz, 2008; Nawaz et al., 2009). Then, MBP connects the two adjacent membranes by self-oligomerization creating a cohesive protein meshwork that acts as a physical filter excluding other cytoplasm- and membrane-associated proteins out of the compacting area, only remaining PLP and MBP (Aggarwal et al., 2013). Moreover, MBP interacts with cytoskeletal proteins modulating its assembly (Dyer, Philibotte, Wolf, & Billings-Gagliardi, 1994; Hill & Harauz, 2005; Hill, Libich, & Harauz, 2005). Notably, MBP is subject to various post-translational modifications modulating its charge level, which may regulate its ability to promote sheet segregation and membrane compaction (Harauz & Musse, 2007).

4.2. MBP mRNA transport and translation.

To permit a correct compaction of membranes at appropriate intracellular sites, MBP mRNA is transported from the nucleus to the myelin compartment where is translated locally. The presence of MBP mRNA and ribosomes in purified myelin fraction was the first evidence which suggest MBP mRNA transport (Colman, Kreibich, Frey, & Sabatini, 1982). MBP mRNA is packed and transported in specialized RNA transport granules through cytoplasmic microtubules to the distal parts of the processes (Ainger et al., 1993, 1997) where MBP translation is initiated by participation of several proteins, as Fyn and integrin receptors (**Figure 10**). These RNA transport granules contain all necessary molecules for the transport, as well as mRNA translation machinery. In addition, RNA granules also contain specific molecules to maintain a translationally repressed state until

the periphery is reached. In fact, defects in proteins involved in MBP mRNA transport or in translation repression results in accumulation of MBP at inappropriate subcellular locations, leading to myelination defects (Lyons, Naylor, Scholze, & Talbot, 2009).

As previously mentioned, Fyn kinase has an important role in CNS myelination, being also involved in local MBP translation. Activated Fyn binds to the microtubule associated protein Tau and recruits the cytoskeleton towards axon-glia contact sites (C. Klein et al., 2002). Thus, Fyn facilities the transport of MBP mRNA to the axon-glia site to initiate the myelination by synthesizing MBP (C. Müller, Bauer, Schäfer, & White, 2013). Furthermore, Fyn activation also result in MBP mRNA release from RNA granule protein complex by phosphorylation of repressed proteins, as hnRNP F, allowing MBP mRNA to be translated (White et al., 2012) (**Figure 10**). Interestingly, it has been described that MBP translation triggered by Fyn is coupled to neuronal stimulation and glutamate signaling, supported the idea of Fyn as important neuronal signals integrator (Wake et al., 2011a).

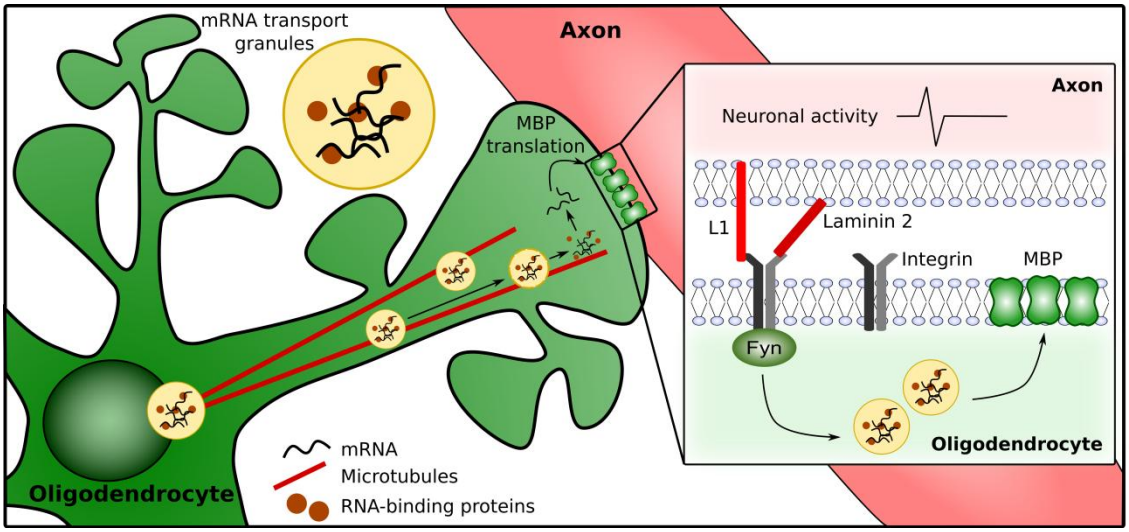

Figure 10. **MBP mRNA transport and localized translation**. MBP mRNA is transported through microtubules within mRNA transport granules towards oligodendrocyte processes where is locally translated. Fyn integrates neuronal signals and allow MBP mRNA release from transport granules and be translated.

In addition, α6β1 integrin receptor activates Fyn (Holly Colognato et al., 2004; L. S. Laursen et al., 2009) and stimulates MBP synthesis through interactions with a mRNA-binding protein, hnRNP-K (Lisbeth S. Laursen, Chan, & ffrench-Constant, 2011). Moreover,

Fyn knock-out mice show a reduction in MBP levels (Lu, Ku, Chen, & Feng, 2005), while the presence of a constitutively active α6β1 integrin mutant promotes MBP translation (Lisbeth S. Laursen et al., 2011). The regulation of MBP translation is also regulated by transcription factors as CREB which may be phosphorylated by CAMKII (Sun, Enslen, Myung, & Maurer, 1994), PKC (Xie & Rothstein, 1995) and growth factor-induced kinases like ribosomal S6 kinase (Xing, Ginty, & Greenberg, 1996).

5. Oligodendrocyte and Alzheimer´s disease.

AD has been traditionally considered to be a gray matter (GM) disease. However, evidence of diffuse white matter (WM) pathology from AD patients and animal models have also been reported (Firbank et al., 2007; Kavcic, Ni, Zhu, Zhong, & Duffy, 2008; Roher et al., 2002a). WM is an essential component of neural networks and is critical for many high order cognitive processes including attention, executive functioning, non-verbal/visual-spatial processing, and generalized processing speed, all of which are impaired in AD. It was generally believed that atrophic changes observed in the WM were a consequence of axon retraction caused by Wallerian degeneration due to neuronal cell body loss. However, there is no correlation between GM and WM damage (Brun & Englund, 1986; de la Monte, 1989). Moreover, it has been observed at early stages of AD pathology that WM atrophy occurs before GM degeneration as neuronal loss, plaque formation or cognitive decline, suggesting that axonal or myelin chemical abnormalities provoke neuronal body loss degeneration (Bartzokis et al., 2003, 2004; Brun & Englund, 1986; Kavcic et al., 2008; Price et al., 2001).

Myelination process occurs in a specific chronological pattern in which different brain regions are myelinated at different time points. In fact, myelin synthesis of prefrontal and temporal areas continues until the end of the fifth decade of life. Imaging techniques revealed that late-myelinating regions, such as temporal and frontal lobes characterized by the presence of small caliber fibers, are the first to be affected by AD degenerative process (Bartzokis et al., 2003; Stricker et al., 2009; Teipel et al., 2007). In addition, oligodendrocyte progenitors cells in these regions have reduced myelin turnover and

thus, a diminished capacity for myelin repair than oligodendrocytes present in early-myelinating areas (Power, Mayer-Pröschel, Smith, & Noble, 2002).

It is well established that WM integrity progressively deteriorates with normal aging (Damoiseaux et al., 2009; Inano, Takao, Hayashi, Abe, & Ohtomo, 2011), but evidence from whole brain imaging studies suggests that this natural tendency is exacerbated and accelerated by AD (Bartzokis et al., 2003; de la Monte, 1989; Stricker et al., 2009). Postmortem and *in vivo* magnetic resonance imaging (MRI) studies have largely demonstrated a substantiated WM impairment in AD, finding reduced white matter volume and alterations of white matter microstructure (Bartzokis, 2011; Roher et al., 2002a), such as differences in the physical organization of the myelin lipid bilayer (Chia, Thompson, & Moscarello, 1984). A recent study, in which several imaging measurements of myelin status and psychological test are combined, has demonstrated that age-related demyelination is associated with memory impairment, especially in dementia states (Kavroulakis et al., 2017). It has been described that AD patients present loss of myelin in specific regions of the brain, such as cortical GM and WM (Roher et al., 2002b), and large decrease in the number of $Olig2^+$ cells in the WM and GM of superior temporal gyrus and sensory motor cortex. In contrast, the WM of the mild frontal gyrus exhibit increased density of $Olig2^+$ cells (Behrendt et al., 2013). In the case of corpus callosum, it is also affected in AD brains and its impairment correlates with the progression and severity of the disease (Teipel et al., 2002).

Interestingly, several studies have observed WM disruption in asymptomatic individuals with increased risk for AD and in patients with mild cognitive impairment (MCI) (B. Parente et al., 2008; Bartzokis et al., 2006). Bartzokis and colleagues correlated age-related slow cognitive processing speed with myelin breakdown in late-myelinating WM areas of these subjects. Moreover, the development of a novel brain imaging approach allows evaluating more precisely the myelin content in the brain. In this sense, a recent exhaustive study of asymptomatic individuals with genetic risk factors for AD show that these individuals present brain alterations of myelin content in relation to well established AD markers in cerebrospinal fluid (CSF). Interestingly, they observed a strong association between myelin content reduction and soluble Aβ concentration in CSF. This

study also revealed that age-related changes in myelin are particularly observed in late-myelinating areas, as frontal WM and the genu of corpus callosum, corroborating the facts previously described (Dean et al., 2017). These results indicate that myelin have an important role in preclinical stages in AD, which may be related to the onset of the cognitive decline.

The underlying causes of oligodendrocyte and myelin dysfunction in AD have not been fully clarified. However, several studies propose Aβ as a candidate to promote WM dysfunction. In AD patients, increased levels of Aβ peptide have been correlated with brain regions exhibiting myelin abnormalities (Roher et al., 2002b), being these Aβ deposits mainly in late-myelinating areas (Bartzokis, Lu, & Mintz, 2007). Moreover, WM changes including demyelination, have been also documented in MCI and are potentially related to Aβ and tau pathology (Bartzokis et al., 2003; Dean et al., 2017; Dennis J Selkoe & Hardy, 2016). Specifically, focal demyelination is observed in plaque-associated myelinated axons from AD temporal cortex, whereas plaque-free cortical GM of human AD have no significant loss of myelin or oligodendrocyte density (Stanislaw Mitew et al., 2010).

In this sense, biochemical analysis of total myelin fraction in AD patients revealed increased $A\beta_{1-42}$ levels accompanied by a significant decrease in the amount of MBP, PLP and CNPase. In addition, myelin lipid content is also altered, observing a marked decrease in cholesterol levels, while total fatty acid content was increased (Roher et al., 2002a). Concretely, depending on the brain area MBP levels vary. While in AD frontal WM is significantly lower in comparison with MCI (D.-S. Wang et al., 2004), increased levels of MBP are observed in cortical GM of AD patients (Dennis J. Selkoe, Brown, Salazar, & Marchotta, 1981; Zhan et al., 2015a). Interestingly, in these AD patients the high ratio of degraded MBP over total MBP revealed a strong rate of MBP degradation (Zhan et al., 2015b). Increase of degraded MBP and myelin components as galactocerebroside is also observed within vesicles in periventricular WM of AD (Zhan et al., 2014), suggesting a high myelin damage. Furthermore, it has been described an increase in degraded MBP associated with autophagy specific markers (Zhan et al., 2015a). This findings are consistent with previous studies documenting myelin and lipid changes in GM and WM of

AD (Han, 2007; Han, M Holtzman, McKeel, Kelley, & Morris, 2002; Pernber, Blennow, Bogdanovic, Månsson, & Blomqvist, 2012). However, the mechanisms by which MBP levels are higher in AD remain unclear.

Surprisingly, it has recently been shown that MBP is able to bind to Aβ and inhibit its fibril formation, possibly playing a role in regulating its deposition and formation of senile plaques in parenchyma (Dean et al., 2017; Hoos, Ahmed, Smith, & Van Nostrand, 2009; Liao, Ahmed, Smith, & Van Nostrand, 2009).

5.1. Oligodendrocyte and amyloid β peptide.

In spite of the relevance that the white matter and myelin seem to have in AD pathology, only a few studies have analyzed the effect of Aβ peptide on oligodendrocytes in the context of this disorder. In fact, it has been described that oligodendrocytes express APP and therefore, are able to produce Aβ that may exacerbate the ongoing pathology (Skaper et al., 2009). Overall, previously reported *in vitro* studies have illustrated that various forms of Aβ peptide are able to induce toxicity on oligodendrocytes. As above mentioned, Aβ becomes toxic when it oligomerizes (McKee, Kowall, Schumacher, & Beal, 1998) and myelin can be directly damaged by oligomerized forms of the peptide (Xu et al., 2001).

Precisely, treatment of rat neonate-derived oligodendrocytes with 0.2-20 μM of $A\beta_{1-40}$ or $A\beta_{25-35}$ results in dose-dependent cell death, characterized by nuclear and cytoskeletal disintegration, DNA fragmentation, and mitochondrial dysfunction. In addition, cells treated with $A\beta_{25-35}$ for 24 h resulted in the breakdown and dissolution of oligodendrocyte processes and appearance of shrunken cell bodies (Xu et al., 2001). Moreover, the use of $A\beta_{25-35}$ at 10 μM induces ceramide-mediated apoptosis in oligodendrocytes (J.-T. Lee et al., 2004). Interestingly, *in vivo* experiments analyzing the effects of stereotaxic injection of $A\beta_{1-42}$ at high concentration (500 μM) in rat corpus callosum resulted in considerable axonal damage, and loss of myelin and mature oligodendrocytes (Jantaratnotai, Ryu, Kim, & McLarnon, 2003).

On the other hand, contradictory results have been reported when analyzing whether differentiation stage in the oligodendroglial linage plays a role in cell susceptibility. In this sense, after $A\beta_{1-42}$ treatment for 4 h both immature and mature oligodendrocyte cell population presented an increased abundance of cells with pyknotic nuclei (Desai et al., 2010). These data indicate that cultured oligodendrocytes exhibit a differentiation state-independent sensitivity to Aβ toxicity. However, two years later it was described that when using $A\beta_{1-42}$ 10 μM for 48 h the treatment promote cytotoxicity in mature oligodendrocytes, but not to OPCs (Horiuchi et al., 2012). In the same study, it was shown that the presence of 1 μM of Aβ peptide in the differentiation medium for 4 days reduces OPCs myelin sheath formation by inhibition of F-actin distribution. However, no changes were observed in the number of MBP^+ cells or in the expression of MBP and PLP (Horiuchi et al., 2012). Additionally, Aβ peptide may lead to increase caspase-3 expression and apoptotic cell death in progenitor and differentiated cells (Desai et al., 2010).

Hypothesis and Objectives

Hypothesis and Objectives

Oligodendrocytes are glial cells in charge of developing myelin sheaths in the central nervous system. The presence of oligodendrocyte progenitor cells and the generation of new mature oligodendrocytes in the adult brain contribute to myelin maintenance and regeneration. However, under pathological conditions, as in Alzheimer´s disease, it is observed a myelin and white matter decline that may be related to the cognitive impairment associated with the disorder. In addition to this, oligodendrocytes have been shown to be vulnerable to amyloid β peptide, one of the main hallmarks of Alzheimer´s disease. Therefore, we hypothesize that oligomeric amyloid β peptide directly modulates oligodendrocyte proliferation and differentiation, altering myelin maintenance and contributing to white matter impairment in the progression of Alzheimer´s disease.

To that end, the following specific objectives were designed:

Aim 1. To characterize the changes of myelin-related proteins expression triggered by oligomeric amyloid β peptide in primary oligodendrocyte culture and cerebellar organotypic slices.

Aim 2. To describe the molecular mechanisms underlying amyloid β oligomer-mediated changes in myelin basic protein synthesis in cultured oligodendrocytes.

Aim 3. To evaluate molecular and functional features of oligodendrocytes and myelin in a triple transgenic Alzheimer's disease mouse model.

Aim 4. To study myelin integrity at ultrastructural level in a triple transgenic mouse model of Alzheimer's disease.

Aim 5. To analyze myelin-related protein alterations in white matter and cerebrospinal fluid of Alzheimer's disease patients.

Experimental procedures

Experimental procedures

1. Animals.

All experimental procedures followed the European Directive 2010/63/EU, and were approved by the Ethic Committees of the University of the Basque Country UPV/EHU. Animals were housed in standard conditions with 12 h light cycle and with *ad libitum* access to food and water. All possible efforts were made to minimize animal suffering and the number of animals used.

Experiments were performed in Sprague Dawley rats and in the triple transgenic mouse model of Alzheimer´s disease (3xTg-AD), which harbours the Swedish mutation in the human amyloid precursor protein (APPSwe), presenilin knock-in mutation (PS1M146V), and tau P301L mutant transgene (tauP301L) (Oddo *et al*., 2003).

2. Cell Culture.

2.1. Optic nerve-derived primary oligodendrocyte culture.

Primary oligodendrocyte cultures were performed as previously described (Barres *et al*., 1992) with modifications (Matute, Sánchez-Gómez, Martínez-Millán, & Miledi, 1997). Optic nerves were extracted from P12 Sprague Dawley rats and meninges were removed in supplemented (2 µl/ml gentamicin, 1 mg/ml BSA and 2 mM glutamine) HBSS (Sigma-Aldrich) under magnifying scope. Then, optic nerves were cut in small pieces and enzymatically digested with collagenase (1.25 mg/ml; Sigma-Aldrich), trypsin (0.125%; Sigma-Aldrich) and deoxyribonuclease (0.004%; Sigma-Aldrich) for 40 min at 37°C. Afterwards, the enzymatic reaction was stopped by 10% FBS in DMEM (Gibco), centrifuged at 1000 rpm for 5 min and the pellet was resuspended in 1 ml of the same solution. By using needles (23, 25 and 27G), mechanical dissociation was performed and the resulting cell suspension was filtered through a 40 µm nylon mesh (Millipore).

Cell number was determined by tripan blue staining (Sigma-Aldrich) with 10 µl of sample and the rest of the cell suspension was centrifuged at 1000 rpm for 10 min. The obtained pellet was resuspended in chemically defined Sato medium, consisting of a supplemented (4.5 g/l glucose and 0.11 g/l sodium piruvate) DMEM base with several factors that favour oligodendrocyte survival and development (**Table 2**). Cells were plated (10^4-10^5 cells per well) on poly-D-Lysine-coated coverslips (12 or 14-mm-diameter) resting in 24-well plates and maintained at 37°C and 5% CO_2 in chemically defined Sato medium. Cultured oligodendrocytes were allowed to adhere for 24 h before corresponding treatments.

Table 2. Sato medium composition

Reagent	Concentration
Dulbecco's Modified Eagle Medium (DMEM)	Base medium
Insulin	5 µg/ml
Penicillin/Streptomycin	100 U/ml
BSA	1 mg/ml
L-Glutamine	2 mM
N-Acetyl L-Cystein	6.3 mg/ml
Ciliary neurotrophic factor (CNTF)	10 ng/ml
Neurotrophin 3 (NT-3)	1 ng/ml
Transferrin	100 µg/ml
Putrescine	16 ng/ml
Progesterone	60 ng/ml
Sodium selenite	40 ng/ml
Triiodotironine (T3)	30 ng/ml
L-Tyroxine (T4)	40 g/ml

2.2. Organotypic cerebellar slice culture.

Organotypic cerebellar slice culture were prepared from cerebellar sections of P5-P7 or P12 Sprague Dawley rat pups according to previously described procedures (Stoppini, Buchs, & Muller, 1991)(Dusart, Airaksinen, & Sotelo, 1997). Briefly, after decapitation, cerebella were extracted and cut into 350 µm parasagittal slices using a tissue chopper (McIlwain) and meninges were removed. Slices were transferred to 0.4 µm culture membranes inserts (Millipore), each containing three slices. Slices were maintained in 6-well plates for seven days in 50% basal medium with Earle´s salt (Life technologies), 25% Hank´s buffered salt solution (Life technologies), 25% inactivated horse serum (Life technologies), 5 mg/ml glucose (Panreac), 0,25 mM L-glutamine (Sigma-Aldrich) and Antibiotic-Antimycotic solution (100 units/ml of penicillin, 100 µg/ml of streptomycin and 25 µg/ml of amphotericin B, Life Technologies) at 37°C in a humidified atmosphere with 5% CO_2. Slices were kept in culture for 7 days before performing the experiments.

3. Human samples.

Patients gave informed consent to all clinical investigations, which were performed in accordance with the principles embodied in the Declaration of Helsinki.

3.1. Brain tissue.

Frozen samples and formalin-fixed paraffin-embedded sections from prefrontal cortex and hippocampus of 15 subject controls and 30 AD patients were obtained from the Neurological Tissue Bank Hospital Clinic-IDIBAPS Biobank (**Table 3**). AD samples were grouped by Braak and Braak (Braak & Braak, 1995) into AD-II, AD-III, AD-IV and AD-V-VI, and by CERAD classification (Mirra et al., 1991) into AD-A, AD-B and AD-C.

Table 3. Characteristics of controls and AD subjects, categorized as stages I to VI of Braak and Braak and A,B or C of CERAD criteria.

Case number	Ref. number	Braak stage NFT	CERAD Aβ	Gender	Age	Age (mean±S.D.M.)	Postmortem delay*	Regions analyzed
C1	1378	-	-	M	78	79.1±4.55	6:00	Cx
C2	1405	II	-	M	80		5:30	Hp
C3	1423	-	A	F	82		5:00	Cx and Hp
C4	1491	-	-	M	83		13:00	Cx
C5	1536	-	-	M	79		4:45	Cx and Hp
C6	1543	II	-	M	80		4:30	Hp
C7	1557	III	-	M	86		10:15	Cx and Hp
C8	1687	II	-	F	69		12:00	Cx and Hp
C9	1697	I-II	-	M	78		6:00	Hp
C10	1733	-	-	M	76		11:30	Cx and Hp
AD1	0575	II	-	F	86	76.83±7.50	13:30	Cx
AD2	1109	II	A	F	75		16:20	Cx
AD3	1357	II	-	F	79		10:30	Cx
AD4	1468	II	-	M	64		10:00	Cx
AD5	754	III	B	M	87		2:30	Cx
AD6	1022	III	B	M	71		10:30	Cx
AD7	1144	III	A	M	73		4:20	Cx
AD8	1759	III	-	M	74		9:00	Cx
AD9	774	IV	B	M	75		10:00	Cx
AD10	849	IV	B	M	70		5:00	Cx
AD11	948	IV	B	M	79		5:30	Cx
AD12	1255	IV	C	M	89		7:00	Cx
AD13	1230	V	C	M	79	76.5±1.95	4:15	Cx
AD14	1286	V	C	M	79		5:00	Cx and Hp
AD15	1622	V	C	M	76		5:00	Cx
AD16	1198	VI	C	F	77		5:00	Cx and Hp
AD17	1392	VI	C	M	77		5:00	Cx and Hp
AD18	1445	VI	C	F	74		6:30	Cx and Hp
AD19	1456	VI	C	F	74		3:30	Cx and Hp
AD20	1585	VI	C	F	74		6:30	Cx and Hp
AD21	1637	VI	C	M	78		7:00	Cx and Hp
AD22	1645	VI	C	F	77		5:30	Cx and Hp

*Time elapsed between death and sample extraction.

Cx, frontal cortex; Hp, hippocampus.

3.2. Cerebrospinal fluid samples.

Cerebrospinal fluid samples from 26 individuals per group with subjective cognitive impairment (SCI), mild cognitive impairment (MCI) and established AD were kindly provided by Prof. Angel Cedazo Minguez (Karolinska Institutet, Stockholm, Sweden).

4. Preparation of $A\beta_{1-42}$ oligomers.

$A\beta_{1-42}$ oligomers were prepared as reported previously (Dahlgren et al., 2002). Briefly, $A\beta_{1-42}$ (ABX) was initially dissolved to 1 mM in hexafluoroisopropanol (Sigma-Aldrich) and separated into aliquots in sterile microcentrifuge tubes. Hexafluoroisopropanol was totally removed under vacuum in a speed vac system and the peptide film was stored desiccated at -80°C. For the aggregation protocol, the peptide was first resuspended in dry DMSO (Sigma-Aldrich) to a concentration of 5 mM, and Hams F-12 (PromoCell) was added to bring the peptide to a final concentration of 100 µM and incubated at 4°C for 24 h. The preparation was then centrifuged at 14,000 g for 10 min at 4°C to remove insoluble aggregates and the supernatants containing soluble $A\beta_{1-42}$ were transferred to clean tubes and stored at 4°C.

5. Protein extract preparation and detection by western blot.

5.1. Oligodendrocyte protein preparation.

After each treatment, cultured oligodendrocytes were washed in cold 0.1 M phosphate buffered saline (PBS) twice and cells were scraped in 40 µl of sample buffer (62.5 mM Tris pH 6.8, 10% glycerol, 2% SDS, 0.002% bromophenol blue and 5.7% β-mercaptoethanol in dH_2O) per treatment (2 wells/treatment and 80,000 cells/well). All this process was performed on ice to enhance the lysis process and avoid protein degradation. After that, samples were boiled at 95°C for 10 min.

5.2. Organotypic slice protein extract preparation.

After 7 days in culture, cerebellar slices were exposed $A\beta_{1-42}$ oligomers for 48h. Then, each slice was resuspended in 80 µl of sample buffer and then, samples were boiled at 95°C for 10 min.

5.3. Protein preparation from animal tissue and human samples.

Mice were anesthetized with isofluorane (Schering-Plough) and optic nerve, corpus callosum and hippocampus were extracted, placed on dry ice and stored at -80ºC.

Animal and human tissue samples were resuspended in 200 µl of RIPA buffer (50 mM Tris pH 7.5, 150 mM NaCl, 0.5% sodium deoxycholate, 0.1% SDS, 1% NP-40 in 0.1 M PBS) supplemented with protease inhibitor cocktails (Roche), and were homogenized with a douncer. Afterwards, they were sonicated for 25 cycles at 80% amplitude (Labsonic M, Sartorius), centrifuged for 10 min, at 1,200 rpm and 4°C, and then supernatants were collected. Total protein content was quantified through Bradford assay (Bio-Rad). Protein extracts from tissues (10 µg per sample) and from CSF samples (11.25 µl) were analyzed by western blot.

5.4. Western blotting.

Protein samples were separated by SDS-PAGE in 3-8% Tris-Acetate and 4-20% Tris-Glycine polyacrylamide gels (Bio-Rad), according to the molecular weight of proteins. Electrophoresis was conducted in a Tris-Tricine buffer (100 mM Tris, 100 mM Tricine, 0.1 SDS% in dH_2O, pH 8.3) or in a Tris-Glycine buffer (25 mM Tris, 192 mM glycine, 0.1 % SDS in dH_2O, pH 8.3) by using the Criterion cell system (Bio-Rad). Gels were transferred to nitrocellulose membrane by using a Trans-Blot® Turbo™ Transfer System (Bio-Rad).

Membranes were blocked for 1 h at room temperature (RT) in blocking solution, which consisted of TBST buffer (20 mM Tris, 137 mM NaCl, 0.1% Tween-20 in dH_2O, pH 7.6) supplemented with either 5% bovine serum albumin (Sigma-Aldrich) or with 5%

PhosphoBlocker Blocking Reagent (Cell Biolabs) for phosphorylated protein detection. Then, they were incubated with specific primary antibodies in the same solution overnight at 4°C with gentle shaking. Afterwards, membranes were washed three times with TBST and incubated in blocking solution containing secondary antibody conjugated to horseradish peroxidase (HRP) for 1h at RT.

Immunoreactive proteins were detected by using enhanced electrochemical luminescence (Super Signal West Dura or Femto, Pierce) and ChemiDoc XRS Imaging System (Bio-Rad). Band signal was quantified by densitometry using Image Lab software (Bio-Rad) and were normalized and provided as the mean ± S.E.M of at least three independent experiments.

Membranes were stripped of antibodies using Restore Western Blot Stripping Buffer (Thermo Fisher Scientific) for 10 min at RT. Membranes were then washed in TBST for three times, blocked and incubated with other primary antibodies.

5.5. Antibodies for Western blot.

The following antibodies were used for protein detection, mouse anti-MBP (1:1000; Biolegend), rabbit anti-Src [pY^{418}] (pSFK; 1:500; Invitrogen), rabbit-Fyn (1:500; Santa Cruz), mouse anti-LCK (1:500; BD Bioscience), mouse anti-SRC (1:1000; Cell Signaling), rabbit anti-integrin β1 (1:1000; Cell Signaling), rabbit anti-phospho-CREB (1:1000; Cell Signaling), rabbit anti-CREB (1:1000; Cell Signaling), mouse anti-CNPase (1:500; Sigma Aldrich), hamster anti-CD81 (1:1000; Bio-Rad), mouse anti-CD63 (1:1000; BD Biosciences), rabbit anti-PDGFR-α (1:200; Santa Cruz), rabbit anti-neurofilament heavy polipeptide (1:1000; Abcam), mouse anti-neurofilament H non- phosphorylated, SMI-32 (1:1000; Biolegend), rabbit anti-PDGFr (1:200; Santa Cruz), rabbit anti-Olig2 (1:1000; Millipore), mouse anti-GAPDH (1:2000; Millipore) and rabbit anti-β-actin (1:5000; Sigma-Aldrich).

6. Immunoprecipitation.

Immunoprecipitation assays were performed to determine which specific protein of SFK family kinase was involved in Aβ-triggered signaling in cultured oligodendrocytes. First, 50 µl of protein A-sepharose beads (Abcam) were incubated with 1 µg of antibody (anti-Fyn, 1:100, Santa Cruz Biotechnology; or anti-phosphotyrosine, 1:500, Sigma-Aldrich) for 4 h at 4°C. Then, samples were centrifuged at 2,000 g for 2 min and supernatants discarded to keep the antibody-beads complex. After that, cells were treated with Aβ at 200 nM for 15 min and were washed with cold 0.1M PBS twice. Cells were scraped in 500 µl RIPA buffer supplemented with protease and phosphate inhibitor cocktail (ThermoFisher Scientific) and were incubated with the antibody-protein A beads complex previously obtained, in RIPA buffer with protease and phosphate inhibitors overnight at 4°C under rotary agitation. The lysate-antibody-beads complex was centrifuged at 4,000 rpm and washed with RIPA buffer for three times followed by other centrifugation to obtain the immunocomplex. Finally, protein elution was carried out in 2x sample buffer after boiling the sample at 95°C for 5 min and centrifugated at 12,000g for 1 min. After elution, proteins were analyzed by Western blot.

7. Inhibitors.

The following inhibitors were used: PP2 (10 µM; Selleckchem), RGDS (100 µM; Tocris), hamster anti- rat CD29 (0.25 mg/ml; BD Pharmingen), hamster IgM (0.25 mg/ml; BD Pharmingen), Ryanodine (50 µM; Sigma), AIP (1 µM, Anaspec), Nifedipine (10 µM; Sigma-Aldrich), Memantine (10 µM; Tocris), AP-5 (100 µM; Tocris), MK801 (50 µM; Tocris), α-bungarotoxin (10 nM; Tocris), CNQX (30 µM; Tocris)

8. Immunofluorescence.

8.1. Cultured oligodendrocytes.

Cells were fixed in 4% paraformaldehyde (PFA) for 10 min, washed in 0.1 M PBS for three times and then stored at 4°C. Cells were permeabilized and blocked in 4% normal

goat serum (NGS, Palex), 0.1% Triton X-100 (Sigma-Aldrich) in 0.1 M PBS (blocking buffer) for 1 h and incubated with primary antibodies overnight at 4°C. Then, cells were washed in 0.1% Triton X-100 in 0.1 M PBS (washing buffer) and incubated with the fluorochrome-conjugated antibodies in blocking solution for 1 h at RT. After that, cells were washed and incubated with DAPI (4 µg/ml, Sigma-Aldrich) for 10 min. Then, cells were washed again twice and coverslips were mounted on glass slides with Fluoromount-G mounting medium (SouthernBiotech).

8.2. Animal tissue and organotypic slices.

Mice were anesthetized with avertine and perfused with 30 ml of PB followed by 30 ml of 4% PFA in 0.4 M PB. The brains were extracted and postfixed with the same fixative solution for 4 h at RT, placed in 30% sucrose in 0.1 M PBS at 4°C and then kept in cryoprotectant solution (30% ethylene glycol, 30% glycerol and 10% PB 0.4 M in dH_2O) at -20°C. The tissue was cut using a Leica VT 1200S vibrating blade microtome (Leica microsystems) to obtain coronal 40 µm-thick sections. In the case of cerebellar organotypic slices, they were fixed in 4% PFA for 40 min at RT followed by washing in 0.1 M PBS for three times. Slices were then taken off the membranes and kept in 0.1 M PBS at 4°C. Free-floating vibratome sections or cerebellar slices were permeabilized and blocked with 0.1% Triton X-100, 4% NGS in 0.1 M PBS for 1 h at RT and were incubated with primary antibodies overnight at 4°C with gently shaken. Slices were then washed three times in 0.1% Triton X-100 in 0.1 M PBS and were incubated with blocking solution containing fluorochrome-conjugated antibodies and DAPI (4 µg/ml) at RT for 1 h. After that, slices were washed for three times in 0.1% Triton X-100 in 0.1 M PBS and were mounted on glass slides with Fluoromount-G mounting medium.

For labeling specific oligodendrocyte lineage markers, an antigen retrieval protocol was performed. Free-floating sections were incubated in R-Universal epitope recovery buffer for heat-induced antigen unmasking (Aptum) for 5 min at 95°C followed by 5 min at RT and then were washed in cold 0.1 M PBS twice. Then, slices were permeabilized in 100% ethanol at -20°C for 10 min and washed in 0.1 M PBS for three times. Sections were permeabilized and blocked in 10% NGS, 0.1% Triton X-100 in 0.1 M PBS for 30 min at RT

and incubated with specific antibodies overnight at 4°C with gentle shaking. Afterwards, slices were washed three times in 0.1 M PBS and incubated with blocking solution containing fluorochrome-conjugated antibodies and DAPI (4 µg/ml) at RT for 1 h. Slices were washed for three times in 0.1 M PBS and were mounted on glass slides with Fluoromount-G mounting medium. For PDGFr-α labeling antigen retrieval protocol was not utilized and Triton X-100 was only used for permeabilization.

8.3. Paraffin-embedded human sections.

Paraffin-embedded human sections (10 µm-thick) were deparaffinized and rehydrated by immersing in xylene followed by incubations with alcohol content solutions (100°, 96° and 75° diluted in dH_2O) and TBS (100 mM Tris-Cl, 300mM NaCl, 4.25 mM $MgCl_2$ and 1.5 mM $CaCl_2$; ph 7.4) for 10 min in each solution. Samples were then boiled in Universal Buffer (Aptum) by using antigen retriever for 20 min and allowed to cool down during 30 min to promote epitope unmasking. After section retrieval, samples were washed in TBS for three times and blocked in 4% BSA in TBS for 1 h at RT and were incubated with the primary antibody mouse anti-MBP (BioLeyend, 1:400) in blocking solution overnight at RT. Then, samples were washed in TBS twice and incubated in blocking solution containing DAPI (4 µg/ml) and the fluorochrome-conjugated antibody, donkey anti-mouse Alexa 647 (Jackson Immunoresearch) for 1 h at RT. After that, samples were washed in TBS and treated with Autofluorescence Eliminator Reagent according to the manufacturer's instructions (Millipore) to reduce lipofuscin-like autofluorescence. Finally, sections were washed and mounted with Fluoromount-G mounting medium.

8.4. Analysis of fluorescence immunostaining images.

Fluorescence immunostaining for cultured oligodendrocytes and cerebellar organotypic slices were examined under a fluorescence microscope (Cell observer. Z1, Zeiss) and the micrographs were taken using the Axiocam digital camera. For oligodendrocyte differentiation analysis in cultured oligodendrocytes, 20-50 fields (524.19 x 524.19 µm per field) per coverslip were counted. To measure MBP occupied area, 43-52

cells were analyzed per condition. The number of oligodendrocyte cells and the area occupied by each MBP^+ cell were determined with the Image J software.

Fluorescence immunostaining images from mouse and human tissue were taken with Leica TCS SP8 laser scanning microscope using 20X objective (human samples), 40X or 63X oil-immersion objectives (mouse experiments) to generate z-stack projections. Images analysis was carried out in 2-3 sections per subject. For MBP and NFL fluorescence intensity analysis, images were taken with the same setting for all experiment and mean value along the stack profile was quantified with LAS AF Lite software (Leica).

To analyze oligodendrocyte stages, 4 random areas of corpus callosum and 2 of DG and CA3 were used per section, containing each ROI 91.39 x 79.81 µm. For nodes of Ranvier abundance analysis, 5 random areas of 44.97 x 43.85 µm per section were counted and to measure node of Ranvier length 50 nodes per animal were randomly selected and analyzed.

8.5. Antibodies.

The following primary antibodies were used: mouse anti-MBP (1:500, BioLegend), mouse-CNPase (1:500, Sigma-Aldrich), rat anti-O4 (1:500, kindly supplied by Dr. Chistine Thompson, University of Glasgow), mouse anti-Olig2 (1:200, Millipore), rabbit anti-NFL (1:200, Cell Signaling), mouse anti-CC1 (1:200, Millipore), rat anti-PDGFr-α (1:300, BD Pharmingen), mouse anti-Nav1.6 (1:250, Alomone Labs) and rabbit anti-Caspr (1:500, Neuromab). Secondary antibodies coupled to Alexa 488, Alexa 594, Texas Red and Alexa 647 were purchased from Invitrogen, Millipore or Jackson Immunoresearch. (1:500).

9. RNA extraction and quantification.

9.1. RNA isolation.

Cultured oligodendrocytes were treated with Aβ at 1 µM for 24 h and total RNA was isolated using PureLink RNA Mini Kit (Ambion) according to manufacturer's instructions.

Cerebellar organotypic slices were treated with Aβ at 200 nM for 48 h and previous to the RNA extraction, organotypic slices were homogenized with 18 and 21G needles and 3 slices were used per condition. RNA was extracted by using the same kit. RNA concentration and integrity was measured by a spectrophotometer Nano Drop™ 2000 (ThermoFisher Scientific).

9.2. Retrotranscription and Real Time-Polymerase Chain Reaction (RT-qPCR).

RNA was reverse transcribed in a 20 µl reaction containing 5X Buffer (Invitrogen), 0.1 M DTT, random primers (Promega), dNTPs (Invitrogen), RNase OUT and Superscript II retrotranscriptase (Invitrogen) following manufacturer's instructions in a Veriti Thermal Cycler (Applied Biosystems). Resulting cDNA samples were diluted in sterile Mili-Q H_2O.

Quantitative Polymerase Chain Reaction (qPCR) was performed in 11.8 µl RNAse-free water (Promega), 5.2 µl SsoFast Evagreen Supermix (Bio-Rad), 1.35 µl properly diluted primers and 0.5 µl cDNA sample. All reaction were performed by triplicates and carried out in cDNA CFX96 Touch Real-Time PCR Detection System (Bio-Rad). Amplification reactions were optimized and 3 min 95°C, and 40 cycles of 10 s at 95°C, 30 s at 60°C. Primers were designed and synthesized by Quiagen or designed to amplify exon-exon junctions using Primer Express (Applied Biosystems) and PrimerBlast (NIH). PCR product specificity was checked by melting curves. Data were normalized to a normalization factor obtained in geNorm Software through the analysis of the expression of four housekeeping genes. Primer sequences are detailed in the **Table 4**.

Table 4. Sequences of primers used in this study.

Gene	Gene Bank No.	Amplicon size	Sequence
Reference genes			
Hprt1	NM_012583	85	Fwd ATGGACTGATTATGGACAGGACTGA Rev ACACAGAGGGCCACAATGTG
B2m	NM_012512.2	84	Fwd ACCGAGACCGATGTATATGCTT Rev TTACATGTCTCGGTCCCAGG
Cyclophilin A	NM_017101.1	114	Fwd CAAAGTTCCAAAGACAGCAGAAAA Rev CCACCCTGGCACATGAATC
GAPDH	NM_017008.4	80	Fwd GAAGGTCGGTGTCAACGGATTT Rev CAATGTCCACTTTGTCACAAGAGA
Cerebellar organotypic			
MBP	NM_001025291.1	114	Fwd CATCCCAAGGAAAGGGGAGAG Rev TGTGAGCCGATTTATAGTCGGAA
CNPase	NM_012809.2	86	Fwd CGCCCACTCATCATGAGCAC Rev CCTGAGGATGACATTTTTCTGAAGA
PDGFr-α	NM_012802.1	146	Fwd TTATGCCTTGAAAGCCACGTC Rev TCACCTCTCCAGGGTAAGTCCA
Cultured oligodendrocytes			
Itgb1	Purchased from QIAGEN Cat no: QT0018756		
Itgb3	Purchased from QIAGEN Cat no: QT02376241		
Itgb5	Purchased from QIAGEN Cat no: QT01570828		
Itgb8	Purchased from QIAGEN Cat no: QT01790313		
Itga5	Purchased from QIAGEN Cat no: QT02344944		
Itga6	Purchased from QIAGEN Cat no: QT01600158		

10. Gene silencing by lentivirus infection.

After 4 h of cell seeding, oligodendrocytes were transduced with lentivirus containing non-targeting or Itgb1-targeting shRNA (12 µl/ml; Santa Cruz Biotechnology) for 24 h in SATO culture media. On the next day, cells were selected by puromycin (1 µg/ml) for 12 h and were treated in fresh media with Aβ at 1 µM for 24 h and subsequently protein extraction was carried out.

11. mRNA fluorescent *in situ* hybridization (FISH).

After Aβ exposure (1 µM, 24 h) cultured oligodendrocytes were fixed in 4% PFA for 10 min, followed by dehydration with ethanol content solutions (50°, 70° and 100° diluted in dH_2O) and storage at -20°C. Coverslips were rehydrated by incubations with decreasing concentration of alcohol solution and detection of MBP mRNA was carried out using the QuantiGene ViewRNA ISH Cell Assay (Affymetrix Panomics) according to manufacturer's instructions with minor modifications. FISH assay was performed in presence and absence of protease treatment. Background fluorescence was established with a negative probe (BACILLUS S. dapB dihydopicolinate reductase L38424, VF1-11712) and MBP detection was performed using a specific MBP-targeting probe (NM_017026 VC1-15251), both purchased from Affymetrix Panomics. Following *in situ* hybridization, non protease-treated-cells were blocked with 3 mg/ml BSA, 100 mM glycine and 0.25% Triton X-100 in 0.1M PBS and incubated with an anti-MBP antibody (1:500, Bioleyend) overnignt at 4℃. After several washes cells were incubated with secondary antibody for 1h and were washed in 0.1M PBS. Finally, coverslips were incubated with DAPI in 0.1M PBS for 10 min, were washed for three times and mounted with Fluoromount-G mounting medium.

11.1. Image analysis.

Images were acquired with a fluorescence microscope (Cell observer. Z1, Zeiss) using 40X oil-immersion objective. Image acquisition was determined automatically on a random field and pixel intensities were within the linear range, being these settings applied for all samples. Image analysis of experiments carried out with protease was performed using the Radial Profile Angle plugin of Image J software and values of normalized integrated intensity were obtained. Concerning the experiments carried without protease, Image J macro was designed and used to automate the analysis. MBP labeling allowed us to select the cell occupied area and to determine RNA fluorescence intensity only inside cells. In both cases, concentric circles at 10 µm intervals emerging from the center of the cell nucleus were generated and MBP mRNA and protein fluorescence signals were quantified. Results were expressed as fluorescence intensity in

nuclear area (round zone with a 20-µm radius from the nucleus) and periphery (from 20 µm to the end of the cell) (**Figure 11**).

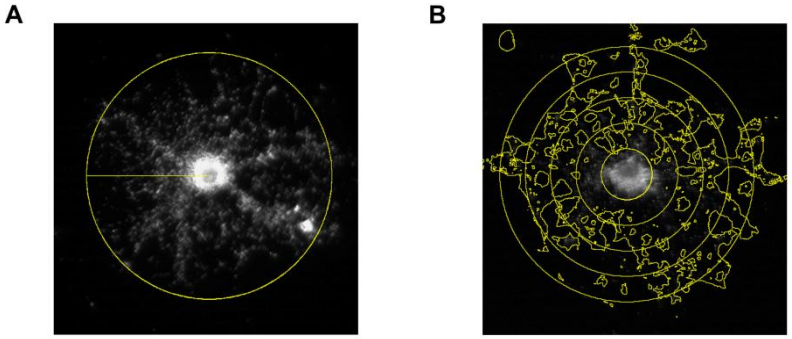

Figure 11. Image analysis of FISH experiments. (A) Fluorescence intensity of MBP mRNA was measured by using Radial Profile Angle when protease was applied to samples. **(B)** In the absence of protease, MBP protein labeling was used to determine by threshold the area occupied by cell and then, MBP mRNA fluorescence intensity values were acquired.

12. Lysophosphatidylcholine (LPC)-induced organotypic demyelination.

LPC-induced demyelination experiments were performed in cerebellar organotypic slices from P12 rats (Birgbauer, Rao, & Webb, 2004). Slices were cultured 7 days *in vitro* and treated 15-16 h with LPC 0.5 mg/ml. After that, slices were exposed to Aβ 200 nM for 48h and were fixed or proteins were extracted 1 and 6 days after Aβ treatment exposure. PP2 inhibitor (10 µM, Selleckchem) was added 30 min before Aβ insult.

13. Cell viability assay.

Cultured oligodendrocyte cell viability was measured 24 h after Aβ treatment by Calcein-AM method (Life Technologies). Cells were incubated with Calcein-AM at 1 µM and 37°C for 30 min in fresh culture medium and then, were washed in pre-warmed 0.1 M PBS for three times. Emitted fluorescence was measured by a Synergy HT (Biotek) spectrophotometer using excitation wavelength at 485 nm and emission at 528 nm. Values were represented as means or a percentage of cell survival in comparison with control cells (control cells, 100% viability).

14. Extracellular vesicles (EVs) purification.

Cultured oligodendrocytes were exposed to Aβ 1 µM for 24 h (520,000 cells/condition) and then, oligodendrocyte protein extraction was performed (as described previously) and culture media collected to EVs isolation (Royo et al., 2017). Culture supernatants were centrifuged at 1,500 g for 10 min to remove lifted cells and cellular debris. The resultant supernatant was centrifuged at 10,000 g for 30 min and the pellet was resuspended in 15 µl 0.1M PBS (microvesicle enriched fraction). Next, the supernatant was ultra-centrifuged at 100,000 g and 250,000 g for 75 min, and the final pellets containig small EVs and exosomes were resuspended in 15 µl 0.1M PBS. For analysis, the pellets were resuspended in non-reducing 1X sample Buffer (without β-mercaptoethanol) and boiled at 37°C for 5 min, at 65°C for 10 min and at 95°C for 15 min, followed by centrifugation at 13,000 rpm for 15 min. Cell lysates and the supernatants were analyzed by Western blot.

15. Electrophisiology.

After being anesthetized with isofluorane, brain and optic nerves from 18-month old mice WT and 3xTg-AD were rapidly removed and optic nerves were placed in an interface perfusion chamber with artificial cerebrospinal fluid (aCSF) containing 126 mM NaCl, 3 mM KCl, 2 mM $CaCl_2$, 1.25 mM NaH_2PO_4, 2 mM $MgSO_4$, 26 mM $NaHCO_3$, 10 mM d-glucose in H_2O bubbled with a mixture of 95% O_2 and 5% CO_2 at 37ºC at least for 30 min before evoked compound potentials (CAPs) recordings. Then, propagated compound action potentials (CAPs) were evoked using a bipolar silver electrode placed on one end of the optic nerve. Stimulus pulse (30 µs duration delivered every 15 s) strength was adjusted to evoke supramaximal stimulation (Tekkök & Goldberg, 2001). CAPs were recorded at 37°C with a suction electrode connected at the opposite end of the optic nerve and back-filled with aCSF. Optic nerves were perfused (1 mL/min) with aCSF continuously bubbled with 95% O2/5% CO2. The signal was amplified 5.0003 and filtered at 30 kHz and control CAPs were recorded for 30 min. TTX (1 µM) was applied at the end of the experiment to obtain the stimulus artifact, which was subtracted from all the records.

For corpus callosum recordings, brain was cut in coronal 400 µm-thick sections by using a Leica VT 1200S vibrating blade microtome (Leica microsystems) in a cutting solution at 0°C (215 mM sucrose, 2.5 mM KCl, 26 mM $NaHCO_3$, 1.6 mM NaH_2PO_4, 1 mM $CaCl_2$, 4 mM $MgCl_2$, 4 mM $MgSO_4$, 20 mM glucose and 1.3 mM ascorbic acid). Then, after preincubation with low calcium solution for 30 min at 32°C, sections were incubated in aCFS containing 124 mM NaCl, 2.5 mM KCl, 10 mM glucose, 25 mM $NaHCO_3$, 1.25 mM NaH_2PO_4, 2.5 mM $CaCl_2$, and 1.3 mM $MgCl_2$ for 30 min. Then, evoked compound potentials (CAPs) were recorded with a pulled borosilicate glass pipette (≈ 1 MΩ resistance) by electrically stimulating corpus callosum with a bipolar tungsten wire electrode, stimulation intensities ranging from 30 to 3000 µA. After this, input-output curves were generated by recording the amplitudes of N1 and N2 as a function of stimulation intensity. Using the difference between the corresponding trough and a straight line drawn between the adjacent peaks, the amplitude of each response was obtained. Three to five responses were averaged for each measurement. Conduction velocity values for myelinated and unmyelinated fibers were calculated as the slope of a straight line fitted through a plot of the distance between the recording and stimulating electrodes versus the response latency (time to N1 or N2, respectively). Peak amplitudes and onset latencies were calculated using custom written routines in pCLAMP 10.0 (Molecular Devises)

16. Electron microscopy.

Mice were anesthetized with avertine and perfused with 4% formaldehyde, 2.5% glutaraldehyde (Electron Microscopy Sciences) and 0.5% NaCl in phosphate buffer, pH 7.4, according to Karlsson and Schultz (1965) as described (Möbius et al., 2010). The brains were extracted and postfixed with the same fixative solution overnight at 4ºC and fixative solution was replace by 1% formaldehyde. The tissue was sagitally cut using a Leica VT 1200S vibrating blade microtome (Leica microsystems) to obtain 200 µm-thick sections, regions of interest were punched and incubated in 2% OsO_4 for 4h followed by dehydration with ethanol and propylenoxide. Afterwards, selected tissue areas were embedded in EPON (Serva) for 24h at 60ºC and EPON-block was trimmed using a Leica EM TRIM (Leica). Ultrathin sections (50 nm thickness) were obtained by Leica Ultracut S

ultramicrotome (Leica) and contrasted with 4% uranyl acetate for 30 min followed by lead citrate for 6 min (according to Reynolds, 1963). EM pictures were taken with a Zeiss EM900 electron microscope (Zeiss). Images obtained for *g*-ratio value and inner tongue area quantification were taken at 12,000x, while those for myelin sheath degenerative events counting were taken at 7,000x magnification.

16.1. Analysis of electron microscopy images.

Electron microscopy images of rostral and caudal corpus callosum were taken from randomly selected fields, being 10 images per animal studied (3 animals per group). Electron micrographs were analyzed using NIH ImageJ software. Axonal, inner tongue (including axon) and myelinated fiber areas were measured and used to determine their diameter. The *g*-ratio value was quantified as the fraction of axonal (A) plus inner tongue (I) diameter divided by whole fiber diameter (M). To randomly select fibers, grids were overlaid onto images, and all axons intersecting with grid lines cross were counted (150-300 myelinated axons per animal). Inner tongue area was also measured as inner tongue area (including axon) minus axonal area.

For myelin sheath degenerative events analysis, 10 micrographs per animal were analyzed to determine the abundance of four types of events: myelin fibers with enlarged inner tongue, dense cytoplasm, empty fiber or myelin degenerated. All myelinated axons were counted to calculate the percentage of each degenerative event per total myelinated axons.

17. Statistical analysis.

All data were expressed as mean ± S.E.M. Statistical analysis were performed using absolute values and GraphPad Prism software (GraphPad Software) applying the corresponding statistical treatment for each experiment, as mentioned in figure captions.

Results

Results

1. $A\beta_{1-42}$ oligomers promote oligodendrocyte maturation *in vitro*.

We investigated the role of Aβ oligomers on oligodendrocyte differentiation and maturation *in vitro*. For that, we used primary cultured oligodendrocytes derived from rat optic nerves. During development, these cells present several morphologies and express stage-specific antigenic markers, being oligodendrocyte transcription factor (Olig2) a marker that is maintained throughout oligodendroglial lineage. Late progenitors are characterized by having simple processes and are recognized by the O4 antibody (Bansal *et al*., 1992). When the myelin protein 2',3'-Cyclic-nucleotide 3'-phophodiesterase (CNPase) begin to be expressed and cells adopt a more rounded morphology then they are considered immature cells. Finally, immature cells differentiate into mature myelin-producing oligodendrocytes which have more complex branched processes and express myelin basic protein (MBP) (**Figure 12A**). In order to evaluate the differentiation state of cells after Aβ exposure, we performed immunocytochemistry for the abovementioned stage-specific cell surface antigens and we analyzed the number of cells present in the different stages of development. Unexpectedly, after Aβ 200 nM treatment for 24 h, the number of $O4^+$ and MBP+ cells per mm^2 (49.07 ± 9.36 and 10.91 ± 1.48, respectively) increased significantly compared to non-treated cells (33.48 ± 8.16 and 5.95 ± 0.76, respectively), while the number of immature cells ($CNPase^+$) remained unchanged (**Figure 12B, C**). Morphological complexity of oligodendrocytes is proportional to their differentiation state, so to further analyze morphological differences the MBP-occupied area was quantified. Aβ induced an increase in mature cell size indicating a more mature morphological state (**Figure 12D, E**). These results suggest that Aβ induces changes in the development stages, promoting oligodendrocyte differentiation and maturation.

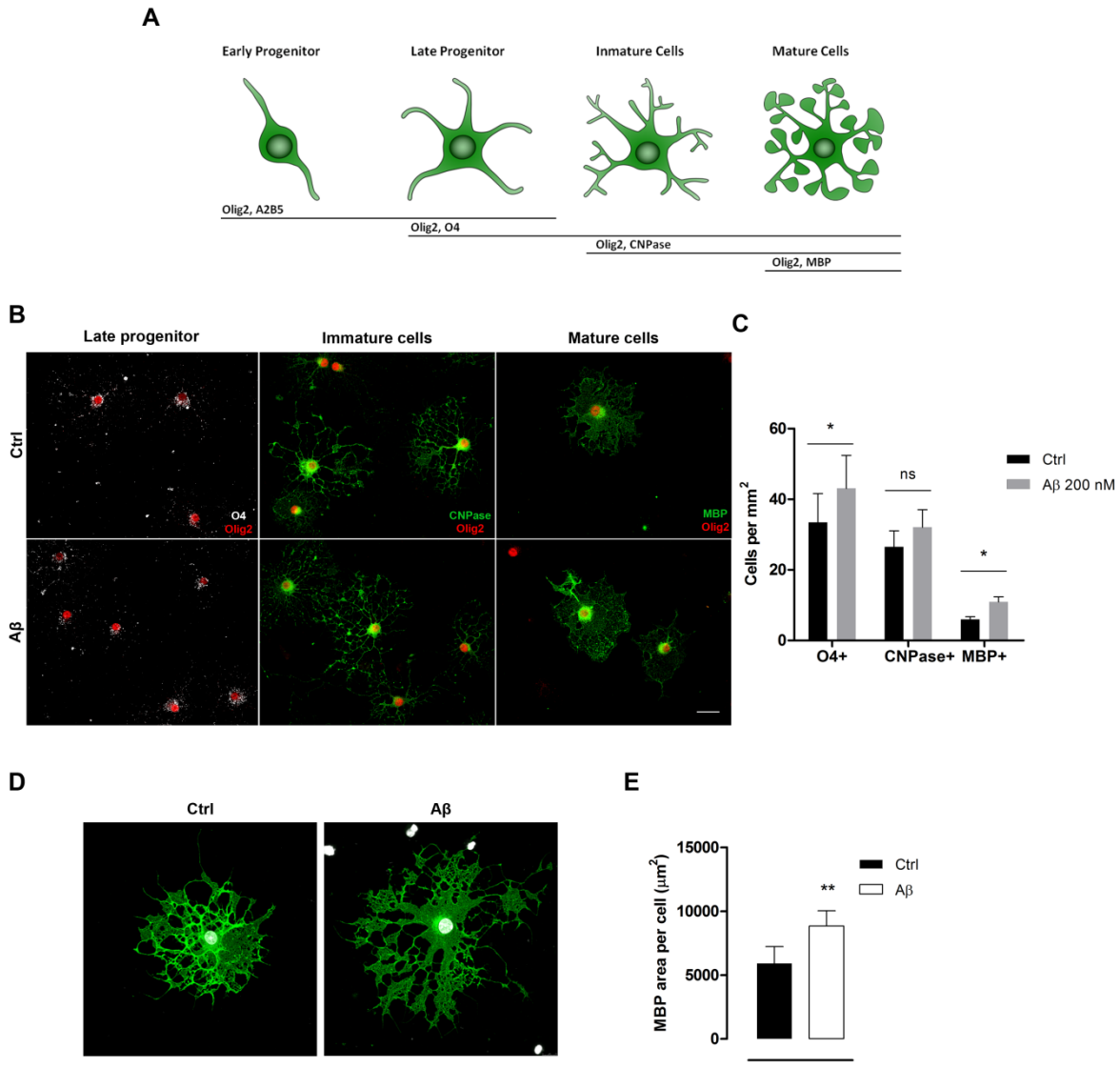

Figure 12. $A\beta_{1-42}$ oligomers promote oligodendrocyte maturation *in vitro*. (A) Diagram of oligodendrocyte development stages. **(B)** Representative micrographs showing double-immunostaining for oligodendrocyte linage marker Olig2, and O4 (red, late progenitors), CNPase (green, immature oligodendrocytes), or MBP (green, mature oligodendrocytes). Cells were treated with Aβ at 200 nM for 24 h. **(C)** The number of specific positive cells was counted after treatment (n=4 cultures). **(D)** Representative immunofluorescence image for MBP staining. **(E)** Analysis of the occupied area by the MBP staining per cell (n=4 cultures.). Data are represented as means ± S.E.M. *p<0.05, **p<0.01 compared to non-treated cells; paired Student´s t test. Scale bar, 25 µm.

2. $A\beta_{1-42}$ oligomers upregulate MBP expression in oligodendrocyte peripheral areas.

To further study the Aβ-induced oligodendrocyte maturation, we analyzed by western blot the expression levels of MBP after Aβ treatment at different concentrations (200 nM and 1 μM) for 24 h (**Figure 13A**). Oligodendrocyte total protein extracts showed increased levels of MBP protein after Aβ exposure (2.78 ± 0.22 and 2.98 ± 0.27 after 200 nM and 1 μM treatment, respectively) compared to non-treated cells (2.28 ± 0.16). However, no significant differences were found between the two Aβ doses used (**Figure 13B**). Regarding the preparation of $A\beta_{1-42}$ oligomers used in this study, it was mainly composed by Aβ oligomers (trimers and tetramers) but also by large fibrils and monomer forms (Lambert *et al*., 1998; Chromy *et al*., 2003; Alberdi *et al*., 2013). Thus, to asses which molecular form of Aβ was responsible for inducing oligodendrocyte maturation, we treated cultured oligodendrocyte with monomeric, oligomeric or fibrillar Aβ preparation using specific protocols as abovementioned (**Figure 13C**). MBP levels were only increased by Aβ oligomeric forms compared to control cells, while Aβ fibrils and monomers did not have effect on MBP expression (**Figure 13D**). Moreover, to assess if Aβ could modulate MBP distribution along the cell, we analyzed this protein levels around the nucleus and at peripheral areas (**Figure 13E**). We tested the effect of Aβ oligomers in cultured oligodendrocytes at 1 μM for 24 h and found that Aβ increased the MBP fluorescence intensity only at peripheral areas, while no significant differences were found at nuclear area (**Figure 13F**). These results indicated that oligomeric Aβ forms upregulate oligodendrocyte MBP expression but only at peripheral areas.

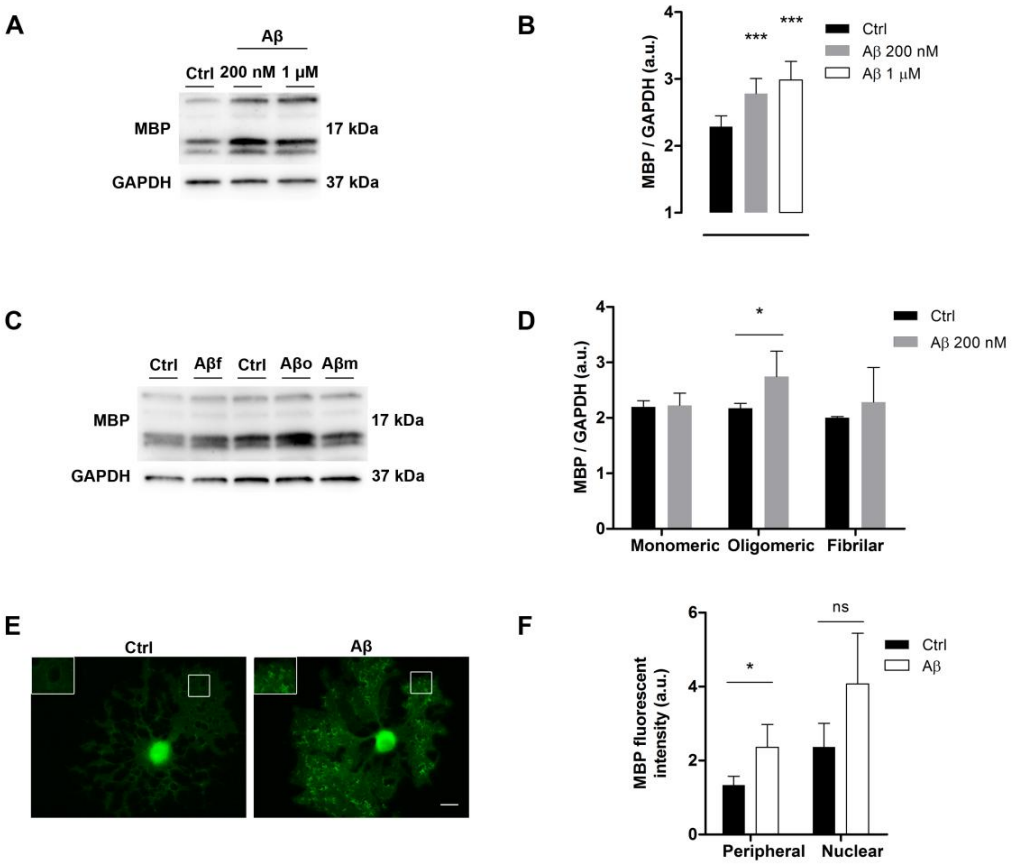

Figure 13. MBP levels are increased after $A\beta_{1-42}$ oligomers treatment in peripheral areas of cultured oligodendrocytes. (A) Western blotting of MBP expression in total cell extracts treated with Aβ 200 nM or 1 μM for 24 h. **(B)** Analysis of MBP levels is shown (n=10-20 cultures). **(C, D)** Cells were treated with fibrillar, monomeric or oligomeric Aβ peptide at 1 μM for 24 h, and MBP levels of total extracts were quantified and detected by western blot (n=3 cultures). Data are represented as means ± S.E.M. of optical density values normalized to corresponding GAPDH. **(E)** Representative MBP-immunolabeled micrographs of Aβ-treated (Aβ) or non-treated (Ctrl) cultured oligodendrocytes. **(F)** Analysis of MBP fluorescence intensity at nuclear and peripheral areas is shown (n=4 cultures). Scale bar, 10 μm. Data are represented as means ± S.E.M. *p<0.05, ***p<0.001 compared to non-treated cells; paired Student´s t test.

3. $A\beta_{1-42}$ oligomers increase MBP mRNA local translation at peripheral areas in primary cultured oligodendrocytes.

Since Aβ oligomers induce MBP upregulation in oligodendrocytes, we asked whether the increase of MBP levels may be due to transcriptional or translational regulation leaded by Aβ oligomers. First, to examine the possible role of Aβ as a transcriptional

regulator, we measured MBP mRNA by quantitative FISH in the presence of protease. The prehybridization proteolytic digestion step with protease would allow us to unmask all mRNA molecules present in the cell and then enhance its detection. We focused on two cell areas, around the nucleus and the cell periphery, and found that Aβ treatment (1 µM for 24 h) did not change MBP mRNA fluorescence intensity in either areas comparing to non-treated cells (**Figure 14A, B**). Therefore, Aβ oligomers do not regulate MBP mRNA synthesis and transport in oligodendrocytes.

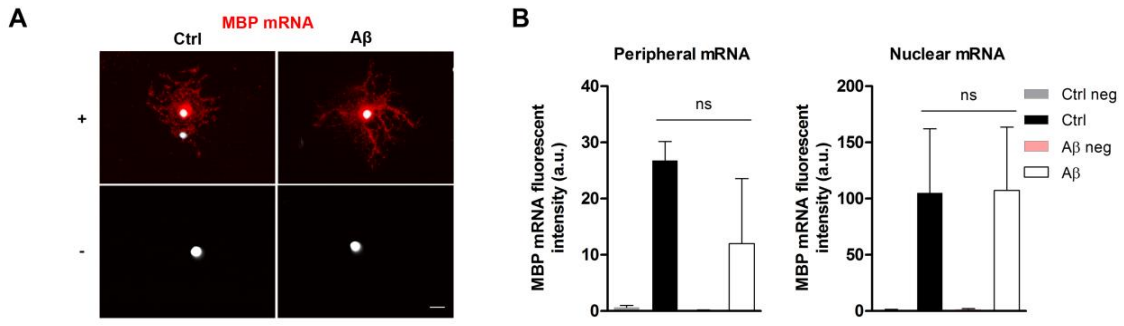

Figure 14. $A\beta_{1-42}$ oligomers do not regulate MBP mRNA synthesis and transport in oligodendrocytes. Cells were treated with Aβ 1 µM for 24 h and MBP mRNA levels were measured by quantitative FISH in the presence of protease. **(A)** Representative epifluorescence images of cultured oligodendrocytes showing MBP positive probe (top panels) and non-targeting probe (bottom panels). **(B)** Quantitative analysis of MBP mRNA fluorescence intensity of peripheral and nuclear areas (n=3 cultures). Scale bar, 10 µm. Data are represented as means ± S.E.M.; repeated-measures ANOVA followed by Bonferroni posttest.

In addition, MBP mRNA has been shown to be transported from the nucleus to oligodendrocyte processes (Trapp et al., 1987; Ainger et al., 1993, 1997) and there, at cell periphery is translated. Next, we quantified the MBP mRNA levels after Aβ exposure (1 µM, 24h) by quantitative FISH in the absence of protease to analyze whether MBP mRNA might be locally translated in oligodendrocytes. Labeling of MBP mRNA showed that Aβ promoted an increase in the amount of unmasked MBP mRNA in oligodendrocyte peripheral areas compared to non-treated cells, while no differences were found in nuclear areas (**Figure 15A, B**). These results strongly suggest that Aβ increase MBP mRNA local translation in cultured oligodendrocytes.

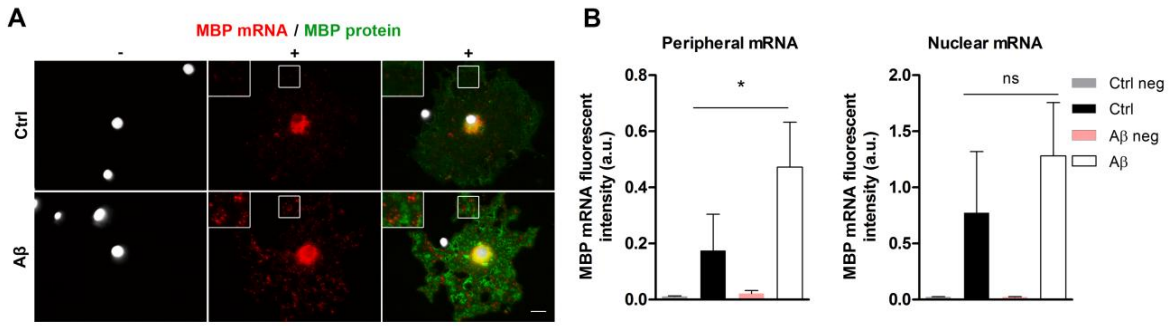

Figure 15. $A\beta_{1-42}$ oligomers increase MBP mRNA local translation in primary oligodendrocyte cultures. (A) Representative micrographs of oligodendrocytes treated with Aβ 1 µM for 24 h. MBP mRNA was visualized by fluorescent probe (red) and MBP protein expression by immunolabeling (green). **(B)** MBP mRNA levels of peripheral and nuclear areas were measured by quantitative FISH (n=3 cultures). Scale bar, 10 µm. Data are represented as means ± S.E.M.; repeated-measures ANOVA followed by Bonferroni posttest.

4. $A\beta_{1-42}$ upregulates MBP expression via integrin β1/Fyn/CREB signaling pathway.

4.1. Integrin β1 mediates Aβ-induced MBP upregulation through Fyn activation in oligodendrocytes.

In order to investigate the molecular pathway underlying Aβ-induced MBP upregulation, we focused on a key protein involved in myelin synthesis, the tyrosine-protein kinase Fyn. In oligodendrocytes, Fyn is the predominant Src family kinase (SFK) that is upregulated during oligodendrocyte differentiation and has been related to myelination process (Kramer-Albers and White, 2011). Moreover, Fyn activation results in local MBP synthesis by regulation of mRNA translation (White *et al*., 2008; Wake *et al*., 2011). To analyze the putative role of Fyn during Aβ-induced MBP increase, we first examined the SFK phosphorylation after exposure of oligodendrocytes to Aβ 200 nM. Cell treatment for 5 and 15 min increased SFK phosphorylation (pSFK) to 145.8 ± 14.65 and 138.20 ± 17.84, respectively, with respect to control levels, 100% (**Figure 16A**). By immunoprecipitation assays, we demonstrated that Fyn was the specific member of SFKs which was activated by Aβ, since kinase Fyn was the one phosphorylated upon Aβ exposure (**Figure 16B**). In contrast, Aβ did not promote tyrosine phosphorylation of LCK and SRC, two members of SFK (**Figure 16C**). We also observed that using PP2, a SFK

inhibitor, Fyn phosphorylation after Aβ treatment for 5 and 15 min was significantly blocked (**Figure 16C, D**).

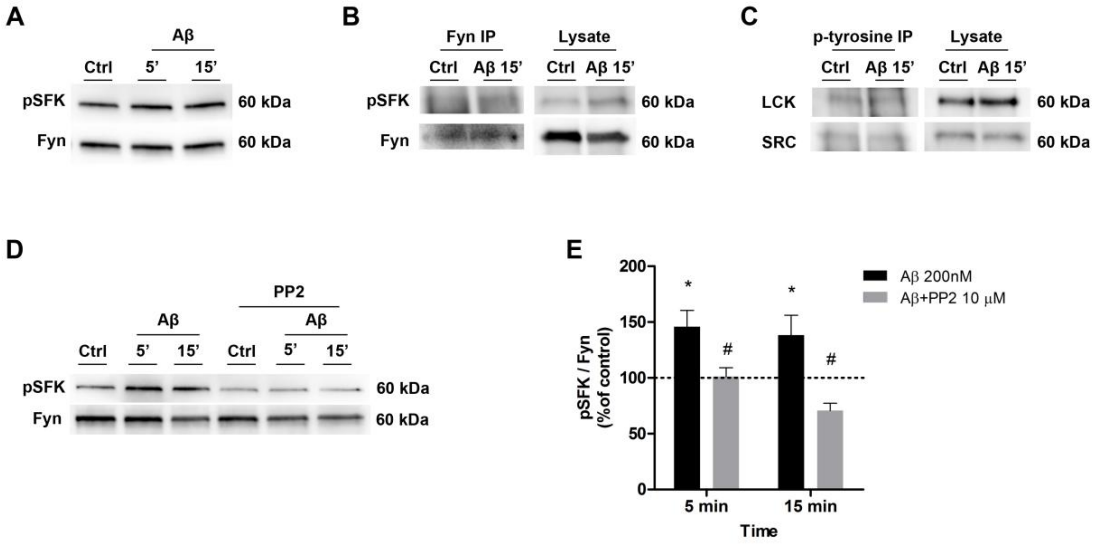

Figure 16. $A\beta_{1-42}$ oligomers induce Fyn kinase activation in cultured oligodendrocytes. (A) Cells were exposed to Aβ 200 nM for 5 or 15 min, and phosphorylation of Src family kinases was examined (pSFK) by western blot. **(B)** Immunoprecipitation (IP) of cells treated with Aβ 200 nM for 15 min was performed with anti-Fyn, followed by immunoblotting with anti-pSFK. **(C)** Western blotting of LCK and SRC in cells immunoprecipitated with phospho-tyrosine antibody after Aβ exposure (Aβ 200 nM for 5 min). Total cell lysates were immunoblotted with the previous antibodies. **(D, E)** Total protein samples were extracted 5 and 15 min after Aβ treatment in the presence or absence of PP2, a SFK inhibitor (30 min), and Fyn phosphorylation was analyzed by western blot (n=5). Data are represented as means ± S.E.M. of optical density values normalized to corresponding Fyn. *p<0.05, compared to non-treated cells; #p<0.05 compared to Aβ alone; paired Student´s t test.

Next, the involvement of a receptor mediating Aβ-induced Fyn activation was studied. One possible candidate for this process could be integrin β1 (Itgb1). It has been shown that in astrocytes Itgb1 activity is modulated by Aβ, promoting astrogliosis (Wyssenbach *et al*, 2016). Moreover, Itgb1 stimulation increases Fyn activity (Lisbeth Schmidt Laursen, Chan, & ffrench-Constant, 2009) and enhances MBP expression of oligodendrocytes (Lisbeth S Laursen, Chan, & Ffrench-Constant, 2011). Thus, to determine if integrin receptors mediate Fyn activation triggered by Aβ, first expression of several integrins subunits was analyzed by RT-qPCR and western blot in isolated

oligodendrocytes. Aβ-induced mRNA expression increase of Itgb1 and integrin β8 (Itgb8), being 139.1 ± 25.42 and 118.8 ± 7.83 vs. 100% of control, respectively (**Figure 17A**). Since Itgb8 has been described to be strongly expressed during oligodendrocyte maturation (Milner *et al*., 1997), and our results show that Aβ induces this maturation, it is difficult to attribute the Itgb8 increase as a direct response to Aβ. Therefore, we focused on studying Itgb1 protein expression and found that its levels were increased up to 56.62% over control after Aβ exposure at 200 nM and 1 µM for 24 h (**Figure 17B, C**).

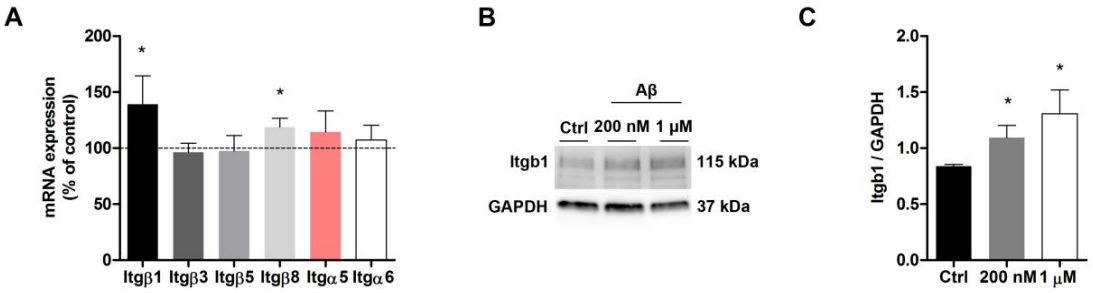

Figure 17. Integrin β1 receptor expression is upregulated after $A\beta_{1-42}$ oligomers treatment. (A) Integrin receptor subunit expression levels in cells treated with Aβ (200 nM, 24 h) were analyzed by RT-qPCR (n=3-4). **(B)** Western blotting of Itbβ1 receptor in total protein extracts of cells treated with Aβ 200 nM or 1 µM for 24 h. **(C)** Quantification of Itbβ1 protein levels is shown (n=3). Data are represented as means ± S.E.M. of optical density values normalized to corresponding GAPDH. *p<0.05, compared to non-treated cells; paired Student´s t test.

Next, we investigated whether this receptor contributes to Fyn activation by Aβ. Western blot analysis showed that Aβ 200 nM for 5 and 15 min induced Fyn phosphorylation (145.8% ± 14.62 and 138.2% ± 17.84 vs. 100% of control, respectively) that was attenuated by preincubation with RGDS peptide (111.8 ± 3.77% and 117 ± 11.92% vs. 100% of control, respectively) which contains the integrin binding sequence and inhibits its function (Wright & Meyer., 1985). Similarly, treatment with an antibody αCD29 (that specifically binds Itgb1) (Mendrick & Kelly., 1993) blocked Fyn phosphorylation (109.5 ± 12.22% and 77.66 ± 14.05%) (**Figure 18A, B**). Overall, these results showed that Itgb1 mediates Aβ-modulated Fyn phosphorylation.

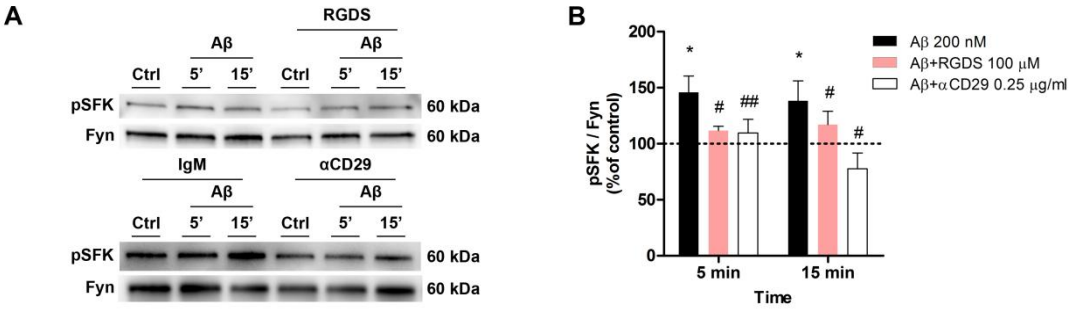

Figure 18. Inhibition of integrin β1 receptor reduces Aβ-induced Fyn phosphorylation in oligodendrocytes. Cells were exposed to Aβ 200 nM for 5 and 15 min after preincubation with RGDS (100 μM, integrin inhibitor) or CD29 antibody (0.25 μg/ml, specific integrin β1 inhibitor). **(A)** Total protein samples were extracted and Fyn levels were detected by western blot. **(B)** Histogram of Fyn levels analysis is shown (n=4). Data are represented as means ± S.E.M. of optical density values normalized to corresponding Fyn. *p<0.05, compared to non-treated cells; #p<0.05, ##p<0.01 compared to Aβ alone; paired Student´s t test.

To investigate the function of integrin receptors and Fyn activation on Aβ-mediated oligodendrocyte differentiation, we analyzed MBP expression of cultured oligodendrocytes by western blot. MBP-increased levels induced by Aβ (200 nM for 24 h) were completely blocked after preincubation with RGDS or PP2 (**Figure 19A, B**), suggesting that Fyn and integrin receptors were involved in Aβ-modulated MBP expression. Then, to confirm the physiological role of the specific receptor Itgb1 in the Aβ-induced MBP upregulation, a lentiviral vector was used to silence Itgb1 and then MBP levels were analyzed. First, we verified that treatment of cells with Itgb1 shRNA lentivirus blocked Itgb1 expression (66.67 ± 7.94% of control and 53.24 ± 7.57% of Aβ) compared to cells treated with control shRNA lentivirus (100%) (**Figure 19C, E**). Moreover, cells with Itgb1 silenced and treated with Aβ did not exhibit increased MBP levels compared to non-silencing cells (**Figure 19C, D**). In summary, these results showed that Aβ treatment increase MBP expression through Itgb1 and Fyn activation in cultured oligodendrocytes.

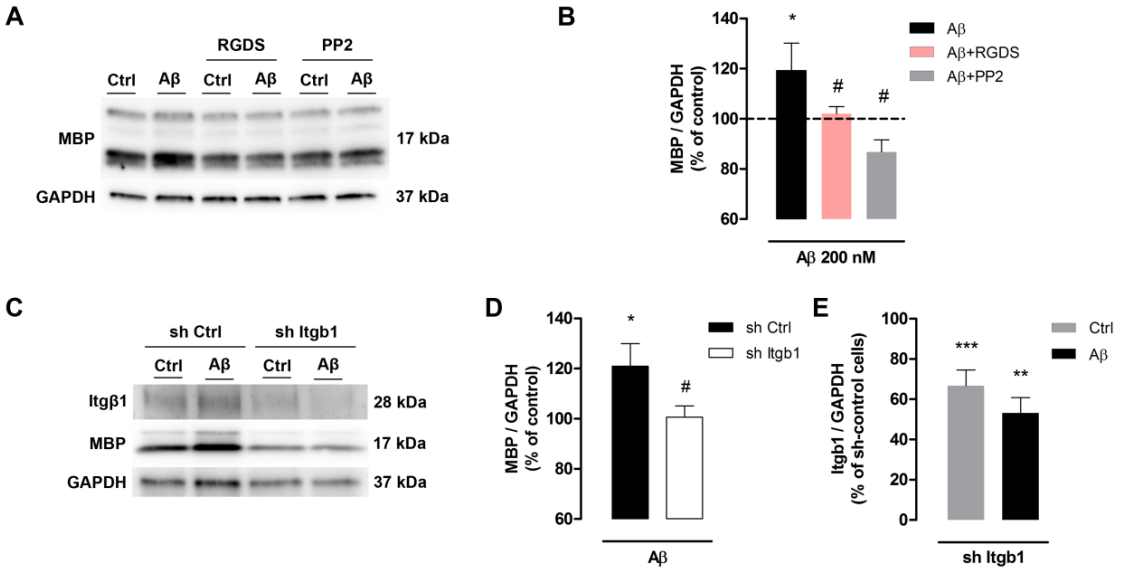

Figure 19. Integrin β1 receptor mediates Aβ-induced MBP upregulation in cultured oligodendrocytes. (A, B) Western blot and quantification analysis of MBP expression in total protein extracts of cells treated with Aβ 200 nM for 24 h and preincubated with RGDS (integrin inhibitor) or PP2 (SFK inhibitor) (n=4 cultures). **(C)** Oligodendrocytes were transfected with control shRNA (sh ctrl) or shRNA targeting Itgb1 (sh Itgb1) for 24 h. After transfection, cells were treated with Aβ for 24 h, and MBP and Itbβ1 protein levels were measured by western blot. **(D)** Histograms show MBP and **(E)** Itgb1 levels after silencing (n=4 cultures). Data are represented as means ± S.E.M. of optical density values normalized to GAPDH. *p<0.05, **p<0.01, ***p<0.001 compared to non-treated cells; #p<0.05 compared to sh ctrl; paired Student´s t test.

4.2. Aβ-induced ER calcium release activates CREB and upregulates MBP expression in cultured oligodendrocytes.

The transcription factor cAMP response element-binding protein (CREB) plays an important role in myelination by stimulating MBP expression and inducing oligodendrocyte proliferation and maturation (Sato-Bigbee and DeVries, 1996; Afshari *et al*., 2001; Meffre *et al*., 2015). To further investigate the possible involvement of CREB in the signaling cascade triggered by Aβ, we analyzed CREB activation after Aβ exposure. CREB was strongly phosphorylated after Aβ 200nM insults for 5 and 15 min. Besides, the Aβ-induced CREB activation was significantly attenuated by RGDS and PP2 preincubation (**Figure 20A, B**), these data indicate that Aβ promoted CREB phosphorylation through integrin receptors and Fyn activation.

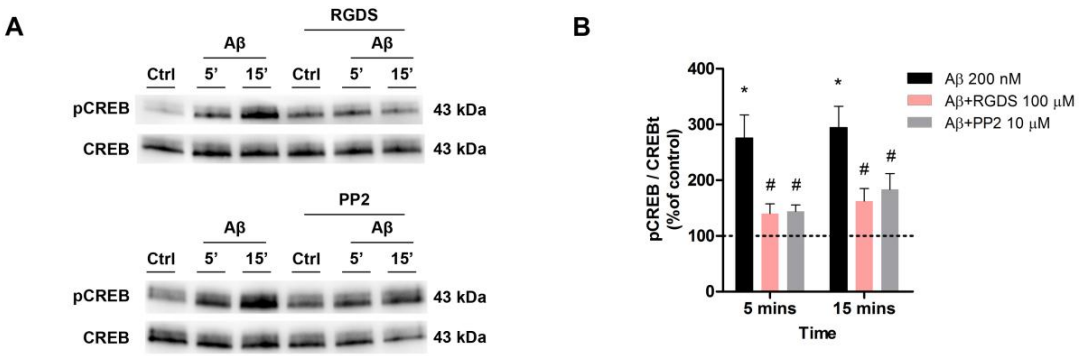

Figure 20. Blockade of integrin receptor and SFK activation attenuates Aβ-induced CREB phosphorylation. **(A, B)** Cells were preincubated with RGDS (integrin inhibitor) or PP2 (SFK inhibitor) and treated with Aβ 200 nM for 5 or 15 min. CREB activation was detected by western blot. Analysis of CREB phosphorylation after Aβ treatment is shown (n=4-6). Data are represented as means ± S.E.M. of optical density values normalized to total CREB. *p<0.05, compared to non-treated cells; #p<0.05 compared to Aβ alone; paired Student´s t test.

CREB can be activated by Ca^{2+} signaling through Ca^{2+}/calmodulin-dependent protein kinase (CAMK) activation. Moreover, Aβ has been related to produce Ca^{2+} homeostasis impairment in neurons (Hashimoto et al., 2003) and astrocytes (Abramov *et al*., 2003; Alberdi *et al*., 2013). Thus, we asked whether Aβ stimuli triggered CREB phosphorylation by increasing Ca^{2+} flux in oligodendrocytes. For that, we treated cultured oligodendrocytes with Aβ 200 nM and preincubated with PP2 and ryanodine (blocker of endoplasmic reticulum ryanodine receptor). By using fluorometric measurements, it was observed an increase in intracellular Ca^{2+} concentration in response to Aβ, which was blocked after PP2 and ryanodine treatment (**Figure 21A**). Moreover, western blot analysis showed that Aβ-induced CREB activation was blocked by using ryanodine and AIP (CAMKII blocker) inhibitors (**Figure 21B, C**). Overall, these results indicate that Aβ activates Fyn through Itgb1, leading a Ca^{2+}-dependent CREB activation.

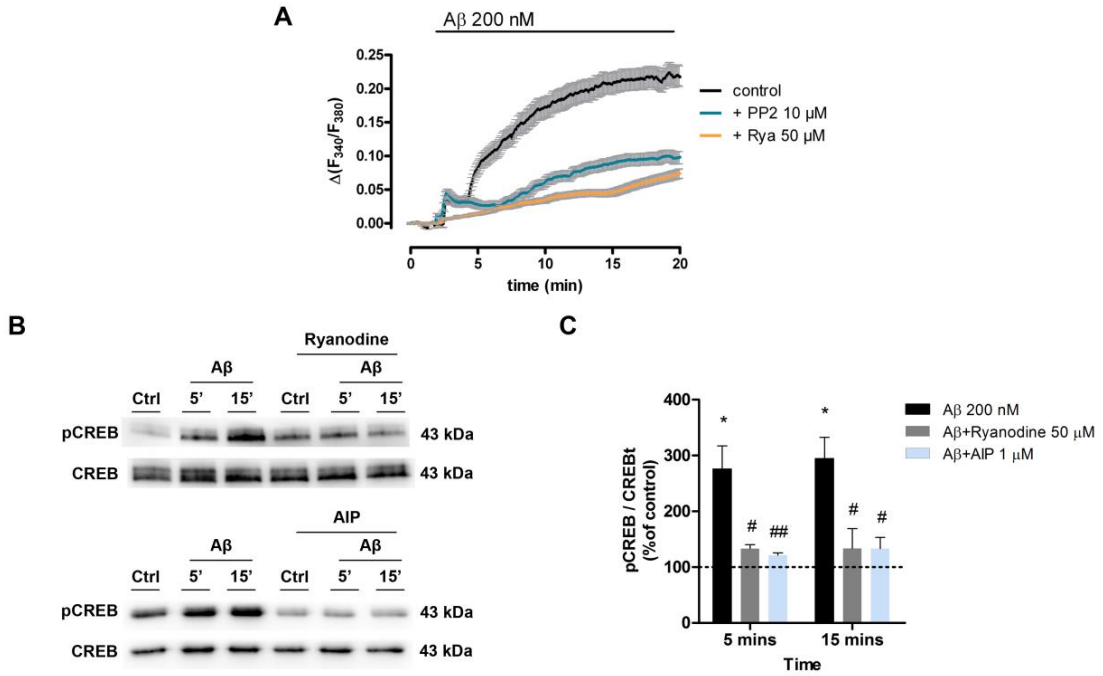

Figure 21. $A\beta_{1-42}$ oligomers induce CREB activation through Ca^{2+} release from the endoplasmic reticulum. **(A)** Cells, loaded with Fura 2-AM, were preincubated with PP2 (SFK inhibitor) or ryanodine (ryanodine receptor blocker) and exposed to Aβ 200 nM. Intracellular Ca^{2+} was measured by microfluorimetry. **(B)** Western blot of phospho-CREB in total protein extracts of cells treated with Aβ 200 nM for 5 or 15 min, and preincubated with ryanodine and AIP (CaMKII inhibitor). **(C)** Quantification of phospho-CREB levels is shown (n=3). Data are represented as means ± S.E.M. of optical density values normalized to total CREB. *p<0.05 compared to non-treated cells; #p<0.05 and ##p<0.01 compared to Aβ alone; paired Student´s t test.

Finally, we determined whether Ca^{2+} release from endoplasmic reticulum (ER) induced by Aβ would contribute to the MBP upregulation. Thus, we preincubated oligodendrocyte cultures with ryanodine and AIP and then treated with Aβ at 200 nM for 24 h. Western blot analysis showed that increase of MBP levels induced by Aβ were blocked by addition of ryanodine receptor and CAMKII inhibitors (**Figure 22A, B**). These data suggest that ER Ca^{2+} release induced by Aβ upregulates MBP expression in oligodendrocytes.

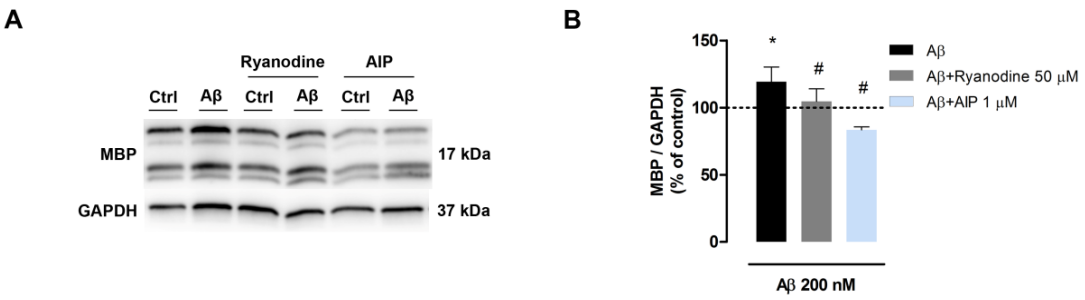

Figure 22. Endoplasmic reticulum Ca^{2+} release promotes Aβ-induced MBP upregulation. (A) Oligodendrocytes, incubated with ryanodine (ryanodine receptor blocker) or AIP (CaMKII inhibitor), were treated with Aβ 200 nM for 24 h and. MBP expression levels in total protein samples were detected by western blot. **(B)** Quantification of MBP levels obtained by western blot (n=3-4 cultures). Data are represented as means ± S.E.M. of optical density values normalized to GAPDH. *p<0.05 compared to non-treated cells; #p<0.05 compared to Aβ alone; paired Student´s t test.

In summary, these results demonstrate that Aβ acts directly on oligodendrocytes to trigger MBP upregulation. Specifically, Aβ activates kinase Fyn through Itgb1, followed by ER Ca^{2+}-dependent CREB activation, resulting in MBP expression increment (**Figure 23**).

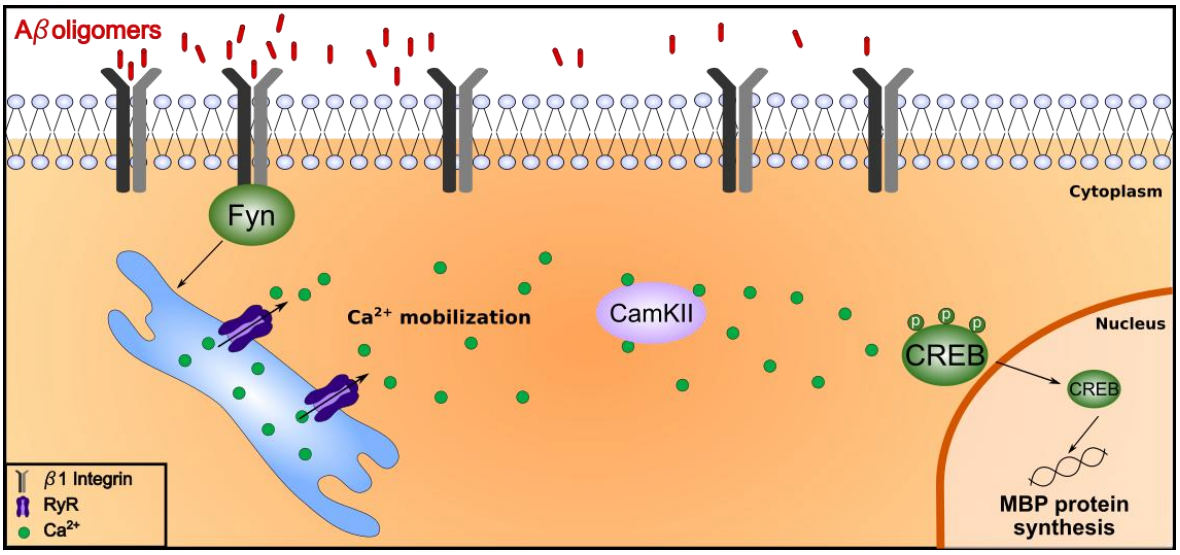

Figure 23. Aβ-signaling pathway underlying MBP upregulation. Model diagram of the signaling cascade activated by Aβ oligomers in oligodendrocytes.

5. $A\beta_{1-42}$ oligomers stimulate extracellular vesicles release containing MBP and CNPase in oligodendrocyte culture.

It has been shown that oligodendrocytes are able to release extracellular vesicles (EVs) which carry myelin-related proteins as MBP (Krämer-Albers et al., 2007). Since we observed an Aβ-induced MBP overexpression, we asked whether Aβ could stimulate the secretion of EVs containing myelin proteins. For this purpose, primary cultured oligodendrocytes were treated with Aβ 1 μM for 24 h and EVs were isolated from culture media by differential centrifugation, finally obtaining microvesicle- (10,000 g) or exosome-enriched fractions (100,000 and 250,000 g) (**Figure 24A**). The western blot analysis showed that MBP and CNPase levels were significantly increased in microvesicle-enriched pellet obtained from supernatants of Aβ-treated cells. In addition, CNPase expression was also detected in 100,000 g pellets and it was observed a 98.11% increase in CNPase amount after Aβ treatment as compared to supernatants of control cells, while MBP was not detectable in this EVs fraction. No MBP and CNPase levels were found in 250,000 g supernatants (**Figure 24B, C**). Consistently, after Aβ treatment we observed higher levels of exosomal marker proteins CD81 and CD63, in 10,000, 100,000 and 250,000 g pellets (**Figure 24D, E**), indicating that more EVs were secreted. Thus, these results demonstrate that Aβ promote oligodendrocyte secretion of EVs containing myelin proteins.

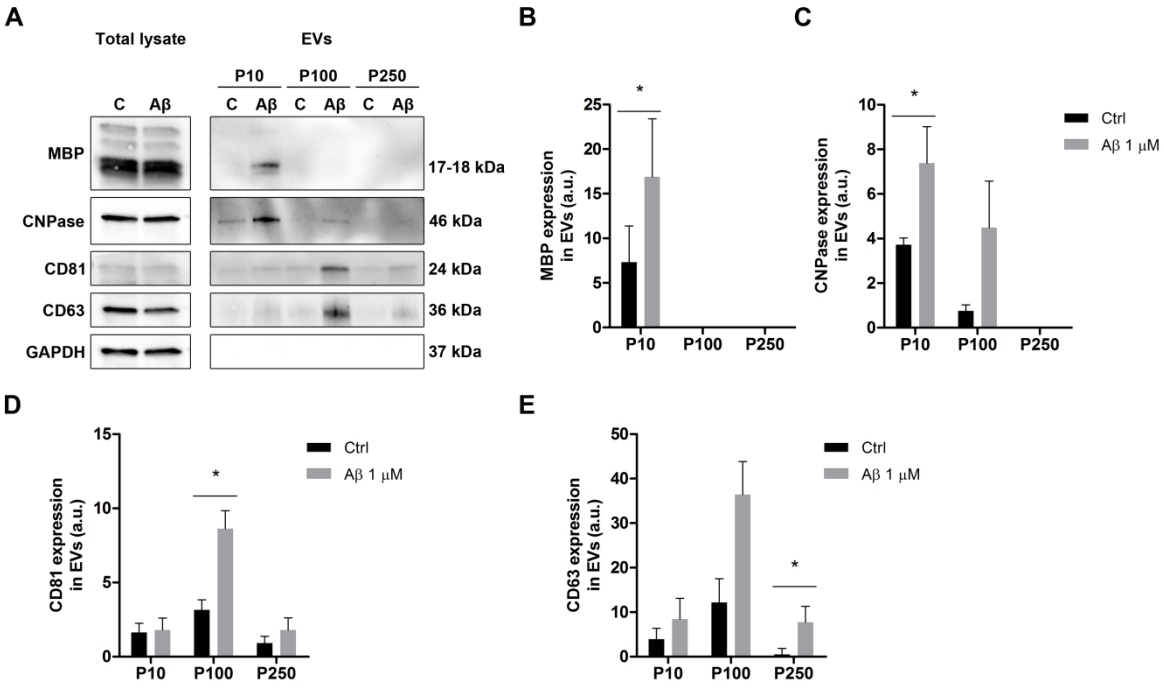

Figure 24. Aβ stimulates cultured oligodendrocyte EVs release containing MBP and CNPase. (A) Western blot of MBP, CNPase, CD81, CD63 and GAPDH in total cell lysate and EVs pelleted by differential centrifugation from culture media of cultured oligodendrocytes treated with Aβ (1 μM, 24 h) **(B-E)** Quantification of these protein levels obtained by western blot (n=4). Data are represented as means ± S.E.M. *p<0.05 compared to non-treated cells; paired Student´s t test.

6. $A\beta_{1-42}$ oligomers enhance oligodendrocyte survival *in vitro*.

To examine the role of $A\beta_{1-42}$ oligomers in oligodendrocyte survival, cell viability was determined by using the fluorescent vital staining Calcein-AM. Since oligodendrocyte basal death is observed due to culture-induced stress, we were able to observe that Aβ treatment significantly increased oligodendrocyte survival, in a dose-dependent manner, reaching a protection plateau at 10 μM (**Figure 25A**). In addition, to discard any unspecific signal due to an interaction between the Calcein-AM probe and Aβ, we added Aβ oligomers to culture media for 24 h in absence of cells and Calcein fluorescence intensity was measured. No differences were found between non-treated and Aβ-treated media (**Figure 25B**). Then, we investigated the molecular mechanisms underlying Aβ-enhanced viability. Thus, cells were treated with Aβ at 1 μM for 24 h and preincubated with PP2, AIP, ryanodine or nifedipine (Ca^{2+}-channel blocker). We found that Aβ-promoted cell

viability was blocked by using indicated inhibitors, indicating that Fyn activation and intracellular Ca^{2+}-increase are important to oligodendrocyte survival (**Figure 25C**).

Finally, we examined the oligodendrocyte culture viability in the presence of naturally Aβ peptide secreted to the conditioned media of N2a neuroblastoma cells that overexpress wild-type human APP (WT) or 670/671 Swedish mutation human APP (SWE) (Wang *et al.*, 2006). We observed that natural Aβ improved the cellular viability of cultured oligodendrocytes in a similar way of synthetic peptide preparation, indicating that endogenous overproduction of Aβ also enhance oligodendrocyte survival (**Figure 25D**).

These results demonstrate that natural and synthetic Aβ peptides have a protective effect on cultured oligodendrocyte by enhancing its cell viability.

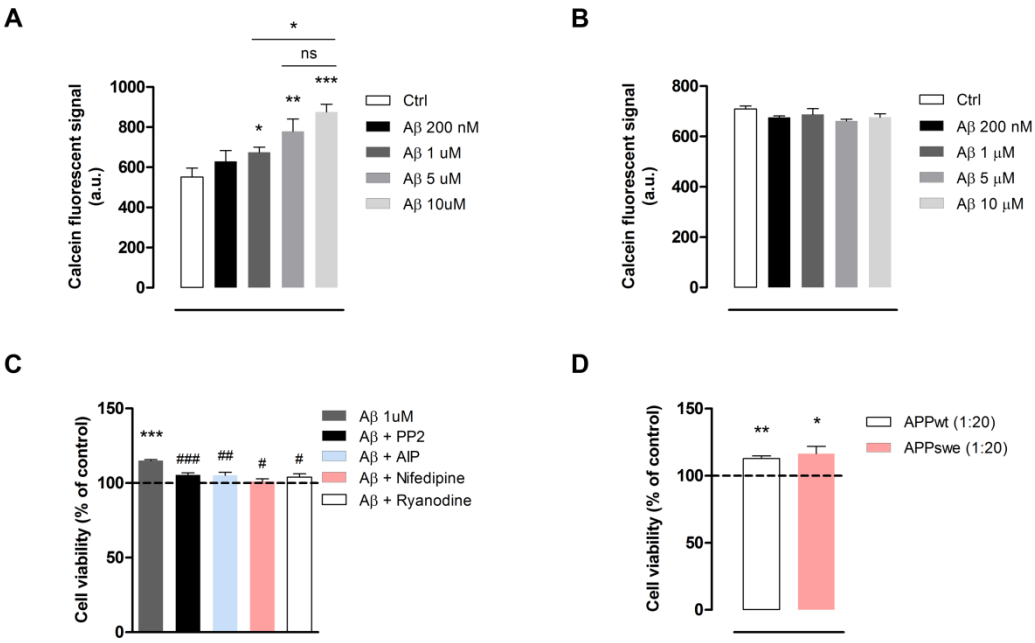

Figure 25. $Aβ_{1-42}$ oligomer treatment protects cultured oligodendrocytes against culture basal death. (A) Cells were treated with increasing concentrations of Aβ (200 nM-10 µM) for 24 h and viability was quantified by Calcein-AM assay (n=6-20). **(B)** Cell culture medium without cells in the presence or absence of Aβ was incubated for 24 h and chemical interaction between Aβ and Calcein-AM was analyzed (n=3). **(C)** Oligodendrocyte viability was measured by Calcein-AM method after incubation with Aβ 1 µM alone or combined with intracellular inhibitors, PP2, AIP, nifedipine (calcium channels, 10 µM) or ryanodine **(D)** Cultured oligodendrocytes were incubated for 24 h with diluted conditioned media (1:20 in SATO) from N2a

cells transfected with wild-type human APP (APPwt) or the 670/671 Swedish mutation human APP (APPswe), and cell viability was measured by Calcein-AM assay (n=4). Data are represented as means ± S.E.M. *p<0.05, ** p<0.01, ***p<0.001 compared to non-treated cells; #p<0.05, ##p<0.01, ###p<0.001 compared to Aβ alone; one-way Anova (A, B); paired Student´s t test (C, D).

7. $A\beta_{1-42}$ oligomers upregulate myelin-related protein expression in cerebellar organotypic cultures.

In order to corroborate the results observed in isolated oligodendrocytes and to assess the contribution of Aβ to myelination process, we used rat cerebellar organotypic cultures as a more complex cellular system and an alternative to animal models. Organotypic cultures are a useful approach for pharmacological and myelination studies as they partially maintain tissue architecture, anatomical relations and network connections (Stoppini *et al*., 1991). Moreover, they are increasingly being used as models to investigate underlying mechanisms of and treatment strategies for neurodegenerative disorders. Thus, we treated rat cerebellar slices after 7 days *in vitro* (7DIV) with Aβ at 200 nM for 48 h, and we analyzed the expression of the myelin-related proteins MBP and CNPase, and oligodendrocyte progenitor receptor PDGFr-α (platelet-derived growth factor receptor α). Aβ induced a significant increase in the expression of these oligodendrocyte-related proteins, as shown by both RT-qPCR (**Figure 26A**) and western blot (**Figure 26B, C**). Among these data, the greatest increment was observed in MBP protein levels, being 66.4 ± 22.59% higher in Aβ-treated slices compared to untreated ones. Then, morphological studies were performed to analyze the integrity of organotypic cerebellar slices. We identified myelin sheaths and axons by immunofluorescence staining using antibodies against MBP and neurofilament-L (NFL), respectively. First, epifluorescence micrographs showed that correct myelination process was occurring in cerebellar slices as shown by the co-localization between myelin (MBP) and axons (NFL). Moreover, an increase in MBP abundance associated with NFL was observed in organotypic slices exposed to Aβ (**Figure 26D**). Therefore, these results verify that Aβ promotes myelin-related protein upregulation, which may be related to myelination process in organotypic culture.

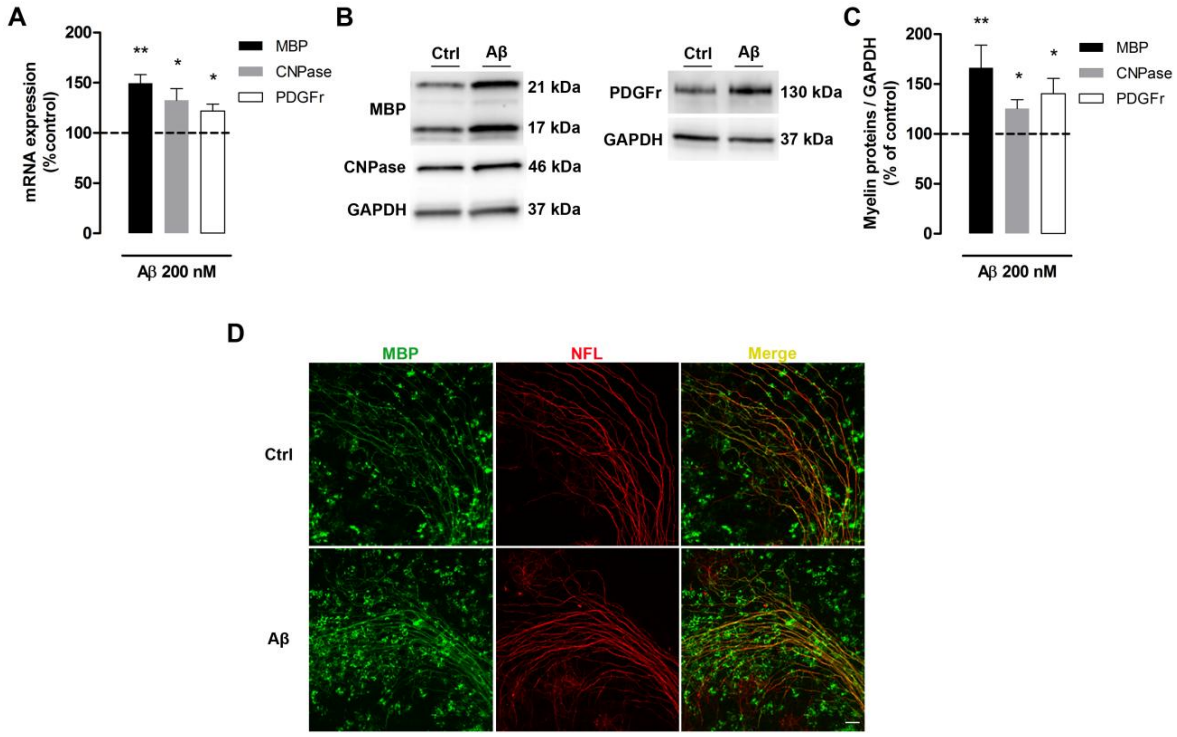

Figure 26. $A\beta_{1-42}$ oligomers upregulate myelin-related protein expression in cerebellar slices. (A) RT-qPCR analysis of oligodendrocyte-related mRNA levels, MBP, CNPase and PDGFr-α in cerebellar slices treated with Aβ at 200 nM for 48 h. **(B)** Western blot for the indicated proteins in total protein extracts from cerebellar slices (n=3 cultures). **(C)** Protein expression analysis is shown (n=4-13 cultures). Data are represented as means ± S.E.M. of optical density values normalized to GAPDH. *p<0.05, **p<0.01 compared to non-treated cells; paired Student´s t test. **(D)** Representative immunofluorescence micrographs of cerebellar organotypic slices with or without Aβ. Immunostaining for the axonal marker neurofilament L (NFL, red), myelin marker (MBP, green), and colocalization of these markers is shown in merge images (yellow). Scale bar, 50 µm.

We previously found that Aβ activates kinase Fyn to increase MBP protein expression in primary oligodendrocyte cultures. Therefore, to examine whether MBP upregulation induced by Aβ in organotypic slices is mediated by SFK, we treated cerebellar slices with Aβ together to PP2. Aβ-induced increased levels of MBP were blocked after PP2 treatment, with 156.2 ± 26.40 vs. 95.13 ± 3.46 of MBP expression in Aβ vs. Aβ with PP2, respectively (**Figure 27A, B**).

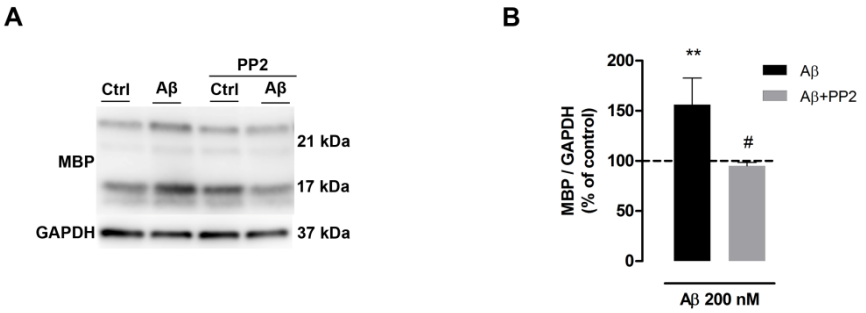

Figure 27. SFK activation participates in Aβ-induced MBP upregulation in organotypic slices. **(A, B)** MBP expression was analyzed by western blot (n=4) after A (200 nM for 48 h) and A together PP2 inhibitor (SFK inhibitor) exposure of cerebellar organotypic slices. Data are represented as means ± S.E.M. of optical density values normalized to GAPDH. **p<0.01 compared to non-treated cells; #p<0.05 compared to Aβ alone; paired Student´s t test.

As it is shown above, Aβ promoted MBP synthesis in physiological conditions, so we asked if Aβ could enhance remyelination in a pathological context, such as lysophosphatidylcholine (LPC)-induced demyelination model (**Figure 28A**). LPC is a bioactive lipid with detergent-like properties and its use is well established as demyelination model in rat cerebellar slices, in which remyelination occurs spontaneously after LPC insult (Birgbauer et al., 2004). In this sense, it has been widely used to investigate the capacity of exogenous molecules to modulate remyelination process (Huang et al., 2011; Mi et al., 2009; Miron et al., 2010). Therefore, we first characterized the LPC model to assess myelin recovery after LPC insult. We induced demyelination with a 16 h treatment of LPC (0.5 mg/ml), showing a sustained MBP level decrease 1 day after (1DIV) LPC removal (27.76% over normally myelinated control). Then, it was observed an incomplete myelin recovery 6 days (6DIV) after LPC insult (37.96% over normally myelinated control) (**Figure 28B, C**). Moreover, to assess the role of Aβ on remyelination, cerebellar slices were exposed to Aβ at 200 nM after LPC exposure and MBP levels were analyzed 1 and 6 days after Aβ application. Importantly, slices treated with Aβ showed a significant increase in MBP expression relative to controls at same time points.

Furthermore, to investigate if SFK activity modulated the MBP increase leaded by Aβ after LPC-induced demyelination, slices were treated with Aβ in the presence or absence of PP2 and results showed that Aβ-induced MBP upregulation was attenuated by PP2

treatment (**Figure 28D, E**). Finally, epifluorescence images of MBP staining revealed that Aβ treatment subsequent to LPC-induced demyelination enhances remyelination by SFK activation (**Figure 28F**).

In conclusion, these data corroborates that Aβ induces MBP upregulation and enhances remyelination after demyelination process in cerebellar organotypic culture.

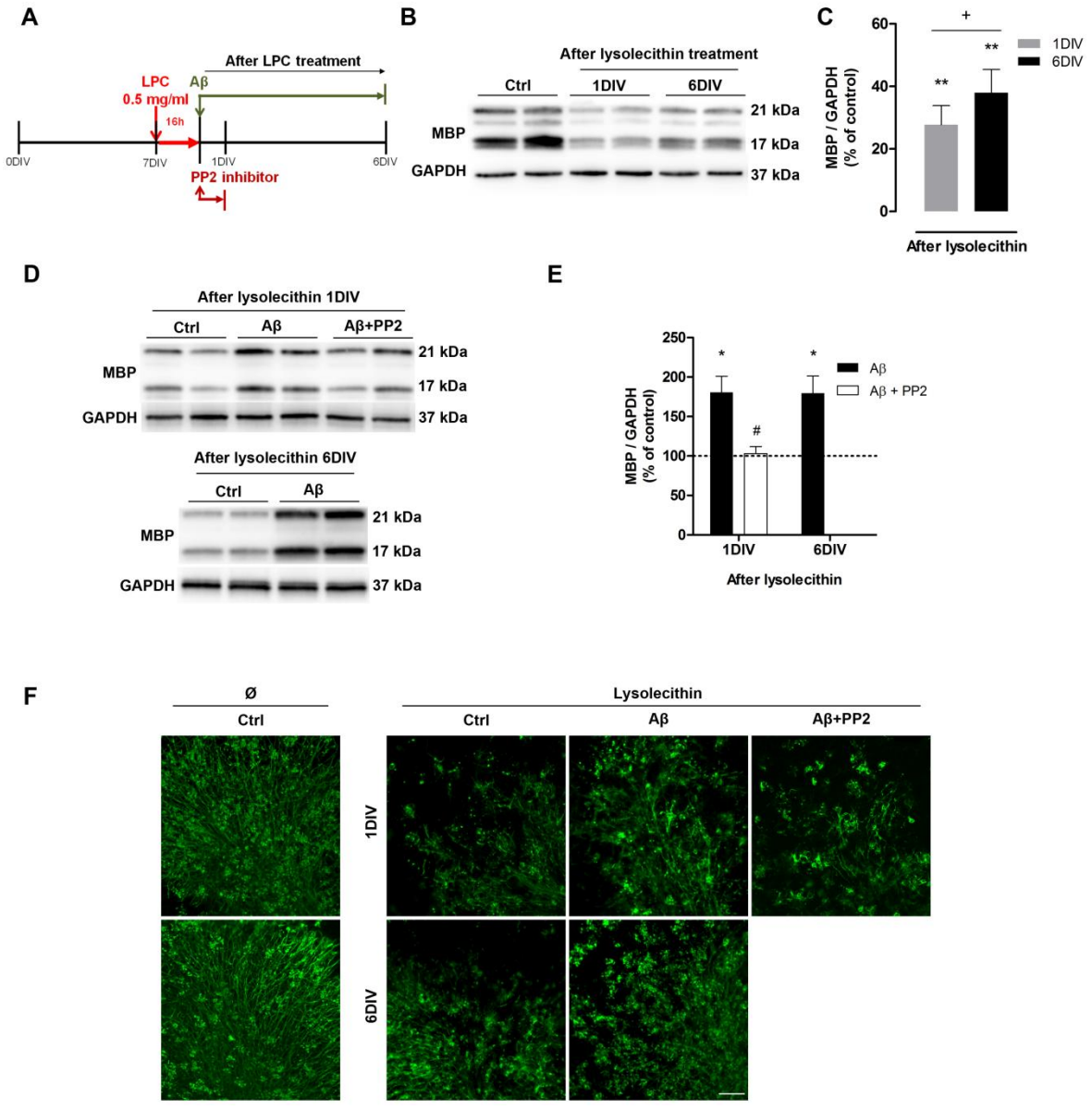

Figure 28. SFK activation by $A\beta_{1-42}$ oligomers enhances remyelination following lysolecithin-induced demyelination in cerebellar slices. (A) Schematic diagram of experimental paradigm. **(B)** Characterization of LPC-induced demyelination model by western blot. **(C)** Cerebellar slices were treated with LPC for 16 h and total protein samples were extracted 1 (1 DIV) and 6 (6 DIV) days after LPC treatment and MBP expression was analyzed (n=6-9 cultures). **(D)** Western blot of MBP expression was analyzed after LPC treatment in the

presence or absence of Aβ (200 nM) and PP2 (SFK inhibitor). **(E)** Data analysis of MBP expression in 1DIV and 6DIV after LPC exposure (n=3-7 cultures). Data are represented as means ± S.E.M. of optical density values normalized to GAPDH. *p<0.05, **p<0.01 compared to non-treated cells; +p<0.05 compared to 1DIV; #p<0.05 compared to Aβ alone; paired Student´s t test. **(F)** Representative images of MBP levels from cerebellar slices treated with LPC, Aβ and PP2 at two different time points. Scale bar, 50 µm.

8. AD transgenic mice exhibit MBP increased levels in hippocampus and corpus callosum at adult ages.

To further assess oligodendrocyte differentiation and myelination in *in vivo* AD model we used the triple transgenic mouse (3xTg-AD), a murine model of this pathology. MBP is an essential myelin protein for generating and maintaining compact myelin sheaths, thus we first analyzed its expression by western blot in hippocampal samples of 6-, 12- and 18-month-old 3xTg-AD and wild-type mice (WT) (**Figure 29A**). It was observed that, at all ages with the exception of 3 months, MBP expression levels were increased in 3xTg-AD compared to WT mice, reaching up to 117.57 % over WT at 18 months (**Figure 29B**). Moreover, MBP increased levels were localized at specific areas of 18-month-old transgenic mice hippocampus, dentate gyrus (DG), CA2-3 and CA3. No differences in MBP expression were found in CA1 and CA2 hippocampal regions comparing 3xTg-AD and WT (**Figure 29D, E**).

In addition, Aβ is accumulated in an age-dependent manner in this AD model having remarkable increased levels from 15 months of age (Oddo *et al*., 2006). Thus, to examine whether Aβ amount correlates with MBP levels, we measured Aβ expression at 18 month-old mice and found a significant positive correlation between MBP and Aβ levels (r=0.9249, p=0.0122) (**Figure 29C**). Thereby, these results indicate that MBP is upregulated in the hippocampus of AD transgenic mice and this expression is positively associated with Aβ oligomer levels.

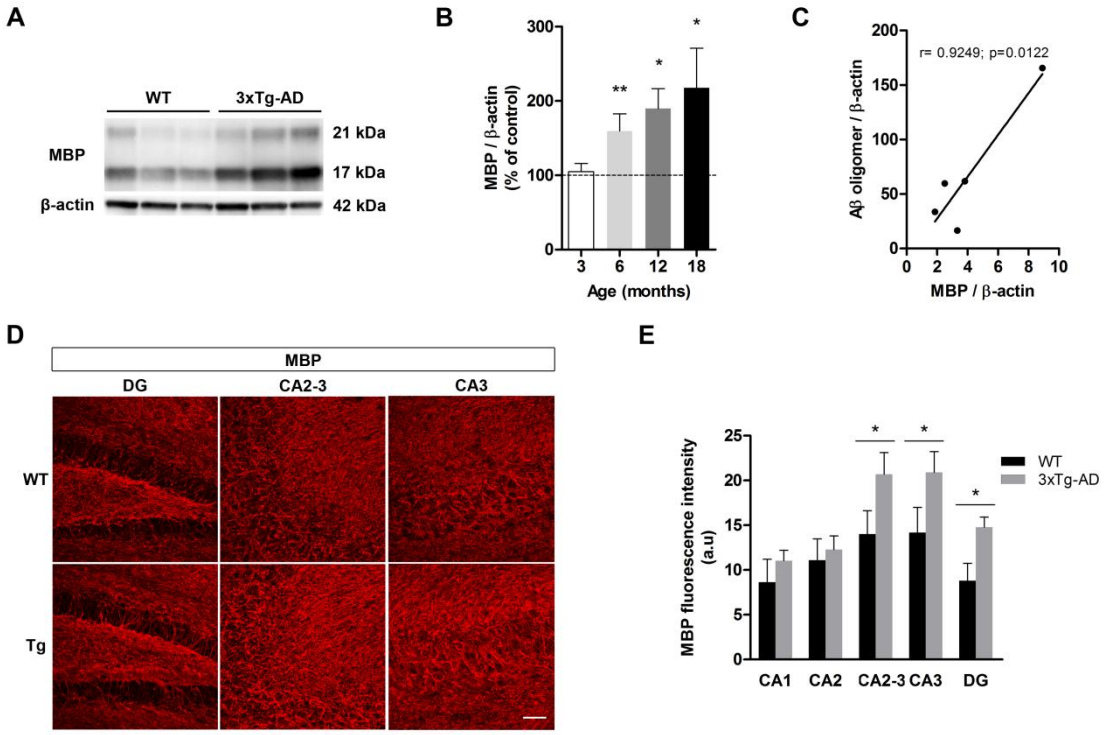

Figure 29. MBP expression is upregulated in AD transgenic mice hippocampus. (A) Western blot of MBP expression in hippocampus of 18-month-old 3xTg-AD mice compared to WT. **(B)** Quantification of MBP levels in hippocampus of 6-, 12- and 18-month-old 3xTg-AD mice in comparison with WT is shown (n=5-6 animals per age). Data are represented as means ± S.E.M. of optical density values normalized to corresponding β-actin. *p<0.05, **p<0.01 compared to WT; paired Student´s t test. **(C)** Correlation between MBP and Aβ oligomer levels in hippocampus of 18-month-old 3xTg-AD mice (n=5 animals). **(D)** Representative confocal z-stack projections of MBP in the dentate gyrus (DG), CA2-3 and CA3 regions of sections taken form 18-month-old transgenic and WT mice. **(E)** Analysis of hippocampus MBP fluorescence intensity is shown (n=5-6 animals). Scale bar, 40 µm. Data are represented as means ± S.E.M. *p<0.05, **p<0.01 compared to WT; paired Student´s t test.

Next, we tested by western blot a non-phosphorylated form of neurofilament heavy chain at 18-month-old mice. SMI-32 antibody is used to detect axonal damage as maker of neurodegeneration (Su, Cummings, & Cotman, 1996), since in healthy axons neurofilament heavy chain (NFH-200) is phosphorylated and this correlates with accurate axonal transport (Watson, Fittro, Hoffman, & Griffin, 1991). No significant differences were found in SMI-32 immunoreactivity between hippocampus samples of 3xTg-AD and WT. (**Figure 30A, B**). Moreover, hippocampal histological sections stained for light neurofilament (NFL) were analyzed and no differences were found in NFL intensity

fluorescence (**Figure 30C, D**). These results suggest that 3xTg-AD hippocampus do not present compromising axons, being MBP upregulation independent of axonal integrity.

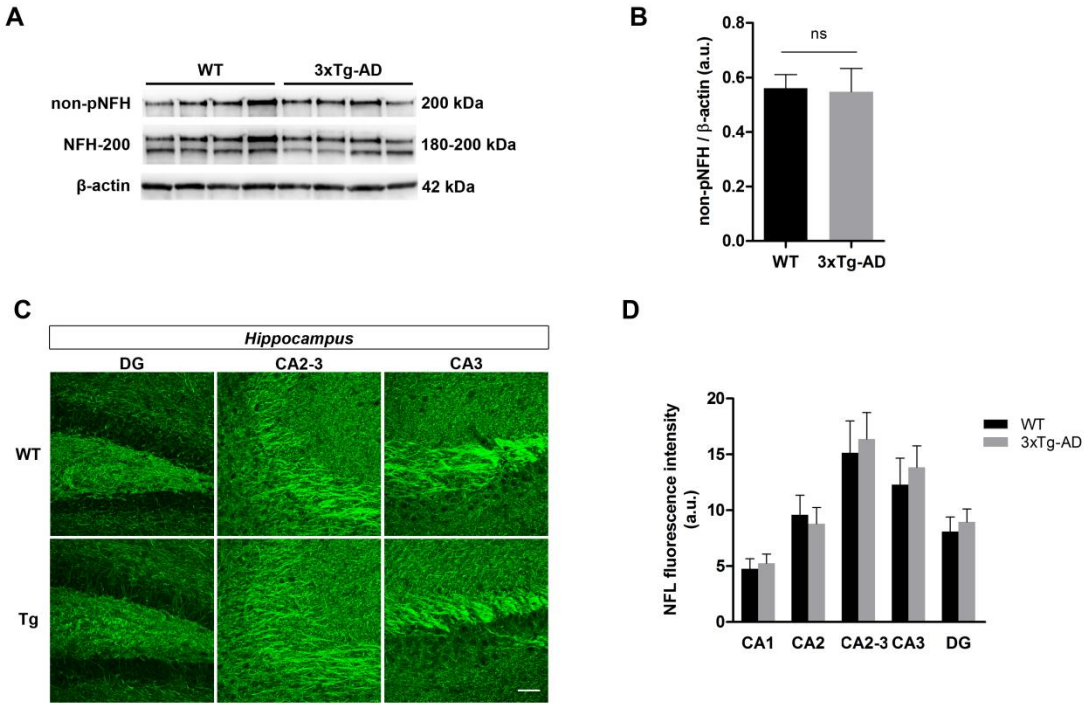

Figure 30. Hippocampus of AD transgenic mice does not present aberrant phosphorylation in axonal neurofilaments. (A) Non-phosphorylated neurofilament H (non-pNFH) and neurofilament H (NFH-200) levels in hippocampus of 18-month-old 3xTg-AD and WT mice were detected by western blot. **(B)** Quantification of SMI-32 immunoreactivity is shown (n=6). Data are represented as means ± S.E.M. of optical density values normalized to corresponding β-actin. **(C)** Representative confocal z-stack projections of neurofilament-L (NFL) in the dentate gyrus (DG), CA2-3 and CA3 regions of 18-month-old transgenic and WT mice hippocampus. **(D)** Analysis of NFL fluorescence intensity of hippocampus regions (n=6). Scale bar, 40 µm. Data are represented as means ± S.E.M; paired Student´s t test.

In order to extend the study of MBP expression pattern in white matter regions of AD *in vivo*, we also quantified MBP levels in transgenic and WT corpus callosum. 3xTg-AD mice present significant MBP overexpression at 12- and 18-month-old (181.1 ± 22.28 and 165.4 ± 19.98 vs. 100% of control, respectively), while a strong tendency was observed since 6 months (128 ± 7.5) and no significant differences were found in 3-month-old mice (**Figure 31A, B**). Accordingly, this MBP increment observed in 3xTg-AD was corroborated

after quantifying MBP intensity by immunofluorescence of 18-month-old mice (**Figure 31C, D**).

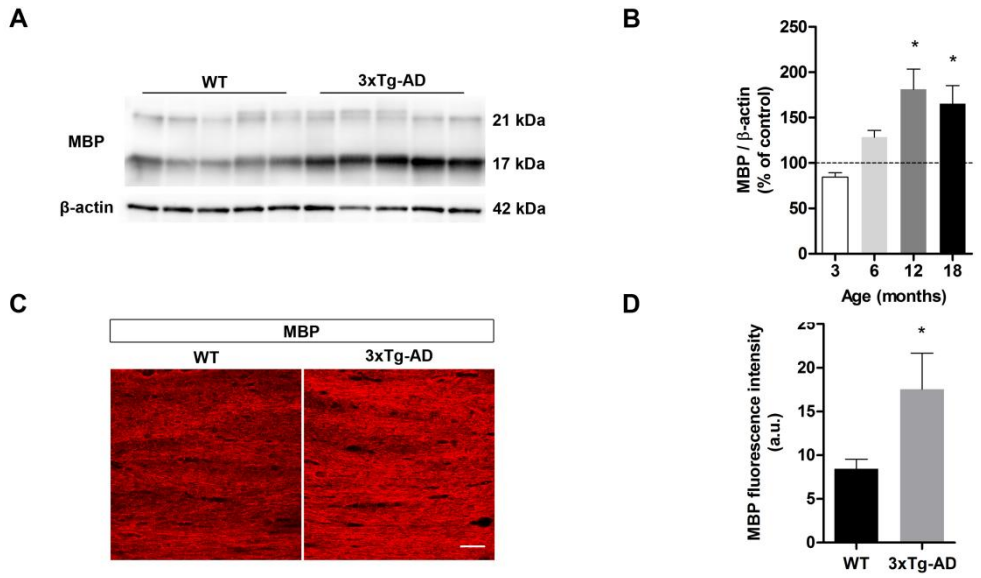

Figure 31. AD transgenic mice present MBP increased levels in corpus callosum. (A) Western blot of MBP expression in corpus callosum of 18-month-old 3xTg-AD and WT mice. **(B)** MBP expression analysis of corpus callosum from 6-, 12- and 18-month-old 3xTg-AD compared to WT mice (n=5-8 animals per group). Data are represented as means ± S.E.M. of optical density values normalized to corresponding β-actin. **(C)** Representative confocal z-stack projections of the corpus callosum of 18–month-old transgenic and WT mice showing MBP. **(D)** Quantification of MBP fluorescence intensity of corpus callosum (n=5 animals). Scale bar, 25 µm. Data are represented as means ± S.E.M; *p<0.05 compared to WT; paired Student´s t test.

Next, non-phosphorylated NFH expression was quantified in corpus callosum and similarly to what occurred in hippocampus, no differences were found in WT and 3xTg-AD at 18 months (**Figure 32A, B**). Concordantly, the quantification of NFL fluorescence intensity remained unchanged (**Figure 32C, D**).

Overall, these data indicate that adult 3xTg-AD mice present changes on MBP synthesis in absence of axonal damage in hippocampus and corpus callosum.

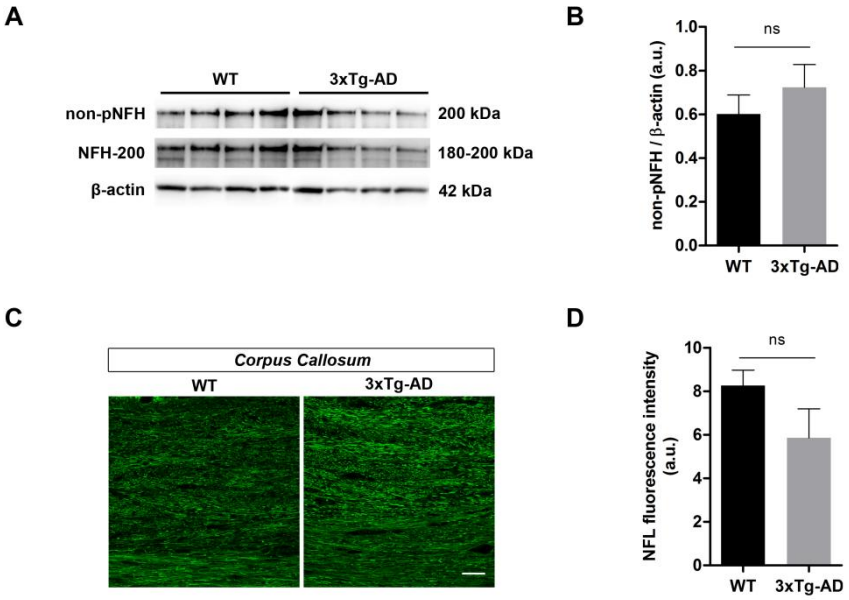

Figure 32. Corpus callosum of AD transgenic mice does not present changes in non-phosphorylated NFH levels. (A) Western blot showing non-phosphorylated neurofilament H (non-pNFH) and neurofilament H (NFH-200) levels in corpus callosum of 18month-old 3xTg-AD and WT mice. **(B)** Quantitative analysis of SMI-32 immunoreactivity in corpus callosum is shown (n=7-8). Data are represented as means ± S.E.M. of optical density values normalized to corresponding β-actin. **(C)** Representative confocal z-stack projections of MBP in the corpus callosum of 18month-old transgenic and WT mice. **(D)** MBP fluorescence intensity quantification of corpus callosum (n=6). Scale bar, 25 µm. Data are represented as means ± S.E.M; paired Student´s t test.

9. Oligodendrocyte proliferation and differentiation are impaired in AD transgenic mice hippocampus and corpus callosum.

As MBP synthesis upregulation occurs in 3xTg-AD mice hippocampus and corpus callosum, we determined if the MBP expression increase was due to oligodendrocyte proliferation and subsequent differentiation in myelin-forming cells. For this purpose, we analyzed oligodendrocyte lineage cells with olig2 antibody, oligodendrocyte progenitor cells with PDGFr-α antibody and mature cells with CC1 antibody to specifically examine each cell population density per mm^3. According to the hippocampal regions where MBP levels are increased in 3xTg-AD, dentate gyrus (**Figure 33A, B**) and CA3 (**Figure 34A, B**) of 6- and 18-month-old mice were analyzed. First, we observed that the density of PDGFr-α^+ cells significantly increased 2-fold in 3xTg-AD dentate gyrus at 6 months compared to WT

(**Figure 33E**), while the proportion of Olig2$^+$ and CC1$^+$ cells remained unchanged (**Figure 33C, D**). In contrast, at 18 months, dentate gyrus of 3xTg-AD did not present a greater number of PDGFr-α$^+$ cell compared to WT. Interestingly, Olig2$^+$ cells density was 43.16 ± 1.24 in 3xTg-AD and significantly increased to 65.6 ± 1.45 in WT, whereas it was observed a marked increasing tendency of CC1$^+$ cells abundance (37.89% over WT). Finally, no significant differences were found in the number of total cells per mm^3 among WT and 3xTg-AD mice (**Figure 33F**).

Moreover, we analyzed the density of oligodendrocyte cells during aging and observed a significant loss of Olig2$^+$ cells comparing 6- and 18-month-old mice, which was attenuated in 3xTg-AD mice (**Figure 33C**). Additionally, there was a decreasing tendency in the abundance of total and CC1$^+$cells, but it was not significant (**Figure 33D, F**).

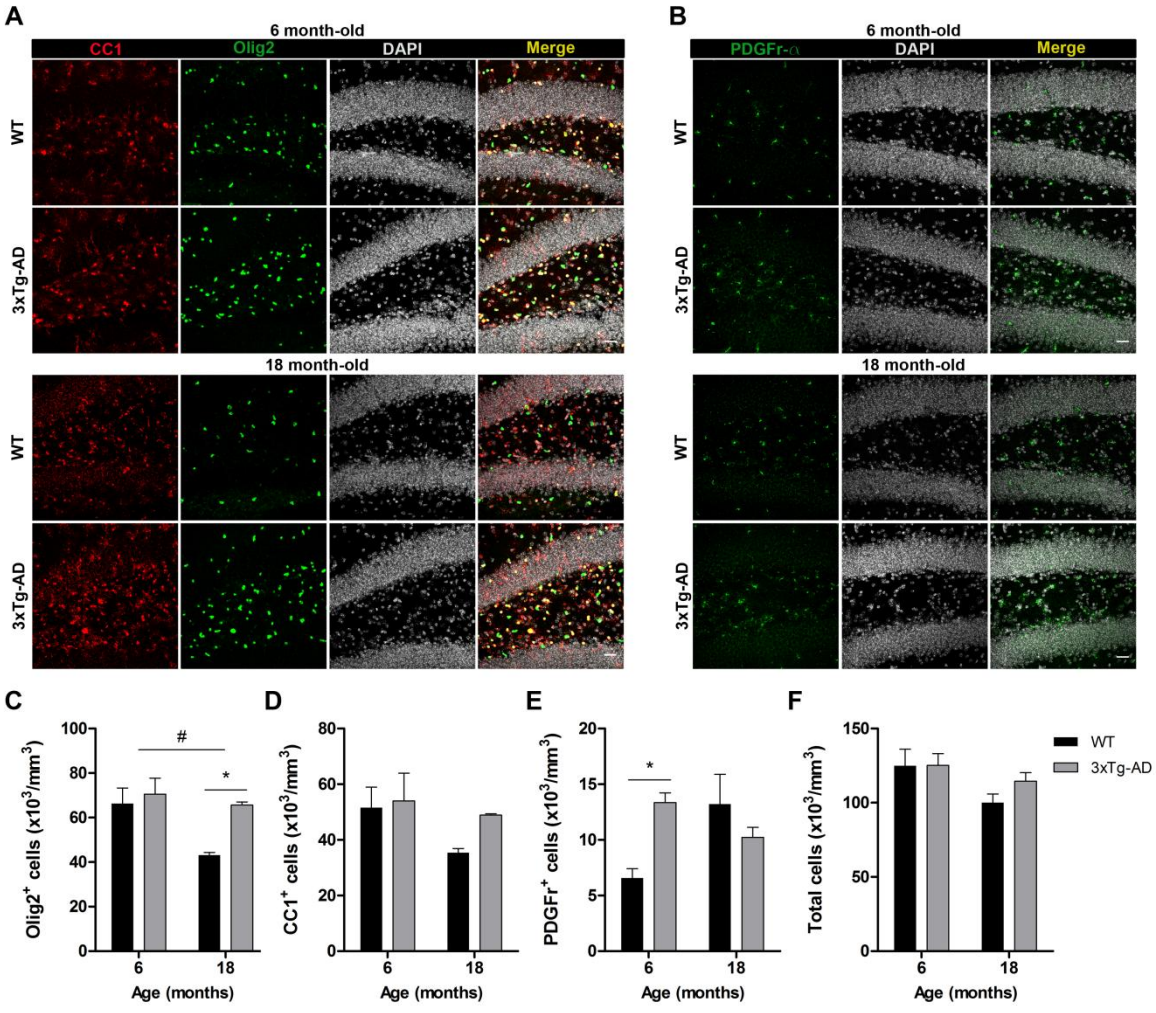

Figure 33. Dentate gyrus of AD transgenic mice presents an increase in the density of OPCs and mature oligodendrocyte at adult ages. Representative confocal z-stack projections of 3xTg-AD and WT hippocampal dentate gyrus at 6 and 18 months. Mature oligodendrocytes were visualized with CC1 (red) and total oligodendrocyte lineage cells with Olig2 (green) **(A)**, and oligodendrocyte progenitor cells with PDGFr-α (green) **(B)**. DAPI staining was used to observe cell nuclei (white). Quantification of $Olig2^+$ cells **(C)**, $CC1^+$ cells **(D),** PDGFr-α^+ cells **(E)**, and total cells **(F)** per mm^3 in the dentate gyrus at both ages (n=3 per group). Scale bar, 25 µm. Data are represented as means ± S.E.M; *p<0.05 compared to WT; # p<0.05 significantly over time; two-way ANOVA followed by Bonferroni posttest.

Moreover, we examined the density of oligodendrocyte populations in CA3 region of WT and 3xTg-AD. Similarly to what we observed in dentate gyrus, a subtle increasing tendency was also observed in $Olig2^+$ and $CC1^+$ cells at 18-month-old 3xTg-AD mice as compared to WT, but it was not significant (**Figure 34C, D**). In addition, no significant differences were found in the proportion of PDGFr-α^+ cells at any ages (**Figure 34E**). Moreover, no differences were observed in the number of total cells per mm^3 among WT and 3xTg-AD mice (**Figure 34F**).

Regarding cell population dynamics during ageing, a significant decrease was observed between 6- and 18-month-old mice in the number of $CC1^+$, although this oligodendrocyte loss was not reflected in the density of total cells (**Figure 34C-F**).

These data indicate that hippocampal dentate gyrus of 3xTg-AD mice present higher density of oligodendrocyte progenitor cells at 6 months which may be leading to a higher abundance of oligodendrocyte lineage cells, including a subtle increment in mature oligodendrocyte cells at 18 months. In contrast, no significant changes were observed in the density of oligodendrocyte populations in CA3.

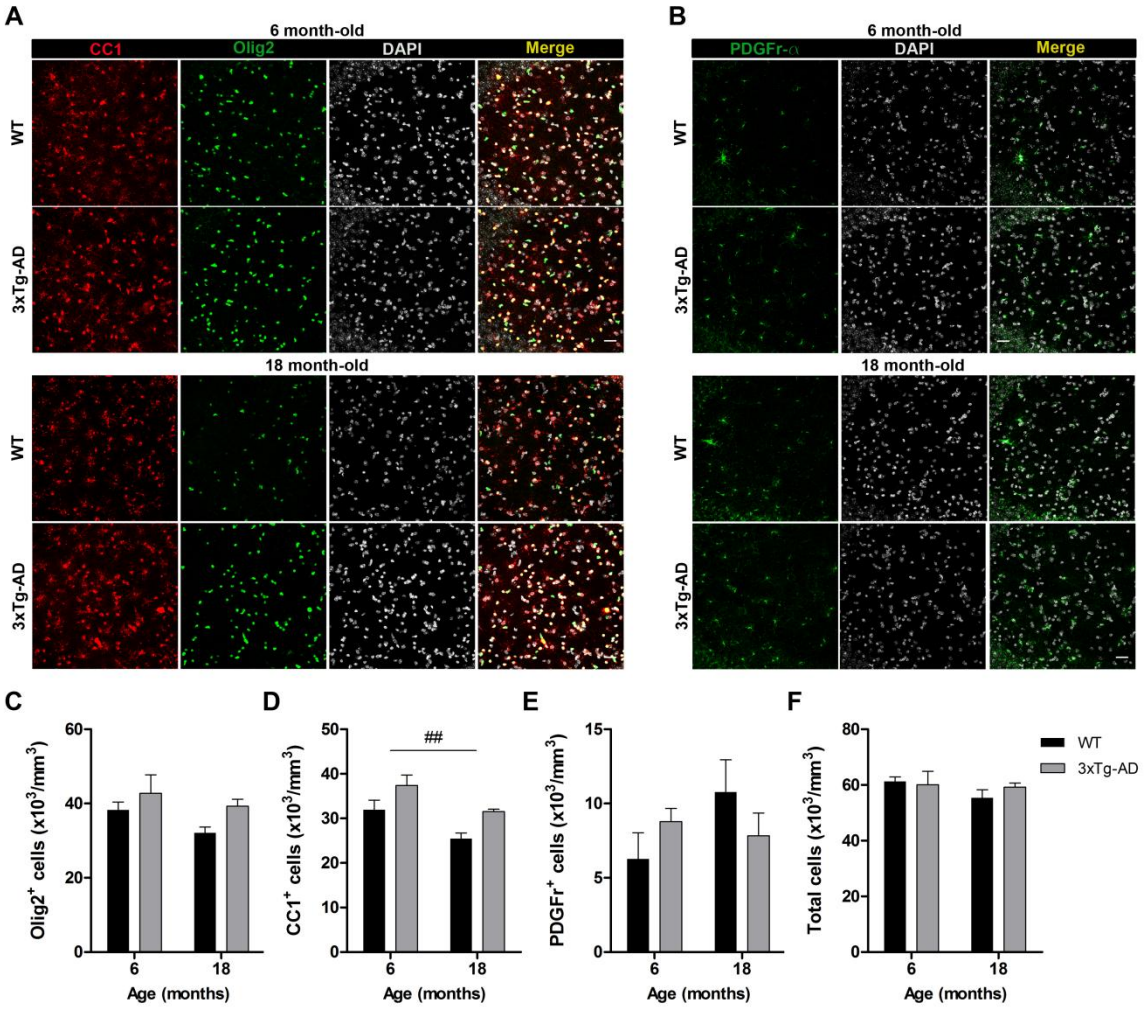

Figure 34. Hippocampal CA3 of AD transgenic mice present an increase in the density of OPCs and mature oligodendrocyte at adult ages. Representative confocal z-stack projections of 3xTg-AD and WT hippocampal CA3 at 6 and 18 months. Mature oligodendrocytes were visualized with CC1 (red) and total oligodendrocyte lineage cells with Olig2 (green) **(A)**, and oligodendrocyte progenitor cells with PDGFr-α (green) **(B)**. DAPI staining was used to observed cell nuclei (white). Quantification of Olig2+ cells **(C)**, CC1+ cells **(D),** PDGFr-α+ cells **(E)**, and total cells **(F)** per mm^3 in CA3 at both ages (n=3 per group). Scale bar, 25 µm. Data are represented as means ± S.E.M; *p<0.05 compared to WT; # p<0.05, ## p<0.01 significantly over time; two-way ANOVA followed by Bonferroni posttest.

In addition, corpus callosum of 6- and 18-month-old mice was also examined (**Figure 35A, B**). Unlike what we observed in the hippocampus, the density of PDGFr-α^+ cells remained unaltered at both ages. Nevertheless, the number $Olig2^+$ and $CC1^+$ cells increased a 30.73% and 29.65% in corpus callosum of 3xTg-AD mice at 18 months, while no significant changes were found at 6 months (**Figure 35C, D**). Interestingly, while the

number of the oligodendroglial lineage is higher in 3xTg-AD, the proportion of each subpopulation remained similar, being 80.71 or 80.04% $CC1^+$ cells and 14.85 or 13.8% PDGFr-α^+ cells in WT or 3xTg-AD, respectively

Moreover, corpus callosum showed a significant decrease in the number of total cells with aging (**Figure 35F**). Concordantly, a 49.91 and 33% of $Olig2^+$ cells was reduced in WT and 3xTg-AD, as well as, the 56.26% and 38.23% of $CC1^+$ cells were loss in WT and 3xTg-AD compared 6 and 18 months mice (**Figure 35C, D**). Similarly, a reduction in PDGFr-α^+ cells was observed with aging (**Figure 35E**). These data suggest that the oligodendrocyte loss occurred in WT due to aging was attenuated in 3xTg-AD mice.

Overall, our results indicate that 3xTg-AD mice exhibit increased densities of oligodendroglial cells, although their progression differs between hippocampus and corpus callosum. While in the first progenitor cells are the ones that are in higher abundance, in corpus callosum we found mature cells to be increased. Regarding cell death, only corpus callosum seems to suffer loss of cell density associated with ageing. Interestingly, this process was shown to be attenuated in transgenic mice and might be mainly affecting cells of the oligodendrocyte lineage.

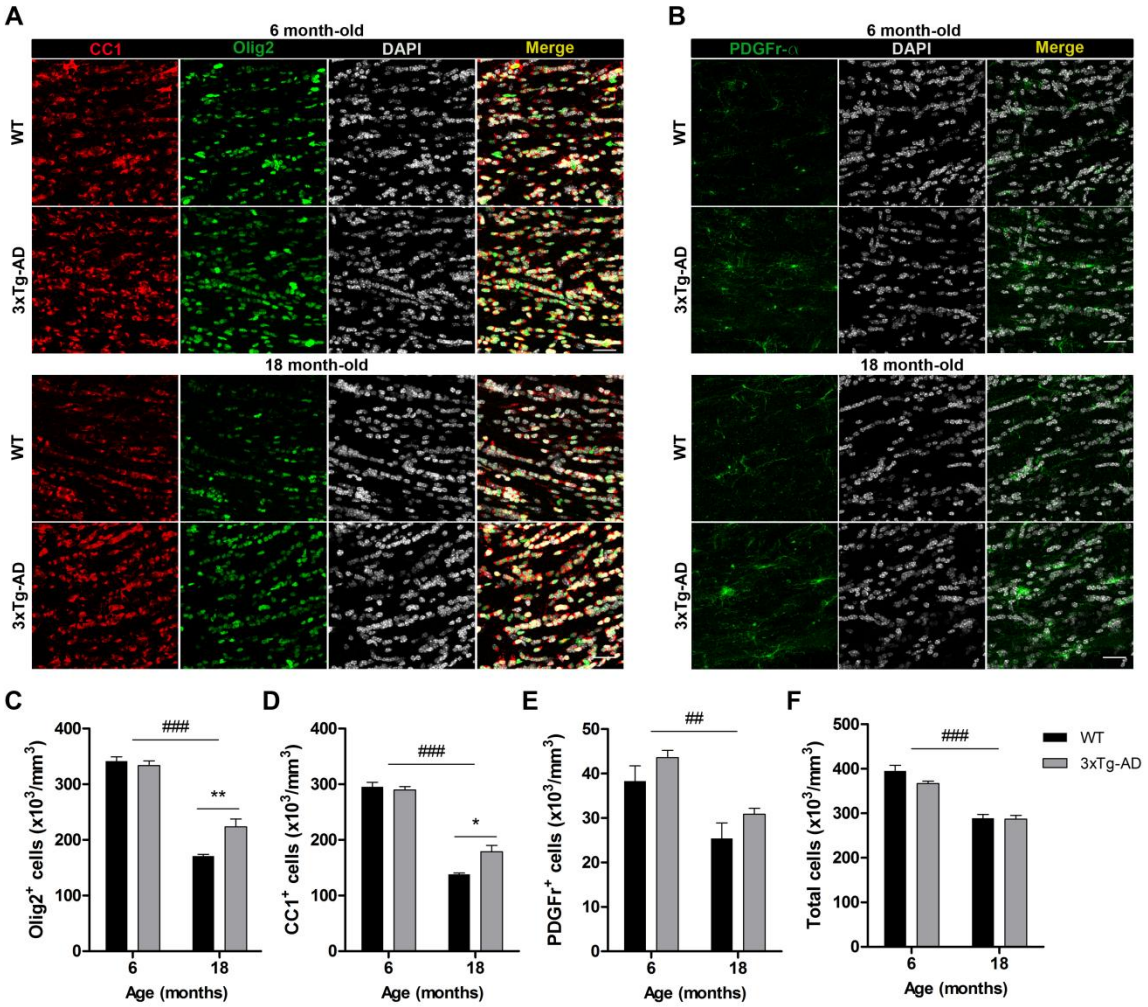

Figure 35. Corpus callosum of AD transgenic mice shows an increase in the density of mature oligodendrocyte and a decrease in oligodendrocyte loss due to aging at adult ages. Representative confocal z-stack projections of 3xTg-AD and WT corpus callosum at 6 and 18 months. Mature oligodendrocytes were visualized with CC1 (red) and total oligodendrocyte lineage cells with Olig2 (green) **(A)**, and oligodendrocyte progenitor cells with PDGFr-α (green) **(B)**. DAPI staining was used to observed cell nuclei (white). Quantification of Olig2+ cells **(C)**, CC1+ cells **(D),** PDGFr-α+ cells **(E)**, and total cells **(F)** per mm^3 in the corpus callosum at both ages (n=3 per group).Scale bar, 25 µm. Data are represented as means ± S.E.M; *p<0.05, **p<0.01 compared to WT; ## p<0.01, ### p<0.001 significantly over time; two-way ANOVA followed by Bonferroni posttest.

10. The density and the structure of nodes of Ranvier are impaired in the corpus callosum of AD transgenic mice.

Since it is described that mature oligodendrocytes generated in adult ages produce more and shorter internodes (Young *et al*., 2013), we characterized nodes of Ranvier in the corpus callosum of adult mice. For that, individual nodes were identified by immunolabeling of the nodal channel Nav1.6 and the paranodal protein Caspr. First, while no differences were found in 6-month-old mice, we found a higher density of nodes of Ranvier in 3xTg-AD at 18 months compared to WT mice (**Figure 36A, B**). Moreover, we observed that the length of nodes of Ranvier was shorter in 3xTg-AD corpus callosum in 18-month-old mice compared to WT, whereas no differences were found at 6 months (**Figure 36C, D**). Accordingly, the distribution of node lengths revealed a significant increase in the number of small nodes (<1 µm) in 18-month-old 3xTg-AD, as well as a severe decrease in intermediate size nodes (1-1.5 µm) in comparison with WT (**Figure 36F**). In contrast, 6-month-old mice did not present differences (**Figure 36E**). Thus, these results demonstrate that corpus callosum of aged 3xTg-AD show more and shorter nodes of Ranvier, in accordance with the increase of mature oligodendrocytes observed in these AD mice.

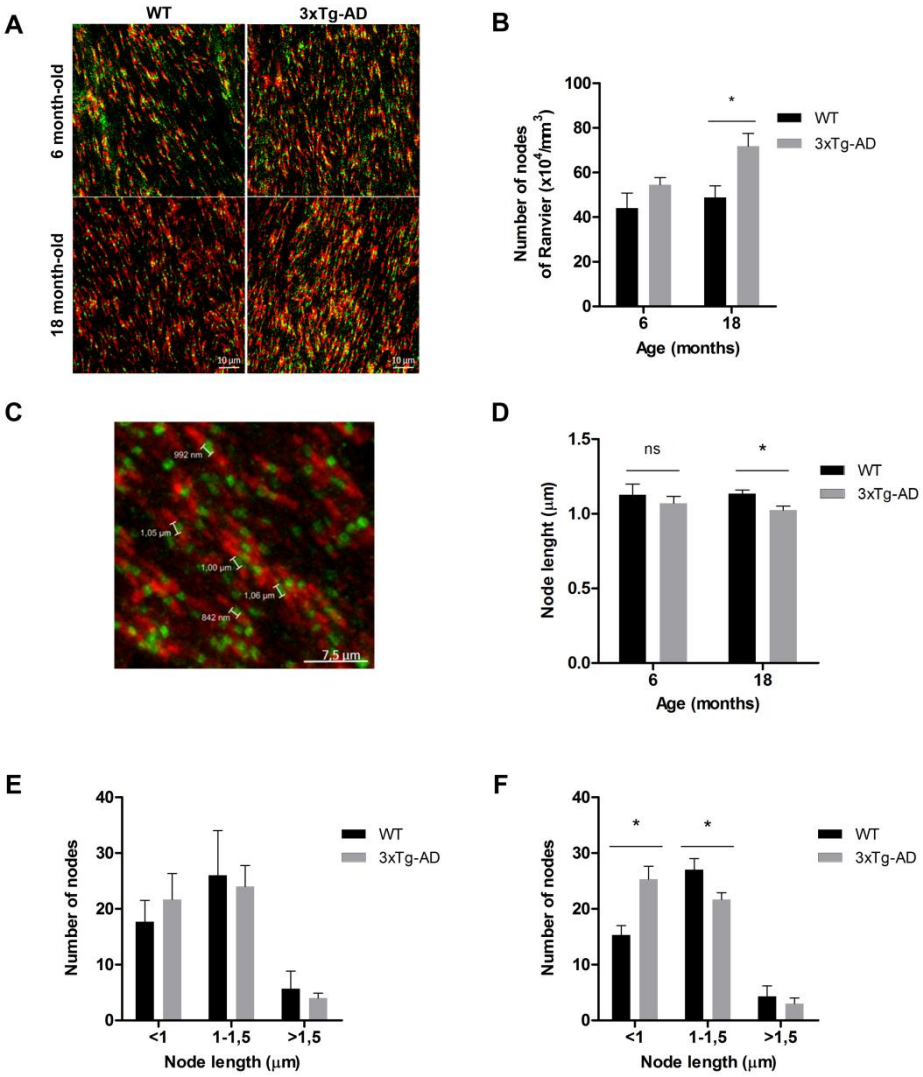

Figure 36. The density and the structure of nodes of Ranvier are impaired in the corpus callosum of AD transgenic mice. (A) Representative confocal z-stack projections of nodes of Ranvier in 3xTg-AD and WT corpus callosum at 6 and 18 months, identified by immunofluorescence labeling for the paranodal protein Caspr (red) and the nodal channel Nav1.6 (green). Scale bar, 25 µm **(B)** Analysis of the number of node of Ranvier at both ages (n=4-5 animals per age). **(C)** Representative micrograph of node length measurement example. Immunostaining for Caspr (red) and Nav1.6 (green). **(D)** Quantification of node lengths in corpus callosum from 3xTg-AD compared to WT mice at 6 and 18 months (n=3 per group). **(E)** Distribution of node lengths at 6 moth-old mice and **(F)** at 18 month-old mice in 3xTg-AD mice comparing with WT mice. Scale bar, 25 µm. Data are represented as means ± S.E.M; *p<0.05, **p<0.01 compared to WT; two-way ANOVA followed by Bonferroni posttest (B, D); paired Student´s t test (E, F).

11. Slow conduction velocity in myelinated axons of AD transgenic mice.

To determine the functional consequences of oligodendrocyte differentiation impairment, we assessed optic nerve conduction at 18-month-old mice by recording compound action potentials (CAPs) comparing WT to 3xTg-AD. First, increase of MBP expression in optic nerves from 18-month-old mice was corroborated (**Figure 37A, B**). Then, optic nerves were acutely isolated from 3xTg-AD and WT mice and CAPs were recorded *ex vivo* (**Figure 37C**). CAP profiles revealed a significantly reduced conduction velocity in 3xTg-AD, as observed by the decrease in the area and in maximum peak of CAP (**Figure 37D, E**).

In order to determine whether axonal dysfunction observed in 3xTg-AD optic nerve is dependent on myelin sheath presence, we examined the conduction velocity in corpus callosum the largest white matter structure in the brain, in which myelinated and non-myelinated axons are present (**Figure 37F**). Thus, we observed that axonal conduction velocity is significantly slower in myelinated 3xTg-AD axons (N1) compared to WT, while no differences were found in unmyelinated ones (N2) (**Figure 37G, H**). These data, combined with our previous results, indicate that white matter abnormalities found in the AD transgenic mice contribute to structural and functional defects in neurotransmission.

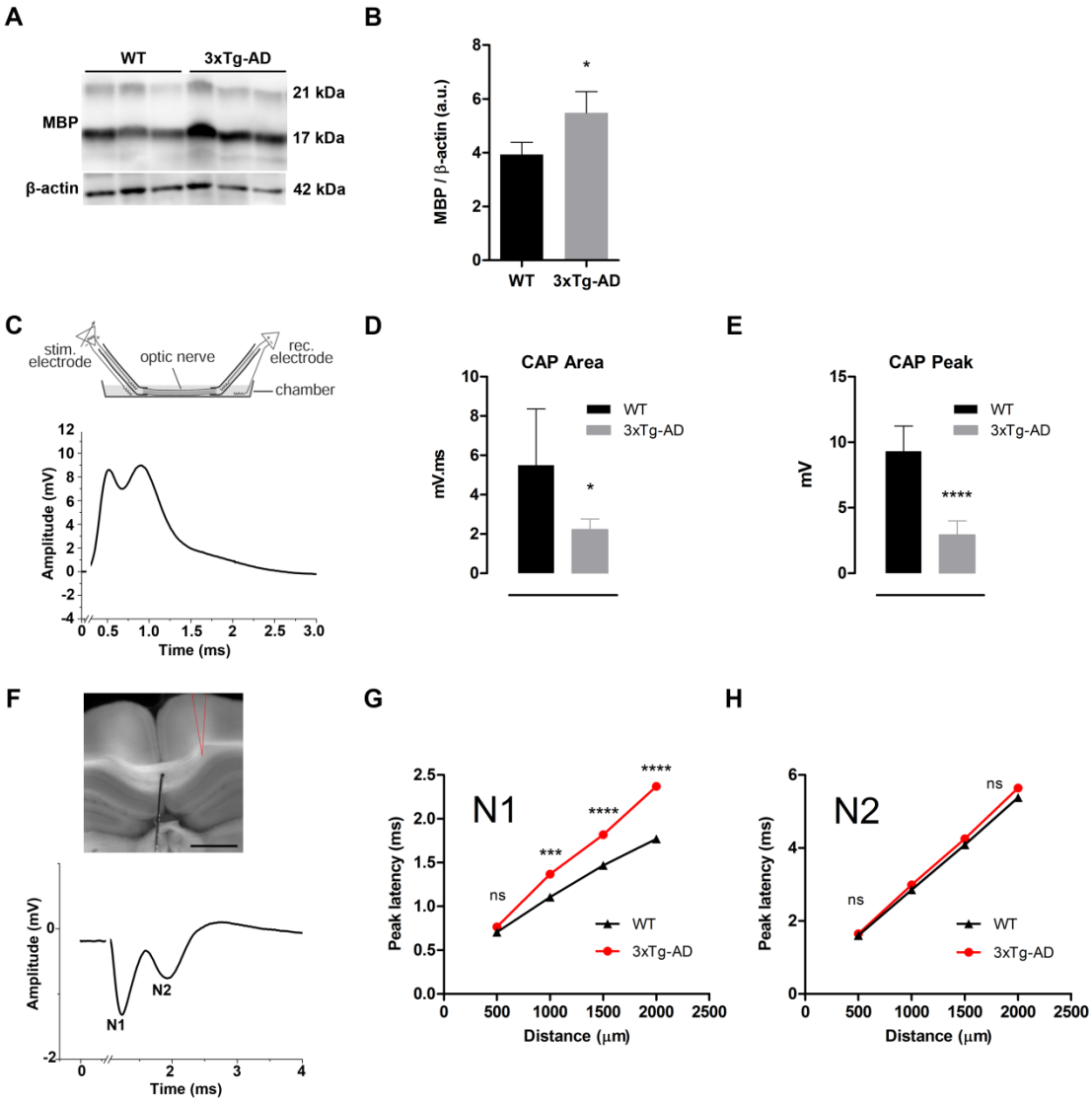

Figure 37. AD transgenic mice present slow conduction velocity in myelinated axons of optic nerve and corpus callosum. (A) Western blot of MBP expression in optic nerve of 18 month-old 3xTg-AD and WT mice (n=3 animals per age). **(B)** MBP expression analysis was shown. Data are represented as means ± S.E.M. of optical density values normalized to corresponding β-actin. **(C)** Scheme of recording compound action potentials (CAPs) from acutely isolated optic nerves. Representative recording traces from control mice. **(D)** Measurement of maximum peak CAP and **(E)** area underneath CAPs in optic nerves. **(F)** Experimental setup showing the stimulating electrode (on the left) and recording electrode (on the right) within corpus callosum of a coronal section. Corpus callosum from WT mice-evoked CAP showing the components arising from myelinated fibers (N1) and unmyelinated fibers (N2). **(G)** Measurement of corpus callosum peak latency of transgenic mice myelinated fibers (N1) and **(H)** unmyelinated fibers (N2). Scale bar, 1 mm. Data are represented as means; *p<0.05, **p<0.01, ***p<0.001 compared to WT; unpaired Student´s t test.

12. AD transgenic mice present myelin-related abnormalities at ultrastructural level.

Our data demonstrate that the density of mature myelin-producing oligodendrocytes and MBP synthesis are markedly increased in adult AD transgenic mice, raising the possibility that oligodendrocyte differentiation impairment affects myelin formation. To explore this hypothesis, we carried out electron microscopy imaging in rostral and caudal corpus callosum of WT and 3xTg-AD mice at 6-, 12- and 18-month-old mice.

First, we analyzed myelin thickness by measuring the *g*-ratio value (**Figure 38I**). Remarkably, rostral corpus callosum cross-sections showed a significant decrease in the *g*-ratio of 3xTg-AD in comparison with WT at all ages, indicating an increment in myelin thickness (**Figure 38A-E**). Specifically, it was observed that only axons with small caliber ranging from 0.5 to 1 and 0 to 0.5 µm showed increased myelin thickness at 12 and 18 months 3xTg-AD, respectively, compared to WT (**Figure 38G, H**). In contrast, the decrease in the *g*-ratio value was independent of the axon diameter size in 6-month-old 3xTg-AD in comparison to WT (**Figure 38F**).

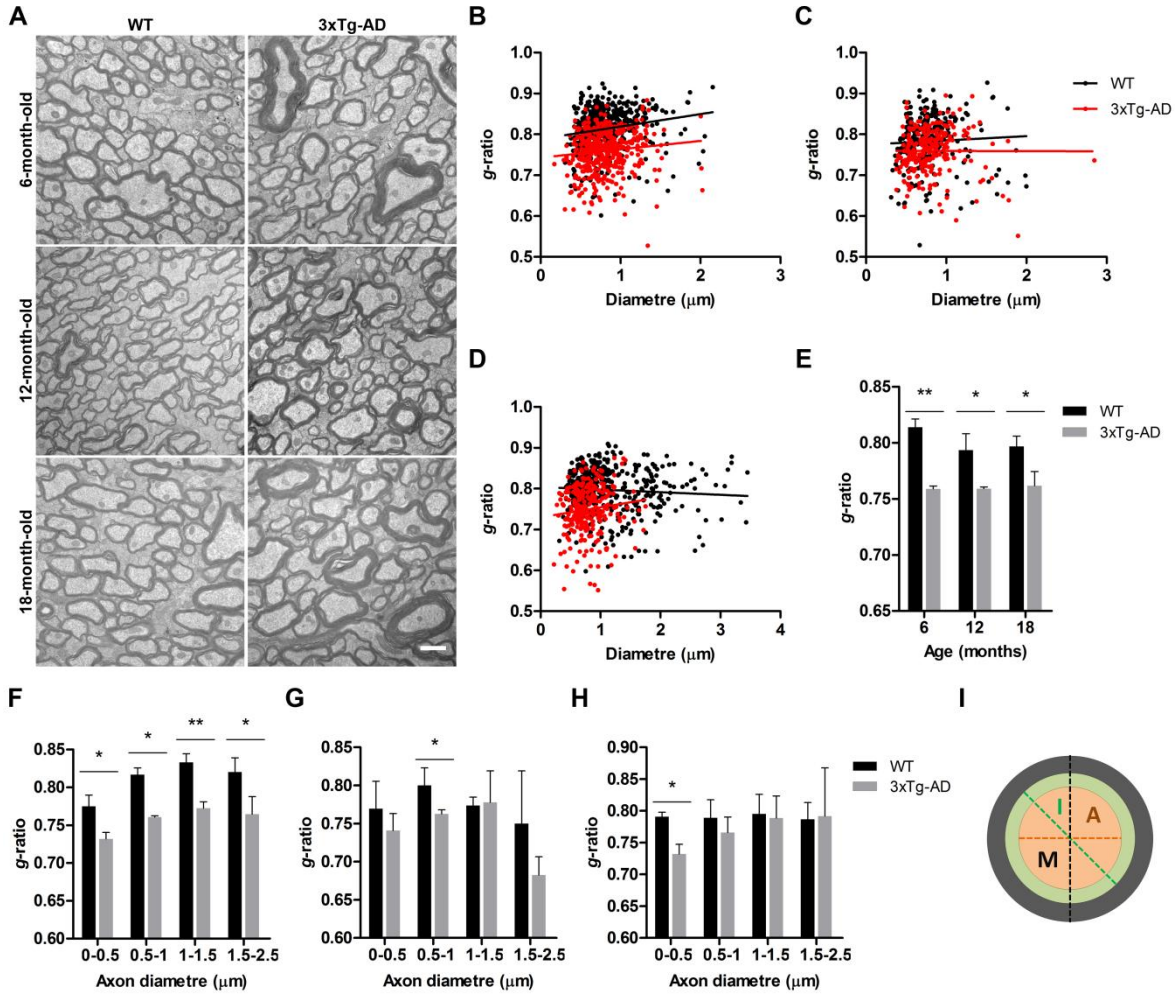

Figure 38. Rostral corpus callosum of AD transgenic mice shows an increased myelin thickness at adult ages. (A) Representative electron micrographs of rostral corpus callosum cross-sections from WT and 3xTg-AD at 6, 12 and 18 months. **(B)** Scatter plots of *g*-ratio of individual axons (y axis) and the corresponding diameter for all axons assessed at 6, **(C)** 12 and **(D)** 18-month-old mice. **(E)** Analysis of *g*-ratio value at all ages (n=3 per group). **(F)** Histograms showing g-ratio grouped by axon diameter in 6-, **(G)** 12- and **(H)** 18-month old WT and 3xTg-AD. **(I)** Schematic cross-section of a myelinated axon illustrating the measured parameters, being *g*-ratio value as I/M. Scale bar, 1 µm. Data are represented as means ± S.E.M; *p<0.05, **p<0.01 compared to WT; unpaired Student´s t test.

Similarly to the outcome observed in the rostral corpus callosum, the caudal zone of 3xTg-AD (**Figure 39A**) showed an increase in myelin thickness at 6 (**Figure 39B**) and 12 months (**Figure 39C**) which was statistically significant compared to WT (**Figure 39E**). However, no significant differences were found at 18 months (**Figure 39D, E**). Moreover, the myelinated axons with 1-1.5 caliber showed myelin thickness differences in 3xTg-AD compared to WT at 6 and 12 months (**Figure 39F, G**).

Overall, these data indicate that corpus callosum of adult 3xTg-AD show an increase in myelin thickness which is mostly present in small-caliber axons.

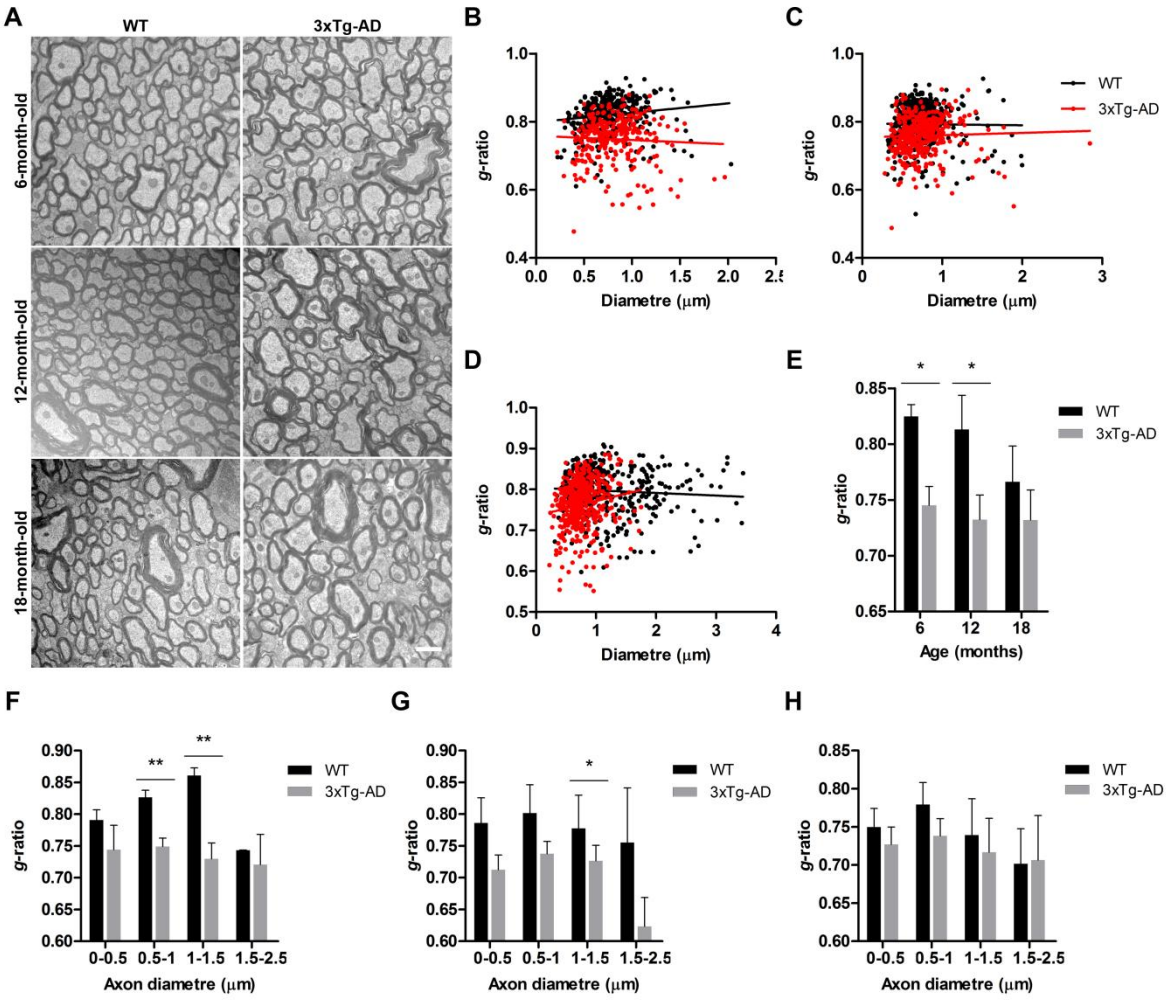

Figure 39. Caudal corpus callosum of AD transgenic mice shows an increased myelin thickness at adult ages. (A) Representative electron micrographs of caudal corpus callosum cross-sections from WT and 3xTg-AD at 6, 12 and 18 months. **(B)** Scatter plots of *g*-ratio of individual axons (y axis) and the corresponding diameter for all axons assessed at 6, **(C)** 12 and **(D)** 18-month-old mice. **(E)** Analysis of *g*-ratio value at all ages (n=3 per group). **(F)** Histograms showing g-ratio grouped by axon diameter in 6-, **(G)** 12- and **(H)** 18-month old WT and 3xTg-AD. Scale bar, 1 μm. Data are represented as means ± S.E.M; *p<0.05, **p<0.01 compared to WT; unpaired Student´s t test.

To further examine the integrity of myelin sheath in WT and 3xTg-AD, we analyzed the inner tongue size of rostral corpus callosum at 6, 12 and 18 months (**Figure 40A**). 3xTg-AD mice showed increased inner tongue size at all ages compared to WT, reaching

up to 263.28% over WT at 18 months (**Figure 40B**). The enlargement of inner tongue observed in 3xTg-AD was strongly associated with small caliber axons (0-0.4 µm) in all ages. In addition, axons with higher diameter also showed myelin with enlarged inner tongue, being affected those from 0.4-0.8 in 6 and 18 months, and all the size range in 12-month-old mice.

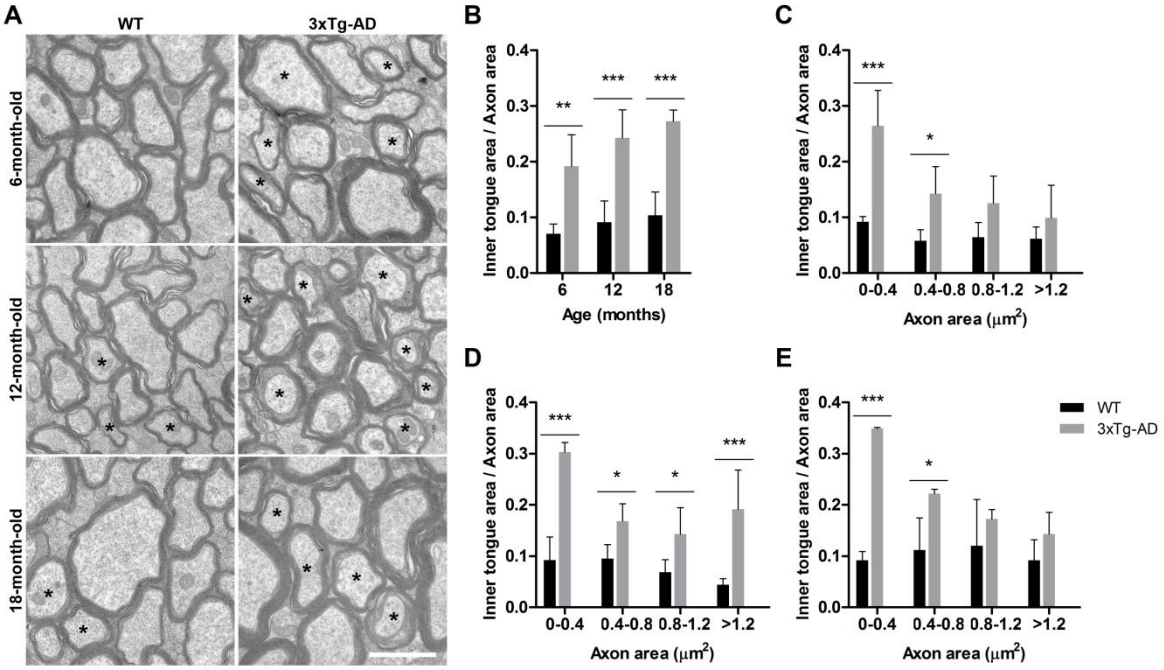

Figure 40. Rostral corpus callosum of AD transgenic mice shows an increment in the inner tongue size at adult ages. (A) Representative electron micrographs of rostral corpus callosum cross-sections from WT and 3xTg-AD at 6, 12 and 18 months. Stars label the myelin fibers with enlarged inner tongue. **(B)** Analysis of inner tongue size from WT and 3xTg-AD mice, measured as inner tongue / axon area (n=3 per group)**.** Data are represented as means ± S.E.M; one-way ANOVA followed by Bonferroni posttest. **(C)** Quantification of inner tongue area grouped by axon area in 6-, **(D)** 12- and **(E)** 18-month old WT and 3xTg-AD. Scale bar, 1 µm. Data are represented as means ± S.E.M; *p<0.05, **p<0.01, ***p<0.001 compared to WT; unpaired Student´s t test.

Moreover, we quantified the inner tongue size in caudal corpus callosum and found that inner tongue area of 3xTg.-AD was increased at 12 and 18 months comparing with WT, while no differences were found in 6-month-old mice (**Figure 41A, B**). Specifically, it was only observed a significant increment of inner tongue size in 3xTg-AD small caliber axons (0-0.4 µm) at 12 and 18 months (**Figure 41D, E**).

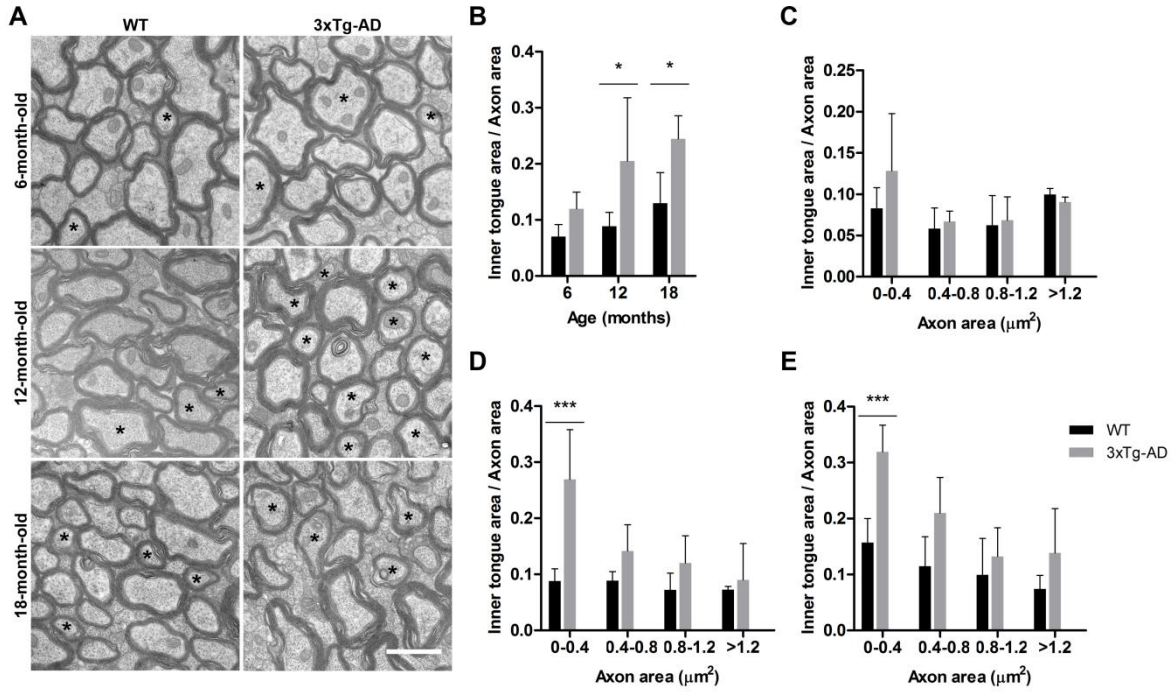

Figure 41. Caudal corpus callosum of AD transgenic mice shows an increment in the inner tongue size at adult ages. (A) Representative electron micrographs of caudal corpus callosum cross-sections from WT and 3xTg-AD at 6, 12 and 18 months. Stars label the myelin fibers with enlarged inner tongue. **(B)** Analysis of inner tongue size from WT and 3xTg-AD mice, measured as inner tongue / axon area (n=3 per group)**.** Data are represented as means ± S.E.M; one-way ANOVA followed by Bonferroni posttest. **(C)** Quantification of inner tongue area grouped by axon area in 6-, **(D)** 12- and **(E)** 18-month old WT and 3xTg-AD. Scale bar, 1 µm. Data are represented as means ± S.E.M; *p<0.05, ***p<0.001 compared to WT; unpaired Student´s t test.

Finally, to extend the analysis of myelin fiber status in the corpus callosum, we evaluated ultrastructural features related to myelin degeneration in 3xTg-AD during ageing. For this purpose, we quantified the following events: enlarged myelin inner tongue (**Figure 42A**), axons with dense cytoplasm (**Figure 42D**), empty fibers (**Figure 42G**), and myelin sheath degeneration (**Figure 42J**) in 6, 12 and 18 month-old mice. First, we observed that the density of myelin fibers with enlarged inner tongue was increased in rostral corpus callosum 3xTg-AD as compared to WT at all ages, reaching up to 23.8% of total myelin sheath in 3xTg-AD, while it only occurred in 12.7% in WT at 18 months. Moreover, the proportion of myelinated axon with enlarged inner tongue increased in an age-dependent manner regardless of genotype (**Figure 42B**), as well as we observed in the caudal zone (**Figure 42C**). In contrast, axons with dense cytoplasm were significantly

increased in 3xTg-AD in comparison with WT at 12 and 18 months in rostral corpus callosum, while were not a pathological feature dependent of age (**Figure 42E**). However, this increment was only observed at 12-month-old 3xTg-AD mice in caudal area (**Figure 42F**). Furthermore, empty myelin sheaths of rostral corpus callosum were examined and found that the proportion of this event was 4.42 fold higher in 3xTg-AD compared to WT at 12 months (**Figure 42H**). No differences were found in the caudal zone of the corpus callosum (**Figure 42I**). Ultimately, since 12-month-old mice degenerative myelin event was significantly increased in 3xTg-AD compared to WT in rostral corpus callosum, maintaining this increment to 18 months (**Figure 42K**). In addition, the incidence of this pathological event was increased with aging. Similarly, it was observed a significant increment in caudal area from 3xTg-AD and WT at 12 months, which in this case was not present in 18-month-old mice (**Figure 42L**). No differences were found in the number of total myelinated axons in 3xTg-AD as compared to WT at all ages in either rostral and caudal corpus callosum (**Figure 42M, N**).

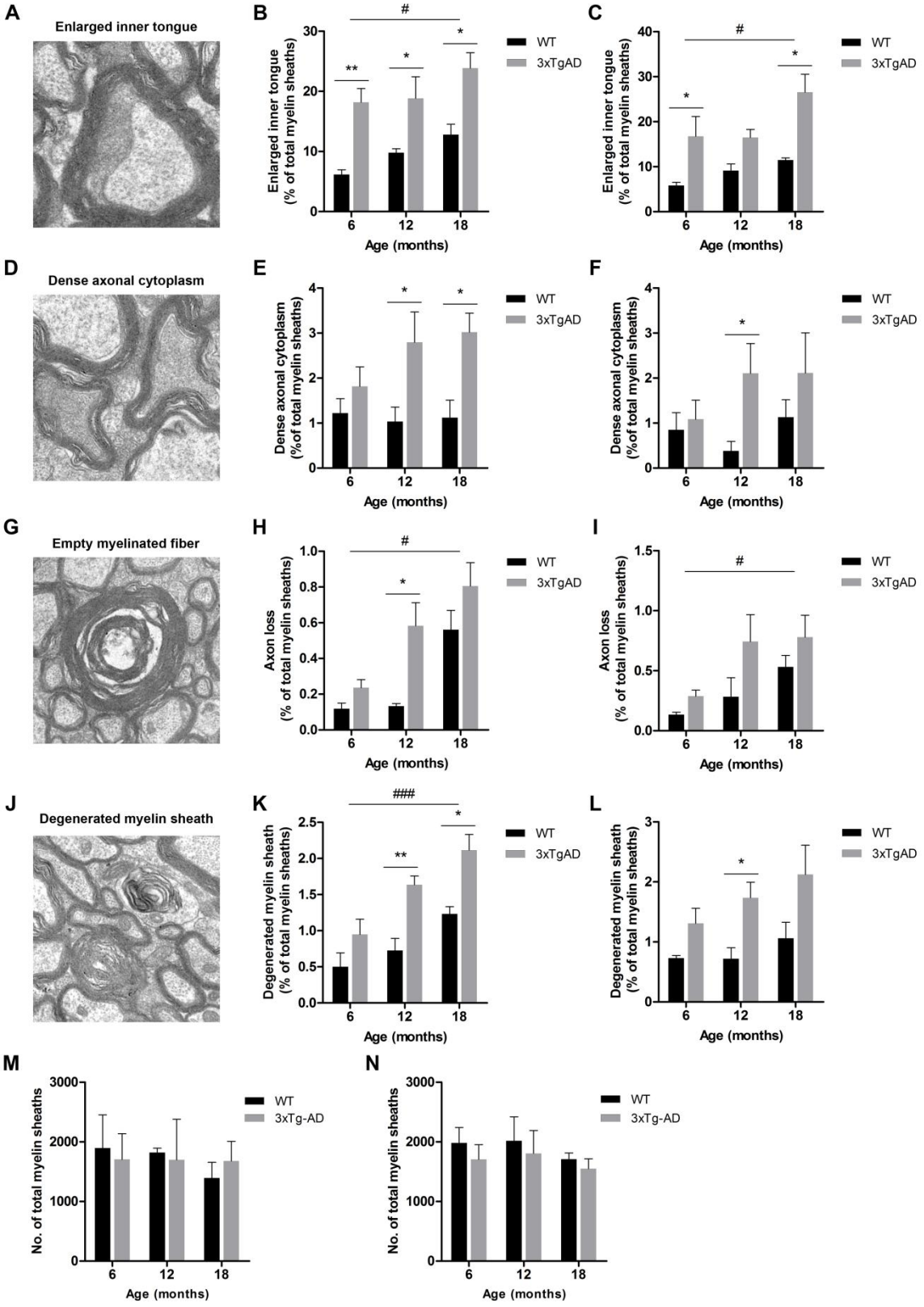

Figure 42. Increased myelin pathology in rostral and caudal corpus callosum of AD transgenic mice. Representative electron micrographs of cross-sections of corpus callosum degenerative events including enlarged inner tongue **(A)**, axon with dense cytoplasm **(D)**, empty fibers **(G)** and degenerative myelin sheath **(J)**. Quantification of enlarged inner tongue **(B, C)**, axon with dense cytoplasm **(E, F)**, empty myelinated fibers **(H, I)** and degenerated myelin sheath **(K, L)** events (n=3 animals per group). Total area analyzed,

2189.71 μm^2. Data are represented as means ± S.E.M; *p<0.05, **p<0.01 compared to WT; #p<0.05, ###p<0.0001 significantly over time; two-way ANOVA followed by Bonferroni posttest.

In summary, the incidence of myelin sheath degenerative events observed in the rostral (**Figure 43A**) and caudal (**Figure 43B**) corpus callosum increased progressively during aging and, remarkably was higher in 3xTg-AD. Concretely, the most common event observed was myelin sheaths with enlarged inner tongue which was detected since 6 months of age, affecting up to 23.8% of myelinated axons in 3xTg-AD. In turn, the prevalence of the other axon and myelin aberrations was smaller, even though it was at least 2 fold higher in 3xTg-AD mice. Moreover, we observed that myelin sheath-associated pathology was more severe in the rostral than in caudal corpus callosum.

Overall, these results demonstrate that oligodendrocyte differentiation and myelin structure are impaired in AD transgenic mice, especially in aged mice. Furthermore, these results suggest that these white matter abnormalities might contribute to the reduction of the conduction velocity in this AD murine model.

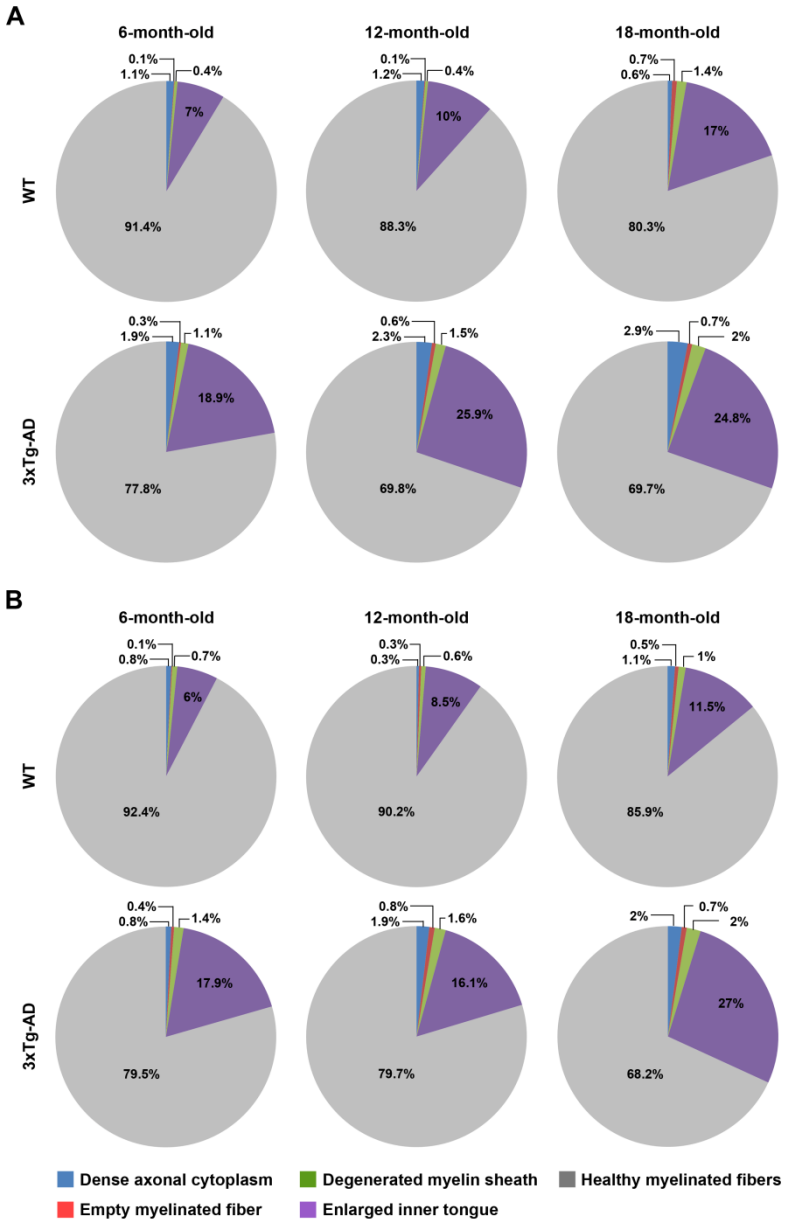

Figure 43. Myelin sheath degeneration in corpus callosum of AD transgenic mice during aging. Pie charts showing the incidence of myelin sheath degenerative events in rostral **(A)** and caudal **(B)** corpus callosum of 6-, 12- and 18-month-old mice WT and 3xTg-AD.

13. Prefrontal cortex and hippocampus of Alzheimer´s disease patients present an increment of MBP levels at advanced stages.

To assess whether oligodendrocyte-produced MBP synthesis is impaired in Alzheimer´s disease, its expression was examined in human *postmortem* samples of prefrontal cortex and hippocampus from healthy subjects and AD patients. Samples from

AD subjects were classified according to Braak stages (II, III, IV or V-VI) (Braak & Braak, 1995) and CERAD criteria (A, B or C) (Mirra et al., 1991). Interestingly, western blot analysis revealed a robust increase of MBP expression in prefrontal cortex of AD patients at CERAD C/Braak V-VI stage as compared to control subjects (**Figure 44A-C**). However, no differences were found at early stages as we observed at CERAD A-B/Braak II, III and V-VI stage. Accordingly, MBP fluorescence intensity was also quantified in prefrontal cortex of last stages and found a 35.77% increase in AD in comparison with control subjects (**Figure 44D, E**). Next, expression of PDGFr-α and Olig2 were examined and it was observed no significant changes in prefrontal cortex of control and AD patients, suggesting that total oligodendrocyte lineage and progenitor cells remained unchanged (**Figure 44F-H**).

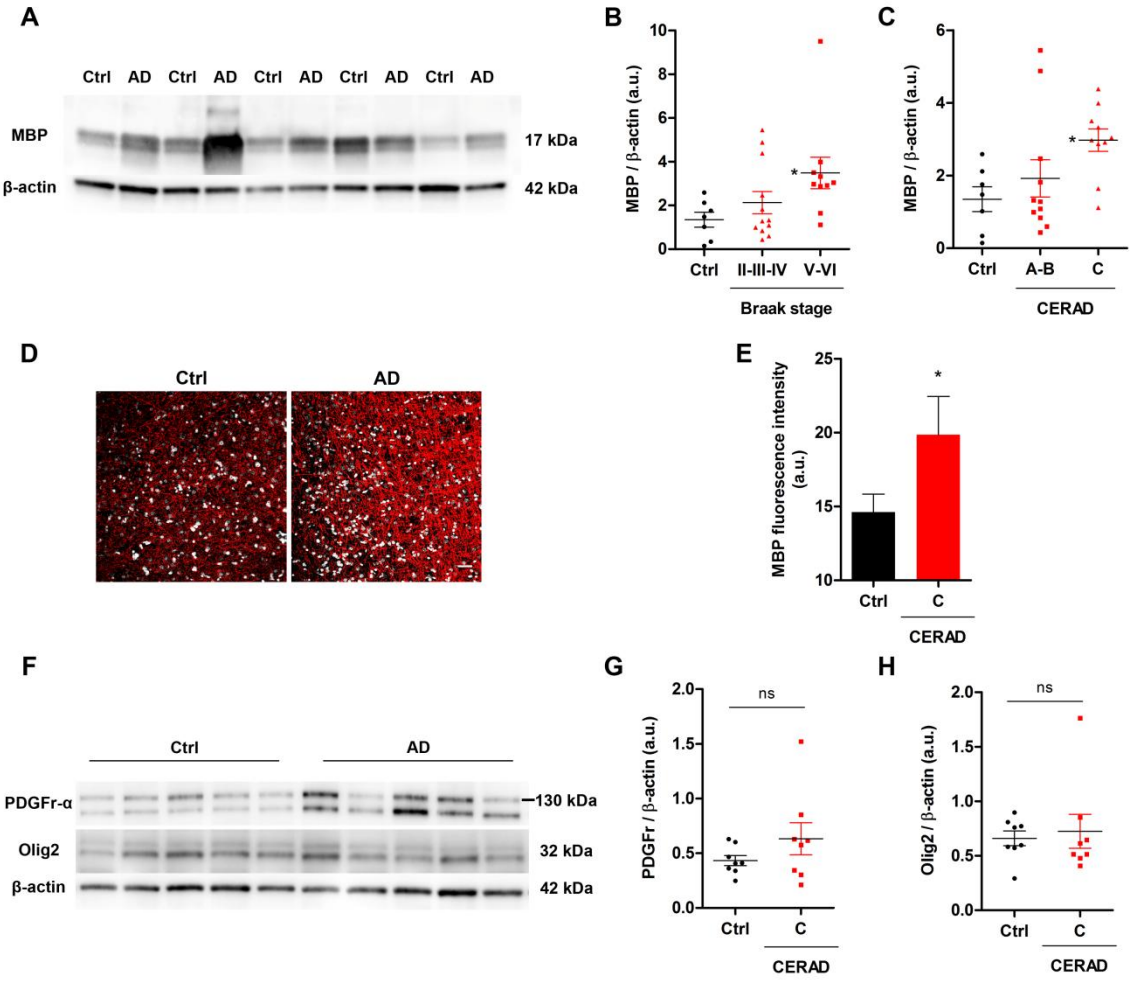

Figure 44. MBP increased levels in prefrontal cortex from AD patients at advanced stages. (A) Western blot of MBP expression in postmortem prefrontal cortex from controls (Ctrl) and AD patients at CERAD C/Braak V-VI stage. **(B, C)** Scatter plot showing MBP levels in Ctrl and AD subjects classified into different Braak stages or according to CERAD criteria (n=10-12 per group). Data are represented as means ± S.E.M.

*p<0.05 compared to Ctrl; Kruskal-Wallis test following by Dunn´s multiple comparison tests. **(D)** Representative confocal z-stack projections showing MBP labeling (red) of prefrontal cortex from Ctrl and AD subjects at CERAD C/Braak V-VI stage. Cell nuclei were visualized with DAPI (white). **(E)** Analysis of MBP fluorescence intensity in human prefrontal cortex (n=4 per group). **(F)** PDGFr-α and Olig2 levels in prefrontal cortex of Ctrl and AD patients at CERAD C/Braak V-VI were detected by western blot. **(G, H)** Scatter plot analysis of PDGFr-α and Olig2 protein expression (n=8 per group). Scale bar, 50 µm. Data are represented as means ± S.E.M. *p<0.05 compared to Ctrl; unpaired Student´s t test.

Indeed, MBP expression analysis in hippocampus of healthy and AD individuals was analyzed, observing a marked increased of MBP levels in AD subjects at late stage (CERAD C) as compared to controls (2.364 ± 0.32 vs. 3.99 ± 0.8, respectively) (**Figure 45A, B**). Then, to describe the specific areas of hippocampus associated with MBP upregulation, immunofluorescence assay was performed (**Figure 45C**). It was observed a significant increment in MBP fluorescence intensity of AD hippocampus at dentate gyrus and CA3, while no differences were found at CA1 and fimbria (**Figure 45D, E**). Moreover, PDGFr-α and Olig2 expression was analyzed and found no significant changes between control and AD subjects (**Figure 45E, F**). Importantly, these results demonstrate a MBP synthesis deregulation in Alzheimer´s disease prefrontral cortex and hippocampus at advanced stages.

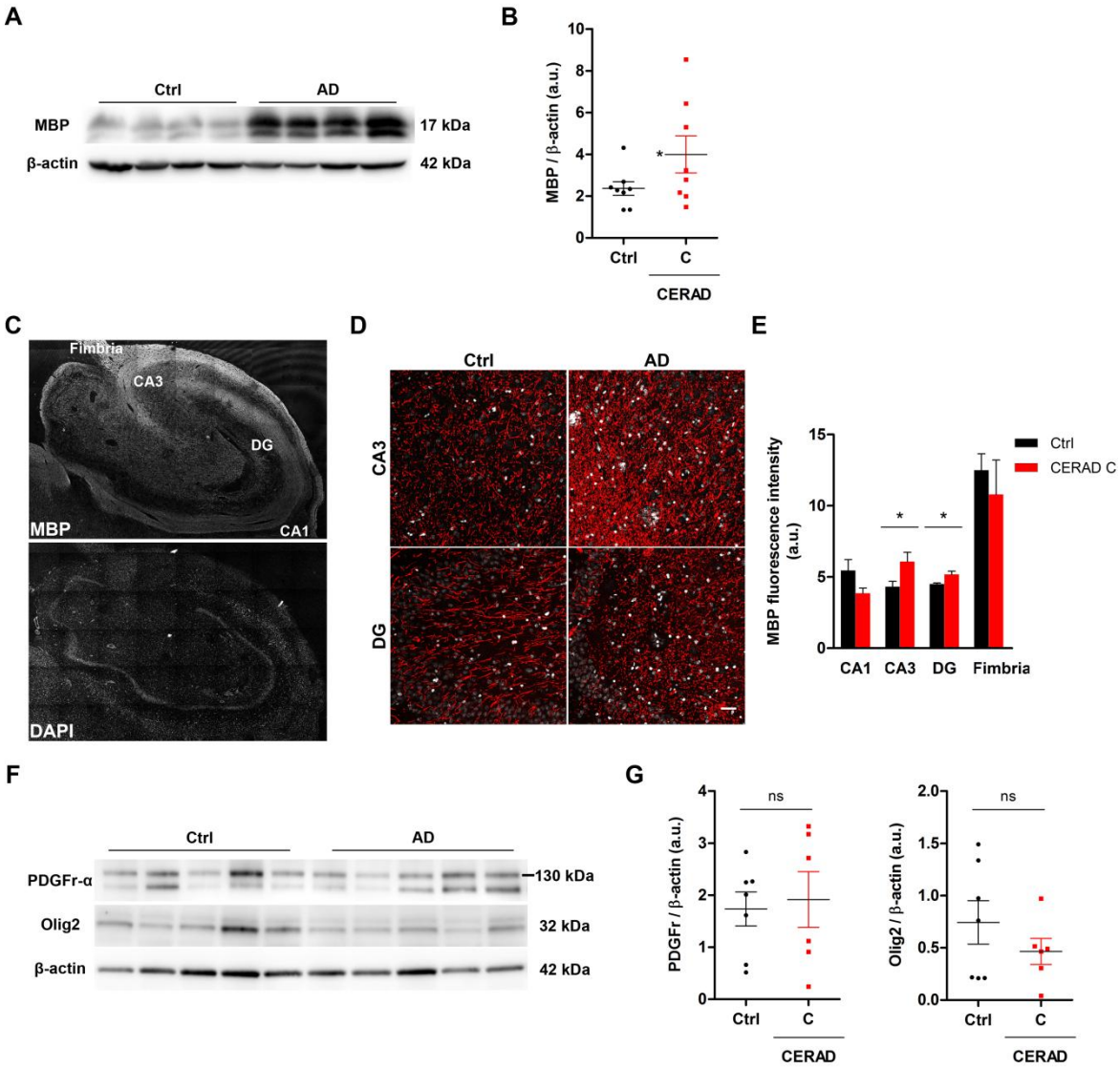

Figure 45. Hippocampus from AD patients show increased levels of MBP at advanced stages. (A) Western blot of MBP expression in postmortem hippocampus from controls (Ctrl) and AD patients at CERAD C/Braak V-VI stage. **(B)** Scatter plot of MBP levels in Ctrl and AD subjects classified according to CERAD criteria (n=8 per group). **(C)** Tile-scan confocal images showing the distribution of MBP expression along the hippocampus of a Ctrl subject. **(D)** Representative confocal z-stack projections showing MBP labeling (red) in the CA1, CA3, dentate gyrus (DG) and fimbria from Ctrl and AD subjects at CERAD C/Braak V-VI stage hippocampus. Cell nuclei were visualized with DAPI (white). **(E)** Quantification of MBP fluorescence intensity in human hippocampus (n=3 per group). **(F)** PDGFr-α and Olig2 levels in hippocampus of Ctrl and AD patients at CERAD C/Braak V-VI were detected by western blot. **(G, H)** Scatter plot analysis of PDGFr-α and Olig2 protein expression (n=6-7 per group). Scale bar, 50 µm. Data are represented as means ± S.E.M. *p<0.05 compared to Ctrl; unpaired Student´s t test.

14. Cerebrospinal fluid of mild cognitive impairment patients presents MBP and CNPase increased levels.

It has been identified myelin-related proteins, as MBP and CNPase in human cerebrospinal fluid (CSF) (Banik, Mauldin, & Hogan, 1979; Whitaker, 1998). Since we have detected increased levels of MBP in the brain of AD patients, we asked whether the amount of this myelin protein was also modified in the CSF samples. For that, we analyzed MBP and CNPase levels in CSF samples from controls, mild cognitive impairment and AD subjects. Western blot analysis showed that MCI patients had remarkably higher levels of MBP and CNPase as compared to controls, while no differences were found between AD and controls samples (**Figure 46A**). In addition, both proteins correlate positively in CSF samples of each diagnostic group, being the correlation higher in MCI and AD groups (**Figure 46B**).

These data indicate that myelin proteins such as MBP and CNPase are present in the CSF from controls subjects, as well as from MCI and AD patients, being significantly increased in MCI (**Figure 46C**).

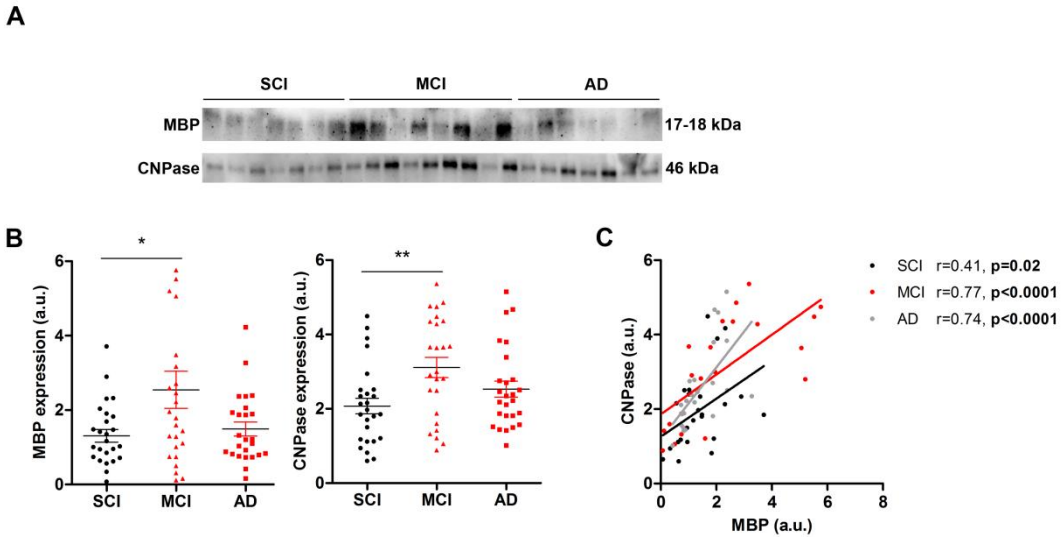

Figure 46. MBP and CNPase levels are increased in MCI cerebrospinal fluid. (A) Western blot of MBP and CNPase expression in CSF from SCI, MCI and AD patients **(B)** Scatter plot analysis of MBP and CNPase levels obtained by Western blot (n=25-26 per group). Data are represented as means ± S.E.M. *p<0.05, **p<0.01 compared to SCI; one-way ANOVA followed by Bonferroni posttest. **(C)** Correlation analysis between MBP

and CNPase levels from SCI, MCI and AD subjects. Each symbol represents an individual (SCI, black; MCI, red; AD, grey). Spearman correlation test.

Discussion

Discussion

AD is characterized by a progressive evolution of cognitive deficits which correlate with the amount of Aβ soluble oligomers. Although it is a disorder mainly associated to neuronal damage, evidences of white matter (WM) disruption previous to neuronal damage have been observed in AD brains (Roher et al., 2002). In the present study we showed that pathogenic Aβ-mediated activity modulates oligodendrocyte differentiation and myelination, promoting MBP upregulation by regulating local mRNA translation. Specifically, we have described the molecular pathways underlying this modulation in which integrin β1 and Fyn are involved. Interestingly, oligodendrocyte differentiation impairment leads to disruption in myelin integrity resulting in failures in neurotransmission *in vivo* in AD model. Moreover, AD patients exhibited increased MBP levels, being myelin proteins dysregulation observed in CSF samples from patients with mild cognitive impairment, expanding the knowledge of new biomarkers for AD. These results strongly support the role of Aβ over oligodendrocytes function as key piece in the progression of AD.

1. $A\beta_{1-42}$ oligomers regulate oligodendrocyte MBP synthesis by promoting mRNA local translation *in vitro*.

The presence of senile plaques composed by insoluble aggregates of the amyloid β peptide (Aβ) is considered one of the main pathological features of AD. It has been described that soluble forms of this peptide are toxic and its presence correlates with the progression of the disease, becoming Aβ a key feature in AD (Santos et al., 2012). Classically, AD studies have been focused on understanding neuron pathology and describing Aβ-mediated neuronal loss. However, white matter damage (WM) is an important feature in AD patients and several evidences have established a direct relation between Aβ and myelin disruption (Desai et al., 2010; Roher et al., 2002b). In spite of the importance that WM and myelin has in AD, a few studies have analyzed the Aβ involvement in the alteration of glial cells function is still poorly studied.

In this thesis, we first analyzed the role of $A\beta_{1-42}$ oligomers in oligodendrocyte differentiation and myelination. Interestingly, we observed that low concentrations of oligomeric Aβ promote myelin-related proteins synthesis, increasing the expression of MBP and CNPase, as well as oligodendrocyte progenitor receptor PDGFr-α. This protein upregulation was observed after stimulating cerebellar organotypic slices with Aβ. In accordance with this, Aβ oligomers also promoted MBP synthesis increase in primary oligodendrocyte culture, in which these glial cells are isolated, indicating that Aβ-mediated MBP upregulation is due to a direct effect on oligodendrocytes. Increased levels of MBP synthesis triggered by Aβ were accompanied by a larger occupied area by cell bodies and processes of individual mature oligodendrocyte. This morphological aspect observed in response to Aβ may reflect later stages of oligodendrocyte maturation characterized by processes extension and MBP synthesis.

In relation with this, cells treated with Aβ showed significant increased levels of MBP only at peripheral areas, raising the possibility of mRNA local translation. Thus, since it is known that MBP mRNA is transported from the nucleus to the oligodendrocyte processes where it is translated locally (Trapp et al., 1987; Ainger et al., 1993, 1997), we analyzed MBP expressing-mRNA by FISH and found that, indeed, Aβ induced MBP mRNA translation at a local level in cultured oligodendrocytes. However, we did not observe an Aβ-mediated regulation of MBP mRNA synthesis in cultured oligodendrocytes, although number of MBP transcripts was increased in Aβ-treated organotypic slices, as measured by RT-qPCR. In this sense, it is possible that modulation of RNA synthesis highly depends on the duration of Aβ treatment. While organotypic slices were stimulated with Aβ for 48 h, the treatment period in cultured oligodendrocytes was shorter (24 h), which may contribute to the opposing results obtained in relation to induction of MBP transcription. Alternatively, Aβ effects may vary depending on the culture method; while cultured oligodendrocytes are isolated cells, organotypic slices are three-dimensional structures composed of different cell types that may also react to Aβ stimuli.

To further analyze the role of Aβ in AD, we induced lysophosphatidylcholine-mediated demyelination to cerebellar organotypic slices (Birgbauer et al., 2004). Since alterations in myelination patterns in AD have been reported observing focal demyelinated areas (Desai

et al., 2009), we used this well-established model to examine the Aβ-mediated effects on oligodendrocytes under pathological conditions. Remarkably, after demyelination Aβ enhanced remyelination process which is in line with our previous results, pointing to Aβ as a positive modulator of oligodendrocyte myelination. In contrast, a previous *in vitro* study showed that treatment with 1 μM $A\beta_{1-42}$ for 4 days reduced oligodendrocyte myelin sheath formation, while no changes were observed in the number of MBP^+ cells and in MBP expression (Horiuchi, Maezawa, Itoh, Wakayama, Jin, et al., 2012). These differences could be due to methological issues; in this report by Horiuchi and co-workers both Aβ time exposure and oligodendrocyte differentiation stage in which stimuli was added were different in comparison with our study. Therefore, this data may indicate that the sensitivity to Aβ depends on the oligodendrocyte differentiation stage. This hypothesis is in accordance with results observed in the same study in which Aβ for 48 h promote cytotoxicity in mature oligodendrocytes, but not to OPCs (Horiuchi, Maezawa, Itoh, Wakayama, Jin, et al., 2012).

In addition, it has been proposed that oligodendrocytes are able to dispose of overproduced myelin components by releasing extracellular vesicles (EVs) with myelin-specific cargo (Krämer-Albers et al., 2007). As MBP upregulation is observed after Aβ exposure, we also analyzed oligodendroglial EVs release in response to oligomeric Aβ. For that, specific EVs markers and myelin-related proteins, such as MBP and CNPase, were examined in EV-enriched fraction. MBP and CNPase levels were increased after Aβ stimuli, as well as the EV specific markers CD81 and CD63, suggesting that Aβ stimulate the release of EVs containing MBP and CNPase. The increase in EVs release in response to Aβ could be a cellular mechanism to maintain myelin production balance and avoid cellular damage, as reported previously (Frühbeis, Fröhlich, & Krämer-Albers, 2012). However, due to the role of oligodendrocyte EVs in promoting and maintaining neuronal viability (Frühbeis et al., 2013), the dysregulation in oligodendroglial EV secretion triggered by Aβ may contribute to neuronal pathology in AD.

Overall, these findings provide a specific role of Aβ in MBP synthesis regulation by promoting local mRNA translation and stimulating its release including in EVs.

2. Integrin β1 mediate oligomeric Aβ-promote MBP upregulation through Fyn and CaMKII activation.

In this study we have demonstrated for the first time that oligomeric Aβ directly act on oligodendrocytes to induce MBP synthesis. In addition to this, we have described the molecular pathway underlying this protein modulation. Our data indicate that integrin β1 (Itgb1) receptor participates in Aβ-mediated MBP expression increase through Fyn activation. Aβ signaling also induces the release of Ca^{2+} from the endoplasmic reticulum (ER) followed by CaMKII activation, finally resulting in MBP synthesis increase.

Several Aβ oligomer receptors have been described through which this peptide promotes a wide range of cellular effects (Viola & Klein, 2015). Among them, integrin receptors have been proposed to interact with Aβ oligomers. Various properties have been attributed to integrin activity in oligodendrocyte, as its role in oligodendrocyte proliferation and survival, or its influence on cytoskeletal remodeling to permit a correct differentiation and myelination (O'Meara, Michalski, & Kothary, 2011). Remarkably, Itgb1 is involved in synaptic dysfunction triggered by Aβ signaling (Woo et al., 2015). Moreover, Itgb1 is activated by Aβ in isolated astrocytes leading to oxidative stress and astrogliosis (Wyssenbach et al., 2016). However, the activation of integrin receptor by oligomeric Aβ in oligodendrocytes has not been reported up to now.

In this study, we found that Itgb1 and Itgb8 mRNA expression increased in the presence of Aβ. As previously mentioned, Itgb8 has been found to be highly expressed along oligodendrocyte maturation process, while Itgb1 expression decreases (Milner *et al*., 1997). In this sense, since Aβ induces cell maturation *in vitro*, it is likely that the observed Itgb8 upregulation is an indirect consequence of Aβ-promoted oligodendrocyte differentiation. Thus, we focused our research efforts on analyzing the role of Itgb1 in MBP regulation and found that, in the presence of Aβ oligomers, its protein levels were increased. Therefore, this increment in Itgb1 protein expression may result in an increased abundance and availability of molecules of this receptor in the cell surface, exacerbating Aβ-induced MBP upregulation. In addition, due to the influence of Itgb1 on cytoskeleton-remodeling proteins, which are necessary for myelin processes outgrowth

(O'Meara et al., 2011), Itgb1 may also be responsible for the increased occupied area in Aβ-treated oligodendrocytes.

Since Aβ did not modulate MBP mRNA synthesis and transport, MBP upregulation in cultured oligodendrocytes is probably due to mRNA local translation. Integrin $\alpha_6\beta_1$ is known to directly associate with Fyn in oligodendrocytes to mediate oligodendrocyte maturation and local translation of MBP (Colognato, Ramachandrappa, Olsen, & ffrench-Constant, 2004; Laursen, Chan, & Ffrench-Constant, 2011). Fyn activation results in a breakdown of the specialized RNA transport granules by phosphorylation of granule specific proteins, releasing MBP mRNA from its inhibitors and allowing its translation. Thus, we analyzed the role of Fyn in Aβ-mediated MBP synthesis and found that after Aβ stimuli Fyn was phosphorylated and its inhibition, together with iItgb1 blockade, resulted in MBP synthesis reduction. Thus, these data suggest that oligomeric Aβ promotes MBP upregulation by inducing MBP local translation leaded by activated Itgb1 and kinase Fyn.

On the other hand, we analyzed intracellular Ca^{2+} levels in cultured oligodendrocytes and found a disturbance in cellular Ca^{2+} homeostasis in response to Aβ, increasing cytosolic Ca^{2+} amount by releasing it from ER. These results are in accordance with the role of Aβ in regulating intracellular Ca^{2+} flux described in neurons and in astrocytes (Alberdi et al., 2010; Suen et al., 2003; Wyssenbach et al., 2016). In neurons, Aβ-triggered Ca^{2+} intracellular increment is also released from the ER and specifically, through ryanodine receptors (Resende, Ferreiro, Pereira, & Resende de Oliveira, 2008; Suen et al., 2003). According to this, after blocking ryanodine receptors in cultured oligodendrocytes, the increased Ca^{2+} levels triggered by oligomeric Aβ were attenuated, suggesting that ER ryanodine receptors are involved in Aβ-mediated Ca^{2+} mobilization. Remarkably, cytosolic Ca^{2+} increase was promoted by Aβ-induced Fyn activation and its inhibition results in MBP levels decrease, pointing to Ca^{2+} as MBP synthesis modulator. Similarly, it has been described the role of Ca^{2+} in local translation after nerve injury (Yudin et al., 2008). Thus, these data suggest that MBP was locally synthesized in a calcium-dependent manner after Aβ stimuli. In addition, we observed that this secondary messenger promoted CaMKII activation, being also implicated in Aβ-mediated MBP upregulation. In this sense, it have been described the role of CaMKII in local translation in hippocampal dendrites. CaMKII

phosphorylates cytoplasmic polyadenylation element-binding protein (CPEB), which binds to a specific region of mRNA the cytoplasmic polyadenylation element CPE, allowing translation initiation (Atkins, Nozaki, Shigeri, & Soderling, 2004). Interestingly, CPE region is also present in MBP mRNA (Carson et al., 2008). Thus, since we described that CaMKII is involved in MBP synthesis and it is known that the process of transmission of RNA molecules from nucleus to periphery and its local translation is quite analogous in neurons and oligodendrocytes, it is possible that the mechanisms by which CaMKII is mediating MBP synthesis involve CPEG phosphorylation.

On the other hand, CAMKII also regulates CNS myelination and oligodendrocyte maturation, which require a dynamic process extension through activating cytoskeletal remodeling proteins in which CAMKII participates (Waggener, Dupree, Elgersma, & Fuss, 2013). Thus, similarly to Fyn, this protein could be taking part on the increase in the occupied area in oligodendrocytes treated with Aβ in addition to MBP upregulation.

Taken together, we have described that oligomeric Aβ through integrin β1 receptor and subsequent Fyn activation promotes MBP upregulation by mechanisms that involve Ca^{2+} signaling.

3. $A\beta_{1-42}$ oligomers promote oligodendrocyte differentiation and survival.

To further investigate the role of Aβ in oligodendrocyte differentiation, we analyzed oligodendrocyte lineage differentiation patterns after Aβ exposure. Low concentration of oligomeric Aβ promoted an increase in the number of late progenitor $O4^+$ cells and mature MBP^+ cells in primary oligodendrocyte cultures. These data suggest that depending on oligodendrocyte stage of development, Aβ promotes oligodendrocyte differentiation. Thus, Aβ specifically induce the maturation of early to late progenitor and immature to mature cells.

In addition to regulating oligodendrocyte maturation, Aβ also modulates cell survival. In this sense, we observed that oligomeric Aβ has a protective effect on cultured oligodendrocytes by enhancing its cell viability in a dose-dependent manner.

Interestingly, we observed that the molecular mechanisms Aβ-leaded cell death protection are similar to those described for Aβ-mediated MBP synthesis increase, being Src family kinase and CaMKII also relevant in this process. Since we observed that Aβ activates Fyn, and evidences of the role of Fyn kinase in oligodendrocyte survival have been described (O'Meara et al., 2011), it is possible that Fyn is also involved in oligodendrocyte death protection triggered by Aβ.

Similarly to the synthetic oligomeric peptide, natural Aβ secreted from neurons overexpressing human APP with Swedish mutation (SWE) also improved the cultured oligodendrocyte viability. In contrast, a few studies have illustrated that Aβ peptides are able to induce toxicity in oligodendrocytes (Horiuchi, Maezawa, Itoh, Wakayama, & Jin, 2012; J.-T. Lee et al., 2004). However, differences in the forms of Aβ or in the timing of treatment could explain these contradictory results.

On the other hand, since we observed that oligomeric Aβ is able to enhance oligodendrocyte survival as well as to promote its differentiation, these data may suggest a physiological role of Aβ in oligodendrocytes. In this sense, several reports have described that low doses of Aβ enhance memory in young mice, and facilitate induction and maintenance of long term potentiation (Morley et al., 2010). Moreover, it has been described that Aβ is secreted by neurons during excitatory neuronal activity to maintain its appropriate levels and control synaptic activity (Cirrito et al., 2005; Kamenetz et al., 2003). Thus, it seems possible that low concentrations of Aβ have a potential gliotrophic role acting as a survival modulator and enhancer of MBP synthesis in cultured oligodendrocytes. However, as previously discussed, Aβ promotes MBP expression through Itgb1, but also induces this receptor upregulation. This may contribute to a positive feedback amplifying intracellular signals. Therefore, in the context of AD, where a chronic exposition to Aβ occurs, a major dysregulation of MBP synthesis and oligodendrocyte differentiation can take place.

Overall, our results highlight the involvement of soluble $A\beta_{1-42}$ oligomers in oligodendrocyte regulation, including MBP synthesis, cell differentiation and survival, and

further suggest that this peptide may have a relevant role in oligodendrocyte pathology in AD.

4. Oligodendrocyte differentiation is impaired in triple transgenic AD mice at adult ages.

Several animal models have been used to mimic AD disorder and facilitate its study. However, none of them have been successfully able to recapitulate all the pathological features of this disease. The generation of AD triple transgenic mice (3xTg-AD) has brought a great advance in AD research since it develops both amyloid plaque and neurofibrillary tangle pathology in AD-relevant brain regions. In turn, this model acquires extracellular Aβ deposits prior to tangle formation, which is consistent with the amyloid cascade hypothesis.

Although AD has been traditionally considered to be a gray matter (GM) disease, evidence of white matter (WM) pathology from animal models and AD patients have also been reported (Firbank et al., 2007; Kavcic, Ni, Zhu, Zhong, & Duffy, 2008; Roher et al., 2002b). Moreover, early stages of AD pathology show WM atrophy prior to observing GM degeneration suggesting that axonal or myelin chemical abnormalities provoke neuronal loss degeneration (Bartzokis et al., 2003, 2004; Brun & Englund, 1986; Kavcic et al., 2008; Price et al., 2001). Thus, by using this AD mouse model we further examined oligodendrocyte differentiation and myelination. To this purpose, MBP expression was first analyzed specifically in corpus callosum and hippocampus, WM and GM regions which are affected in AD and their impairment correlates with the progression and severity of the disease (Teipel et al., 2002). As AD is an aging-related disorder, we focused our analysis in several ages covering from early AD stage in adult mice to advanced stages observed in older mice. Here, we demonstrated that in 3xTg-AD a marked increase in MBP expression both in corpus callosum and hippocampus is occurring. This increment was observed since 6 months of age and is maintained until 18 months, without any significant differences in axonal damage between wild-type and transgenic mice. Hippocampal MBP expression was analyzed in detail at 18 month-old mice, observing increased levels only in CA3 and dentate gyrus, while CA1 did not show changes. Similarly,

a recent study demonstrated that APP/PS1 transgenic mice show MBP upregulation in hippocampus at early AD stages (Wu et al., 2017a). However, in our model the MBP increase associated with the pathology has not been described to the date, being reported a decrease in 3xTg-AD entorhinal cortex (Desai et al., 2009). Thus, it seems that MBP level alterations, which are not accompanied by axonal damage at early stages of AD, may be region-specific, as previously proposed (Desai et al., 2009). However, in contrast with our results, Desai and coworkers did not observe significant changes in the hippocampus of 6-month-old mice. Therefore, our data suggest that an upregulation of MBP expression occurs in 3xTg-AD since early stages of the pathology, preceding axonal damage and likely being related to primary white matter changes associated with the disease.

The significant increased levels of MBP observed in 3xTg-AD mice may be due to a greater density of mature oligodendrocyte population and/or to an increment in MBP synthesis. To address these possibilities, first we analyzed the number of oligodendrocyte lineage cells, specifically PDGFr-α^+ progenitor cells and $CC1^+$ mature oligodendrocyte cells and found that 3xTg-AD have a higher number of PDGFr-α^+ cells at 6 months of age, while at 18 months they remained unchanged. In contrast, the density of $CC1^+$ mature cells is only increased in 18 month-old mice in the corpus callosum and in hippocampal DG of transgenic mice. However, 3xTg-AD show increased levels of MBP since 6 months of age. This suggests that, while at 6 months MBP alterations occurs mainly through upregulation of its synthesis, at 18 months both MBP synthesis and the number of mature oligodendrocyte population may take part on this process.

In addition, as a result of aging it was observed a marked loss of oligodendrocytes ($Olig2^+$ cells) and specifically mature population. Interestingly, this aging-associated death is attenuated in transgenic mice. One possibility is that the higher number of mature oligodendrocytes observed in 3xTg-AD at 18 months may derive from oligodendrocyte proliferation and subsequent differentiation in mature cells. Alternatively, an enhanced survival of oligodendrocytes may be occurring. These two possibilities, oligodendrocyte maturation and survival are not mutually exclusive. In accordance with our results, increased number of $CC1^+$ mature cells was also detected in hippocampal CA1 in 3xTg-AD

mice (Desai et al., 2010). Similarly, APP/PS1 mice exhibit increased proliferation of $NG2^+$ cells followed by generation of mature oligodendrocytes in corpus callosum (Behrendt et al., 2013). Thus, these evidences reveal the generation of new mature oligodendrocyte in AD mouse model. In fact, our *in vitro* results demonstrate that Aβ oligomers are able to directly enhance oligodendrocyte survival and promote its maturation. Taking this into account, it seems very likely that both oligodendrocyte maturation and survival may be contributing to oligodendrocyte increase observed in 3xTg-AD mice.

Hypothetically, these changes in oligodendrocyte lineage population are leaded by AD-related pathophysiological mechanisms. However, it is possible that a compensatory response to brain damage is also occurring. In this model it has been observed a demyelination process in specific areas as hippocampal CA1 and enthorhinal cortex (Desai et al., 2009). As occurs in other lesions, adult progenitors are able to differentiate into oligodendrocytes capable of remyelinating axons (Zawadzka et al., 2010). Although, we cannot completely rule out this hypothesis, strong evidences point to AD-mediated oligodendrocyte changes, specifically involving the role of Aβ.

In this sense, white matter abnormalities have been reported in the 3xTg-AD and APP/PS1 transgenic mice correlating with elevated levels of intracellular Aβ prior to the manifestation of plaque and tangle pathology (Desai et al., 2010; Wirths, Weis, Szczygielski, Multhaup, & Bayer, 2006). According to this, we observed by western blot a positive correlation between MBP upregulated levels and Aβ amount in the hippocampus of 18-month-old transgenic mice. In addition, we detected alterations in oligodendrocyte population and MBP synthesis at a time point when high amounts of Aβ oligomers and few amyloid plaques are reported, and no signs of concomitant Tau pathology is observed (Oddo et al., 2006). More interestingly, Desai and coworkers described elevated $CC1^+$ mature cells in hippocampal CA1 of 3xTg-AD, similarly to what we observed in corpus callosum, which were reduced by injection with an anti-$A\beta_{1-42}$ engineered intrabody, indicating a direct effect of Aβ in oligodendrocyte survival or differentiation. On the basis of the above and our results obtained *in vitro* in which Aβ directly regulated oligodendrocyte differentiation, we can conclude that impaired oligodendrocyte

differentiation observed in triple transgenic mouse model is mainly triggered by Aβ pathology.

Triple transgenic mice (3xTg-AD) harbor three mutations: human tau ($htau^{p30L}$), human amyloid precursor protein Swedish mutation ($hAPP^{Swe}$) and human presenilin-1 ($hPS1M^{146V}$). $hAPP^{Swe}$ and $htau^{p30L}$ mutant transgenes are expressed exclusively in neurons, while $hPS1M^{146V}$ can be ubiquitously expressed, including in oligodendrocytes. PS1 is the catalytic component of γ-secretase complex, mainly known for its role in amyloidogenic processing of APP (Scheuner et al., 1996). Previous studies have also described that γ-secretase is involved in oligodendrocyte maturation but contradictory results have been reported in oligodendrocyte primary cells and co-cultured with neurons (Lai & Feng, 2004; Watkins, Emery, Mulinyawe, & Barres, 2008). In addition, this familial AD mutation has been shown to increasing oligodendrocyte vulnerability to several insults associated with AD, including Aβ (Desai, Guercio, Narrow, & Bowers, 2011; Pak, Chan, & Mattson, 2003). Previous studies have revealed that oligodendrocyte cells transfected with $PS1M^{146V}$ show no differences in the number of $CC1^{+}$ cells and MBP expression (Desai et al., 2011). This suggests that alterations in oligodendrocyte differentiation patterns observed in 3xTg-AD mice are not directly triggered by $PS1M^{146V}$ mutation expressed in oligodendrocytes. Remarkably, after Aβ treatment the density of mature cells are increased in $PS1M^{146V}$–expressing oligodendrocyte cells, while MBP expression decrease, which highlights the role of Aβ in oligodendrocyte differentiation. In this sense, our results are in accordance with observations about oligodendrocyte lineage in APP/PS1 mice (Behrendt et al., 2013; Wu et al., 2017a), a mouse model of AD in which both mutations are exclusively expressed in neurons, which helps to exclude direct effects of the PS1 mutations in oligodendrocyte lineage. In conclusion, these evidences suggest that Aβ-related insults impact oligodendrocyte independent of PS1 mutant expression, although PS1 mutation may exacerbate Aβ effects.

5. Oligodendrocyte myelination impairment contributes to reduced conduction velocity in AD mice.

AD is characterized by the impairment of several neural processes, including attention, visual-spatial processing and generalized processing speed, in which the correct functioning of WM is essential. Since 3xTg-AD exhibit oligodendrocyte lineage impairment, we aimed to measure the axon impulse transmission in 3xTg-AD. Thus, we analyzed the conduction velocity in optic nerve and corpus callosum of 18-month-old mice by recording compound action potentials (CAPs), both areas being affected by MBP upregulation. First, we observed a significantly reduced conduction velocity in 3xTg-AD optic nerve, raising the possibility that myelin impairment is the main cause of axonal dysfunction in this AD mouse model. According to this hypothesis, we observed that axonal conduction velocity of corpus callosum was markedly slower in myelinated 3xTg-AD axons (N1), while no differences were found in unmyelinated ones (N2). As exclusively myelinated axons show functional failures related to AD pathology, these data suggest that 3xTg-AD develop functional defects in axonal conduction as a result of myelin alterations.

Several factors related to myelin structure can determine and affect the velocity of axonal conduction. Among them, the length and the density of nodes of Ranvier along a fiber markedly influence conduction velocity (Arancibia-Cárcamo et al., 2017). Therefore, to determine in detail the myelin features involved in reducing conduction velocity in AD mouse model, we first examined nodes of Ranvier in the corpus callosum of adult mice and found increased density in 3xTg-AD at 18 months mice, also showing shorter length. At this time, coinciding with this node structure impairment, an elevated density of oligodendrocyte mature cells was detected in transgenic mice. It is described that mature oligodendrocytes generated in adult ages produce more and shorter internodes (Young *et al*., 2013). Therefore, these findings are consistent with the idea of new mature oligodendrocytes leaded by increasing oligodendrocyte differentiation in AD mice. Thus, these data suggest that the higher number in the nodes of Ranvier observed in 3xTg-AD may be produced by newly generated mature oligodendrocyte, consistent with the idea of increased oligodendrocyte differentiation in this AD mouse model. The increase of

nodes of Ranvier in transgenic mice may result in shorter internodal length which is associated with a reduction in conduction velocity (Seidl, 2014; Young et al., 2013).

It has been reported that subtle changes in myelin thickness and integrity are also able to determine axonal function (Waxman, 1997). In addition, several evidences of alterations in myelin structure as node impairment and MBP upregulation are observed in adult AD transgenic mice. To address this issue, myelin structure of corpus callosum was examined by electron microscopy approach. Since patients with AD show corpus callosum atrophy, predominantly in anterior and posterior areas (Teipel et al., 2002), analysis was carried out specifically in both zones. First, we analyzed myelin thickness by measuring the *g*-ratio value and found that 3xTg-AD show thicker myelin sheath at 6-, 12- and 18-month-old mice in corpus callosum. Exceptionally, no significant differences were found at 18 months in caudal zone which may be explained by strong decrease in WT myelin thickness detected in this area. We also observed that myelin thickness increase was independent of the axon diameter size. However, in older transgenic mice thicker myelin sheaths were mostly present in small-caliber axons. The thickness of myelin sheath can have a dominant influence on conduction velocity, leading to conduction velocity reduction when myelin thickness is deviated from the optimal value (Waxman, 1997). These alterations in myelin sheath are not accompanied by axon fiber loss, as proved by both electron microscopy and NFL immunohistochemistry. Thus, hypermyelination observed in the corpus callosum of this AD mice model may negatively affect to axonal transmission.

Similarly to our results, APP/PS1 mice also show increased myelin thickness at early stages of AD (Wu et al., 2017b), pointing to Aβ as a clear candidate in myelin thickness regulation. In this sense, our results *in vitro* demonstrate that Aβ can activate and regulate Itgb1 availability to exacerbate intracellular signals, as CAMKII and leading to MBP upregulation. Since, Itgb1 and CAMKII are also required in myelin thickness determination (Barros et al., 2009; K. K. Lee et al., 2006; Waggener et al., 2013), it is possible that the increased levels of Aβ reported in our mouse model, promote Itgb1 overexpression resulting in myelin thickness increase through CAMKII involvement. However, further research should be conducted to prove this hypothesis.

Appart from hypermyelination, several myelin abnormalities related to aging (Hinman & Abraham, 2007) were observed in 3xTg-AD corpus callosum. A higher density of fibers with enlarged myelin inner tongue, axons with dense cytoplasm, empty fibers and myelin sheath degeneration was found in transgenic mice as compared to WT. We observed that the proportion of myelinated axons with neurodegenerative events increased progressively in an age-dependent manner, but it is exacerbated and accelerated by AD. These results are in accordance with brain imaging studies of AD patients in which WM degenerates with normal aging but it is more severe in AD subjects (Bartzokis et al., 2003; de la Monte, 1989; Stricker et al., 2009). In addition, these results support previous studies focused on 3xTg-AD and APP/PS1, in which they also observed myelin aberrations (Behrendt et al., 2013; Desai et al., 2009, 2010). More interestingly, Desai and co-workers showed a decrease in myelin disruptions in 3xTg-AD by using an anti-$A\beta_{1-42}$ engineered intrabody, demonstrating signs of myelin sheath integrity restoration as compared with WT and mice treated with an irrelevant intrabody (Desai et al., 2010). These data strongly supports the role of Aβ in myelin pathology in AD.

Remarkably, enlarged inner tongue were a consistent feature at all ages examined although appears later in caudal corpus callosum of transgenic mice. Precisely, in both areas, small caliber axons are selectively affected by this enlargement of inner tongue. In this sense, late-myelinating regions that are characterized by the presence of small caliber fibers, are the first to be affected by AD degenerative process (Bartzokis et al., 2003; Stricker et al., 2009; Teipel et al., 2007). Thus, it seems that it could be a relation between axon caliber and the severity of myelin sheath degeneration. However, the precise cause of this fact remains to be fully understood.

In addition to myelin production and maintenance, oligodendrocytes preserve functional axon integrity by providing trophic and metabolic support to neurons through cytoplasmic channels (Philips & Rothstein, 2017). A balance between MBP and CNPase levels is necessary for cytoplasmic channels preservation (Snaidero et al., 2017). In fact, CNPase deficient mice show axonal damage produced by altered cytoplasmic channels, observing a rescue of this axonal alteration when CNPase and MBP levels were restored (Snaidero et al., 2017). In our model, MBP upregulation detected in transgenic mice is not

accompanied by changes in CNPase levels (data not shown). Therefore, the balance between both proteins could be altered, consequently resulting in cytoplasmic channel loss. In this sense, the marked enlargement of inner tongue size presented in 3xTg-AD can be explained by the traffic blockade of the cytosolic cargo due to cytoplasmic channel alteration, leading to secondary swelling of the inner tongue, as observed in the CNPase deficient mice (Rasband et al., 2005). Thus, we propose that MBP upregulation results in an imbalance between MBP and CNPase levels that may lead to myelin sheath alterations, hampering oligodendrocyte-neuron support and influencing disease progression.

Overall, our results show a deregulation of MBP and myelin integrity that promotes hypermyelination associated with AD pathology, which lead to axonal dysfunction. In this sense, evidences observed in different myelin models suggest that the presence of defective myelin sheath is even worse for correct axonal functionality than its absence, since this aberrant myelin is related to uncoupling of oligodendrocyte support of axons (Simons & Nave, 2015).

6. Alzheimer´s disease patients present an increment of MBP levels in prefrontal cortex and hippocampus at advanced stages.

Since, 3xTg-AD mouse model exhibit oligodendrocyte differentiation impairment showing alterations in MBP levels that correlate with Aβ pathology, we analyzed the expression of MBP in control subjects and AD patients at different stages of the pathology. It has been described that prefrontal cortex and hippocampal formation are severe affected in AD, which is reflected in memory impairment observed in patients suffering from the disease (Sampath et al., 2017). Thus, we focused our study on examining MBP levels in these specific areas and found that AD patients showed MBP upregulation both in prefrontal cortex and hippocampal formation at advanced stages of the disease. Specifically, increased levels of MBP were observed in hippocampal DG and CA3, as we observed in 3xTg-AD. Interestingly, MBP expression increase was not accompanied by changes in PDGFr-α and Olig2, which may indicate that no changes in

oligodendrocyte population density, specifically in progenitor cells, were occurring. However, counting of oligodendroglial lineage cells would be necessary to confirm this hypothesis.

In addition, biochemical analysis of total myelin fraction in AD patients revealed increased $A\beta_{1-42}$ levels accompanied by a significant decrease in the amount of MBP (Roher et al., 2002). However, a more detailed analysis of MBP levels have showed that depending on the area, the expression pattern of this protein is different. Precisely, cortical GM and frontal lobe from AD patients exhibit a marked MBP expression increase (Selkoe et al., 1981; Ihara et al., 2010; Zhan et al., 2015). Remarkably, increased levels of MBP were associated with high amount of degraded MBP, which has been related to myelin damage (Ihara et al., 2010). Thus, according to these data, it is possible that MBP upregulation observed in frontal cortex and hippocampal formation of AD patients may be partially related to alterations in myelin integrity as we observed in 3xTg-AD, which may contribute to cognitive impairment in AD patients. However, the mechanisms by which MBP levels are higher in AD remain unclear. It is possible that increased MBP levels are associated with remyelination process after myelin injury in AD brain. Nevertheless, taking together the data obtained in this study in relation with the animal model of the disease and the effects of Aβ directly on oligodendrocytes *in vitro*, we suggest that one of the mechanisms by which MBP protein is upregulated is the direct effect of Aβ. In this sense, further research should be conducted in order to unveil the complete role of Aβ in AD.

On the other hand, several interesting studies have demonstrated that MBP binds to $A\beta_{1-42}$ and inhibits its fibrillar assembly (Hoos et al., 2009). Moreover, diffuse and non-fibrillar deposits of Aβ are often found in region with high abundance of myelinated axons, as white matter (Behrouz et al., 1991). Thus, it may be possible that the inhibition of fibril formation by MBP results in maintaining soluble oligomers and thereby, exacerbate disease pathology as Hoos and coworkers proposed (Hoos et al., 2009). Therefore, since we have described that oligomeric Aβ directly acts on myelin-producing oligodendrocytes and contributes to formation of additional MBP, increased levels of MBP observed in AD patients may contribute to disease progression by inhibiting plaque

formation and promoting the presence of higher concentrations of oligomeric Aβ. In this sense, MBP would not be just a pathogenic hallmark of AD, but a promoter of this pathology progression.

7. Cerebrospinal fluid of MCI patients show increased levels of MBP and CNPase.

It has been reported that white matter and myelin damage may result in an increase of myelin-related proteins in the CSF, specially MBP (Whitaker, 1998; Su et al., 2012). Since we observed MBP upregulation in AD patients, we considered to evaluate myelin proteins as potential candidate biomarkers for AD. For this purpose, we examined MBP and CNPase levels in CSF samples from control subjects, mild cognitive impairment (MCI) and AD patients (AD). Notably, MBP and CNPase levels were significantly increased in CSF from MCI patients, while no differences were found in AD subjects. Interestingly, levels of both myelin-related proteins correlate positively in each group, being more strongly correlated in MCI and AD subjects. Since MBP upregulation was only present in advanced stages of AD brain, we also expected to find high levels of myelin proteins in CSF from AD patients. Surprisingly, only MCI subjects exhibited greater amounts. It is possible that oligodendrocyte and MBP synthesis dysregulation begin at early stages of AD, as previously reported. However, this may be compensated by an efficient mechanism of protein clearance through CSF resulting in elevated MBP levels in preclinical patients, as we have observed. By contrast, as previous studies have described, protein clearance at advanced stages of AD may be diminished (Mawuenyega et al., 2010; de Leon et al., 2017) and consequently, MBP accumulation was detected in the brain of these patients. Additionally, since oligomeric Aβ stimulates oligodendrocyte MBP and CNPase release in EVs, and it has been identified that EVs from human CSF may carry myelin-related proteins, as MBP and CNPase (Chiasserini *et al*., 2014), it could possible that these proteins detected in CSF are included in EVs and participate in the progression of the disease. In this sense, a recent study demonstrated that EVs isolated from CSF from AD patients, destabilize neuronal Ca^{+} homeostasis and are toxic to neurons (Eitan et al., 2016). Thus, future studies will be required to elucidate the role of myelin proteins and EVs in AD pathogenesis.

Overall, we propose that oligomeric Aβ modulates oligodendrocyte differentiation resulting in myelin integrity impairment and contributing to axonal dysfunction, being crucial for AD. Therefore, the comprehension of the mechanisms that regulate oligodendrocyte dysfunction in AD, which results in MBP upregulation and oligodendrocyte lineage impairment, will be crucial for the development of new therapies based on the modulation of oligodendrocyte myelination. In addition, focusing research on finding new biomarkers on oligodendrocyte-related proteins could contribute to early diagnostic of the disease.

Conclusions

Conclusions

1. Amyloid β oligomers promote an increase in oligodendrocyte differentiation and MBP synthesis by modulating mRNA local translation in cultured oligodendrocytes. The mechanism underlying amyloid β -induced MBP upregulation is mediated by integrin β1 receptor followed by Fyn and CaMKII activation.

2. Treatment of oligodendrocyte primary cultures with amyloid β stimulates the release of MBP included in microvesicles and CNPase in both microvesicles and exosomes.

3. Oligodendrocyte primary cell survival was enhanced in the presence of endogenously-produced and synthetic amyloid β. Inhibition of Src-family kinase, ryanodine receptors and CaMKII blocked cell death protection.

4. Amyloid β oligomers upregulate myelin-related proteins expression in cerebellar organotypic slices, being Src-family kinase activation involved in MBP increase. In addition, under pathological conditions after LPC-induced demyelination amyloid β oligomers also enhanced MBP synthesis.

4. *In vivo* analyses of 3xTg-AD showed increased levels of MBP that correlate with Aβ amount, occurring previously to neurofilament damage. These MBP alterations in corpus callosum and hippocampus were accompanied by an increase in oligodendrocyte progenitor cells in early stages, while mature cells were more abundant of old mice.

5. Corpus callosum of 3xTg-AD exhibits impaired myelin integrity, showing more density of nodes of Ranvier and increased thickness of myelin sheaths. Precisely, electrophysiological analysis determined that only myelinated fibers present slow conduction velocity in these mice.

6. Ultrastructural analysis of rostral and caudal corpus callosum of triple transgenic AD mice showed higher abundance of myelin sheath-associated degenerative events, including enlarged inner tongue, dense cytoplasm, empty fibers and myelin degeneration.

7. Frontal cortex and hippocampal formation of AD patients exhibit increased MBP expression. Moreover, higher levels of MBP and CNPase are detected in cerebrospinal fluid of MCI patients in comparison with control subjects.

Bibliography

Bibliography

Aggarwal, S., Snaidero, N., Pähler, G., Frey, S., Sánchez, P., Zweckstetter, M., … Simons, M. (2013). Myelin Membrane Assembly Is Driven by a Phase Transition of Myelin Basic Proteins Into a Cohesive Protein Meshwork. *PLoS Biology*, *11*(6). https://doi.org/10.1371/journal.pbio.1001577

Ainger, K., Avossa, D., Diana, A. S., Barry, C., Barbarese, E., & Carson, J. H. (1997). Transport and localization elements in myelin basic protein mRNA. *The Journal of Cell Biology*, *138*(5), 1077–87. Retrieved from http://www.ncbi.nlm.nih.gov/pubmed/9281585

Ainger, K., Avossa, D., Morgan, F., Hill, S. J., Barry, C., Barbarese, E., & Carson, J. H. (1993). Transport and localization of exogenous myelin basic protein mRNA microinjected into oligodendrocytes. *The Journal of Cell Biology*, *123*(2), 431–41. Retrieved from http://www.ncbi.nlm.nih.gov/pubmed/7691830

Alberdi, E., Sánchez-Gómez, M. V., Cavaliere, F., Pérez-Samartín, A., Zugaza, J. L., Trullas, R., … Matute, C. (2010). Amyloid β oligomers induce Ca2+ dysregulation and neuronal death through activation of ionotropic glutamate receptors. *Cell Calcium*, *47*(3), 264–272. https://doi.org/10.1016/j.ceca.2009.12.010

Almeida, R. G., Czopka, T., ffrench-Constant, C., & Lyons, D. A. (2011). Individual axons regulate the myelinating potential of single oligodendrocytes in vivo. *Development*, *138*(20), 4443–4450. https://doi.org/10.1242/dev.071001

Arancibia-Cárcamo, I. L., Ford, M. C., Cossell, L., Ishida, K., Tohyama, K., & Attwell, D. (2017). Node of Ranvier length as a potential regulator of myelinated axon conduction speed. *eLife*, *6*. https://doi.org/10.7554/eLife.23329

B. Parente, D., Gasparetto, E. L., Cruz, L. C. H. da, Domingues, R. C., Baptista, A. C., Carvalho, A. C. P., & Domingues, R. C. (2008). Potential Role of Diffusion Tensor MRI in the Differential Diagnosis of Mild Cognitive Impairment and Alzheimer's Disease. *American Journal of Roentgenology*, *190*(5), 1369–1374. https://doi.org/10.2214/AJR.07.2617

Back, S. A., Tuohy, T. M. F., Chen, H., Wallingford, N., Craig, A., Struve, J., … Sherman, L. S. (2005). Hyaluronan accumulates in demyelinated lesions and inhibits oligodendrocyte progenitor maturation. *Nature Medicine*, *11*(9), 966–72.

https://doi.org/10.1038/nm1279

Bao, F., Wicklund, L., Lacor, P. N., Klein, W. L., Nordberg, A., & Marutle, A. (2012). Different β-amyloid oligomer assemblies in Alzheimer brains correlate with age of disease onset and impaired cholinergic activity. *Neurobiology of Aging*, *33*(4), 825.e1-825.e13. https://doi.org/10.1016/j.neurobiolaging.2011.05.003

Barros, C. S., Nguyen, T., Spencer, K. S. R., Nishiyama, A., Colognato, H., & Müller, U. (2009). Beta1 integrins are required for normal CNS myelination and promote AKT-dependent myelin outgrowth. *Development (Cambridge, England)*, *136*(16), 2717–24. https://doi.org/10.1242/dev.038679

Bartzokis, G. (2011). Alzheimer's disease as homeostatic responses to age-related myelin breakdown. *Neurobiology of Aging*, *32*(8), 1341–71. https://doi.org/10.1016/j.neurobiolaging.2009.08.007

Bartzokis, G., Cummings, J. L., Sultzer, D., Henderson, V. W., Nuechterlein, K. H., & Mintz, J. (2003). White matter structural integrity in healthy aging adults and patients with Alzheimer disease: a magnetic resonance imaging study. *Archives of Neurology*, *60*(3), 393–8. https://doi.org/.

Bartzokis, G., Lu, P. H., Geschwind, D. H., Edwards, N., Mintz, J., & Cummings, J. L. (2006). Apolipoprotein E genotype and age-related myelin breakdown in healthy individuals: implications for cognitive decline and dementia. *Archives of General Psychiatry*, *63*(1), 63–72. https://doi.org/10.1001/archpsyc.63.1.63

Bartzokis, G., Lu, P. H., & Mintz, J. (2007). Human brain myelination and amyloid beta deposition in Alzheimer's disease. *Alzheimer's & Dementia : The Journal of the Alzheimer's Association*, *3*(2), 122–5. https://doi.org/10.1016/j.jalz.2007.01.019

Bartzokis, G., Sultzer, D., Lu, P. H., Nuechterlein, K. H., Mintz, J., & Cummings, J. L. (2004). Heterogeneous age-related breakdown of white matter structural integrity: implications for cortical "disconnection" in aging and Alzheimer's disease. *Neurobiology of Aging*, *25*(7), 843–851. https://doi.org/10.1016/j.neurobiolaging.2003.09.005

Bauer, N. G., Richter-Landsberg, C., & Ffrench-Constant, C. (2009). Role of the oligodendroglial cytoskeleton in differentiation and myelination. *Glia*, *57*(16), 1691–1705. https://doi.org/10.1002/glia.20885

Baumann, N., & Pham-Dinh, D. (2001). Biology of Oligodendrocyte and Myelin in the

Mammalian Central Nervous System. *Physiological Reviews*, *81*(2). Retrieved from http://physrev.physiology.org/content/81/2/871.long

Bengtsson, S. L., Nagy, Z., Skare, S., Forsman, L., Forssberg, H., & Ullén, F. (2005). Extensive piano practicing has regionally specific effects on white matter development. *Nature Neuroscience*, *8*(9), 1148–50. https://doi.org/10.1038/nn1516

Benninger, Y., Colognato, H., Thurnherr, T., Franklin, R. J. M., Leone, D. P., Atanasoski, S., … Relvas, J. B. (2006). Beta1-integrin signaling mediates premyelinating oligodendrocyte survival but is not required for CNS myelination and remyelination. *The Journal of Neuroscience : The Official Journal of the Society for Neuroscience*, *26*(29), 7665–73. https://doi.org/10.1523/JNEUROSCI.0444-06.2006

Boggs, J. M. (2006). Myelin basic protein: a multifunctional protein. *Cellular and Molecular Life Sciences*, *63*(17), 1945–1961. https://doi.org/10.1007/s00018-006-6094-7

Braak, H., & Braak, E. (1995). Staging of alzheimer's disease-related neurofibrillary changes. *Neurobiology of Aging*, *16*(3), 271–278. https://doi.org/10.1016/0197-4580(95)00021-6

Brinkmann, B. G., Agarwal, A., Sereda, M. W., Garratt, A. N., Müller, T., Wende, H., … Nave, K. A. (2008). Neuregulin-1/ErbB Signaling Serves Distinct Functions in Myelination of the Peripheral and Central Nervous System. *Neuron*, *59*(4), 581–595. https://doi.org/10.1016/j.neuron.2008.06.028

Brun, A., & Englund, E. (1986). A white matter disorder in dementia of the Alzheimer type: a pathoanatomical study. *Annals of Neurology*, *19*(3), 253–62. https://doi.org/10.1002/ana.410190306

Bu, G. (2009). Apolipoprotein E and its receptors in Alzheimer's disease: pathways, pathogenesis and therapy. *Nature Reviews Neuroscience*, *10*(5), 333–344. https://doi.org/10.1038/nrn2620

BUNGE, M. B., BUNGE, R. P., & RIS, H. (1961). Ultrastructural study of remyelination in an experimental lesion in adult cat spinal cord. *The Journal of Biophysical and Biochemical Cytology*, *10*, 67–94. Retrieved from http://www.ncbi.nlm.nih.gov/pubmed/13688845

Buttery, P. C., & ffrench-Constant, C. (1999). Laminin-2/Integrin Interactions Enhance Myelin Membrane Formation by Oligodendrocytes. *Molecular and Cellular*

Neuroscience, *14*(3), 199–212. https://doi.org/10.1006/mcne.1999.0781

Câmara, J., Wang, Z., Nunes-Fonseca, C., Friedman, H. C., Grove, M., Sherman, D. L., … ffrench-Constant, C. (2009). Integrin-mediated axoglial interactions initiate myelination in the central nervous system. *The Journal of Cell Biology*, *185*(4), 699–712. https://doi.org/10.1083/jcb.200807010

Charles, P., Hernandez, M. P., Stankoff, B., Aigrot, M. S., Colin, C., Rougon, G., … Lubetzki, C. (2000). Negative regulation of central nervous system myelination by polysialylated-neural cell adhesion molecule. *Proceedings of the National Academy of Sciences*, *97*(13), 7585–7590. https://doi.org/10.1073/pnas.100076197

Chen, Y., Wu, H., Wang, S., Koito, H., Li, J., Ye, F., … Lu, Q. R. (2009). The oligodendrocyte-specific G protein–coupled receptor GPR17 is a cell-intrinsic timer of myelination. *Nature Neuroscience*, *12*(11), 1398–1406. https://doi.org/10.1038/nn.2410

Chia, L. S., Thompson, J. E., & Moscarello, M. A. (1984). X-ray diffraction evidence for myelin disorder in brain from humans with Alzheimer's disease. *Biochimica et Biophysica Acta*, *775*(3), 308–12. Retrieved from http://www.ncbi.nlm.nih.gov/pubmed/6466674

Chomiak, T., & Hu, B. (2009). What is the optimal value of the g-ratio for myelinated fibers in the rat CNS? A theoretical approach. *PloS One*, *4*(11), e7754. https://doi.org/10.1371/journal.pone.0007754

Chromy, B. A., Nowak, R. J., Lambert, M. P., Viola, K. L., Chang, L., Velasco, P. T., … Klein, W. L. (2003). Self-Assembly of $A\beta_{1-42}$ into Globular Neurotoxins †. *Biochemistry*, *42*(44), 12749–12760. https://doi.org/10.1021/bi030029q

Colman, D. R., Kreibich, G., Frey, A. B., & Sabatini, D. D. (1982). Synthesis and incorporation of myelin polypeptides into CNS myelin. *The Journal of Cell Biology*, *95*(2 Pt 1), 598–608. Retrieved from http://www.ncbi.nlm.nih.gov/pubmed/6183276

Colognato, H., Galvin, J., Wang, Z., Relucio, J., Nguyen, T., Harrison, D., … ffrench-Constant, C. (2007). Identification of dystroglycan as a second laminin receptor in oligodendrocytes, with a role in myelination. *Development*, *134*(9), 1723–1736. https://doi.org/10.1242/dev.02819

Colognato, H., Ramachandrappa, S., Olsen, I. M., & ffrench-Constant, C. (2004). Integrins direct Src family kinases to regulate distinct phases of oligodendrocyte development. *The Journal of Cell Biology*, *167*(2), 365–75. https://doi.org/10.1083/jcb.200404076

Corley, S., Ladiwala, U., Besson, A., & Yong, V. (2001). Astrocytes attenuate oligodendrocyte death in vitro through an alpha(6) integrin-laminin-dependent mechanism. *Glia*, *36*(3), 281–294. https://doi.org/10.1002/glia.1116 [pii]

Cruts, M., Hendriks, L., & Van Broeckhoven, C. (1996). The presenilin genes: a new gene family involved in Alzheimer disease pathology. *Human Molecular Genetics*, *5 Spec No*, 1449–55. Retrieved from http://www.ncbi.nlm.nih.gov/pubmed/8875251

Czopka, T., ffrench-Constant, C., & Lyons, D. A. (2013). Individual Oligodendrocytes Have Only a Few Hours in which to Generate New Myelin Sheaths In Vivo. *Developmental Cell*, *25*(6), 599–609. https://doi.org/10.1016/j.devcel.2013.05.013

Dai, J., Bercury, K. K., Ahrendsen, J. T., & Macklin, W. B. (2015). Olig1 function is required for oligodendrocyte differentiation in the mouse brain. *The Journal of Neuroscience : The Official Journal of the Society for Neuroscience*, *35*(10), 4386–402. https://doi.org/10.1523/JNEUROSCI.4962-14.2015

Damoiseaux, J. S., Smith, S. M., Witter, M. P., Sanz-Arigita, E. J., Barkhof, F., Scheltens, P., … Rombouts, S. A. R. B. (2009). White matter tract integrity in aging and Alzheimer's disease. *Human Brain Mapping*, *30*(4), 1051–1059. https://doi.org/10.1002/hbm.20563

de la Monte, S. M. (1989). Quantitation of cerebral atrophy in preclinical and end-stage alzheimer's disease. *Annals of Neurology*, *25*(5), 450–459. https://doi.org/10.1002/ana.410250506

Dean, D. C., Hurley, S. A., Kecskemeti, S. R., O'Grady, J. P., Canda, C., Davenport-Sis, N. J., … Bendlin, B. B. (2017). Association of Amyloid Pathology With Myelin Alteration in Preclinical Alzheimer Disease. *JAMA Neurology*, *74*(1), 41. https://doi.org/10.1001/jamaneurol.2016.3232

Demuro, A., Mina, E., Kayed, R., Milton, S. C., Parker, I., & Glabe, C. G. (2005). Calcium Dysregulation and Membrane Disruption as a Ubiquitous Neurotoxic Mechanism of Soluble Amyloid Oligomers. *Journal of Biological Chemistry*, *280*(17), 17294–17300. https://doi.org/10.1074/jbc.M500997200

Desai, M. K., Mastrangelo, M. A., Ryan, D. A., Sudol, K. L., Narrow, W. C., & Bowers, W. J. (2010). Early oligodendrocyte/myelin pathology in Alzheimer's disease mice constitutes a novel therapeutic target. *The American Journal of Pathology*, *177*(3), 1422–35. https://doi.org/10.2353/ajpath.2010.100087

Dyer, C. A., Philibotte, T. M., Wolf, M. K., & Billings-Gagliardi, S. (1994). Myelin basic protein mediates extracellular signals that regulate microtubule stability in oligodendrocyte membrane sheets. *Journal of Neuroscience Research*, *39*(1), 97–107. https://doi.org/10.1002/jnr.490390112

Emery, B., Agalliu, D., Cahoy, J. D., Watkins, T. A., Dugas, J. C., Mulinyawe, S. B., … Barres, B. A. (2009). Myelin Gene Regulatory Factor Is a Critical Transcriptional Regulator Required for CNS Myelination. *Cell*, *138*(1), 172–185. https://doi.org/10.1016/j.cell.2009.04.031

Emery, B., & Lu, Q. R. (2015). Transcriptional and Epigenetic Regulation of Oligodendrocyte Development and Myelination in the Central Nervous System. *Cold Spring Harbor Perspectives in Biology*, *7*(9), a020461. https://doi.org/10.1101/cshperspect.a020461

Fewou, S. N., Ramakrishnan, H., Büssow, H., Gieselmann, V., & Eckhardt, M. (2007). Down-regulation of polysialic acid is required for efficient myelin formation. *The Journal of Biological Chemistry*, *282*(22), 16700–11. https://doi.org/10.1074/jbc.M610797200

Fields, R. D. (2008). White matter in learning, cognition and psychiatric disorders. *Trends in Neurosciences*, *31*(7), 361–70. https://doi.org/10.1016/j.tins.2008.04.001

Firbank, M. J., Blamire, A. M., Krishnan, M. S., Teodorczuk, A., English, P., Gholkar, A., … O'Brien, J. T. (2007). Atrophy is associated with posterior cingulate white matter disruption in dementia with Lewy bodies and Alzheimer's disease. *NeuroImage*, *36*(1), 1–7. https://doi.org/10.1016/j.neuroimage.2007.02.027

Fitzner, D., Schneider, A., Kippert, A., Möbius, W., Willig, K. I., Hell, S. W., … Simons, M. (2006). Myelin basic protein-dependent plasma membrane reorganization in the formation of myelin. *The EMBO Journal*, *25*(21), 5037–48. https://doi.org/10.1038/sj.emboj.7601376

Flores, A. I., Narayanan, S. P., Morse, E. N., Shick, H. E., Yin, X., Kidd, G., … Macklin, W. B. (2008). Constitutively Active Akt Induces Enhanced Myelination in the CNS. *Journal of Neuroscience*, *28*(28), 7174–7183. https://doi.org/10.1523/JNEUROSCI.0150-08.2008

Friede, R. L., & Bischhausen, R. (1982). How are sheath dimensions affected by axon caliber and internode length? *Brain Research*, *235*(2), 335–50. Retrieved from

http://www.ncbi.nlm.nih.gov/pubmed/7188332

Gaesser, J. M., & Fyffe-Maricich, S. L. (2016). Intracellular signaling pathway regulation of myelination and remyelination in the CNS. *Experimental Neurology*, *283*(Pt B), 501–11. https://doi.org/10.1016/j.expneurol.2016.03.008

Games, D., Adams, D., Alessandrini, R., Barbour, R., Borthelette, P., Blackwell, C., … Zhao, J. (1995). Alzheimer-type neuropathology in transgenic mice overexpressing V717F β-amyloid precursor protein. *Nature*, *373*(6514), 523–527. https://doi.org/10.1038/373523a0

Gibson, E. M., Purger, D., Mount, C. W., Goldstein, A. K., Lin, G. L., Wood, L. S., … Monje, M. (2014). Neuronal Activity Promotes Oligodendrogenesis and Adaptive Myelination in the Mammalian Brain. *Science*, *344*(6183), 1252304–1252304. https://doi.org/10.1126/science.1252304

Glabe, C. C. (2005). Amyloid accumulation and pathogensis of Alzheimer's disease: significance of monomeric, oligomeric and fibrillar Abeta. *Sub-Cellular Biochemistry*, *38*, 167–77. Retrieved from http://www.ncbi.nlm.nih.gov/pubmed/15709478

Glenner, G. G., & Wong, C. W. (1984a). Alzheimer's disease: initial report of the purification and characterization of a novel cerebrovascular amyloid protein. *Biochemical and Biophysical Research Communications*, *120*(3), 885–90. Retrieved from http://www.ncbi.nlm.nih.gov/pubmed/6375662

Glenner, G. G., & Wong, C. W. (1984b). Alzheimer's disease and Down's syndrome: sharing of a unique cerebrovascular amyloid fibril protein. *Biochemical and Biophysical Research Communications*, *122*(3), 1131–5. Retrieved from http://www.ncbi.nlm.nih.gov/pubmed/6236805

Goate, A., Chartier-Harlin, M.-C., Mullan, M., Brown, J., Crawford, F., Fidani, L., … Hardy, J. (1991). Segregation of a missense mutation in the amyloid precursor protein gene with familial Alzheimer's disease. *Nature*, *349*(6311), 704–706. https://doi.org/10.1038/349704a0

Götz, J., Probst, A., Spillantini, M. G., Schäfer, T., Jakes, R., Bürki, K., & Goedert, M. (1995). Somatodendritic localization and hyperphosphorylation of tau protein in transgenic mice expressing the longest human brain tau isoform. *The EMBO Journal*, *14*(7), 1304–13. Retrieved from http://www.ncbi.nlm.nih.gov/pubmed/7729409

Gravel, M., Peterson, J., Yong, V. W., Kottis, V., Trapp, B., & Braun, P. E. (1996).

Overexpression of 2',3'-Cyclic Nucleotide 3'-Phosphodiesterase in Transgenic Mice Alters Oligodendrocyte Development and Produces Aberrant Myelination. *Molecular and Cellular Neuroscience*, *7*(6), 453–466. https://doi.org/10.1006/mcne.1996.0033

Hammond, T. R., Gadea, A., Dupree, J., Kerninon, C., Nait-Oumesmar, B., Aguirre, A., & Gallo, V. (2014). Astrocyte-Derived Endothelin-1 Inhibits Remyelination through Notch Activation. *Neuron*, *81*(6), 1442. https://doi.org/10.1016/j.neuron.2014.03.007

Han, X. (2007). Potential mechanisms contributing to sulfatide depletion at the earliest clinically recognizable stage of Alzheimer's disease: a tale of shotgun lipidomics. *Journal of Neurochemistry*, *103 Suppl 1*(Suppl 1), 171–9. https://doi.org/10.1111/j.1471-4159.2007.04708.x

Han, X., M Holtzman, D., McKeel, D. W., Kelley, J., & Morris, J. C. (2002). Substantial sulfatide deficiency and ceramide elevation in very early Alzheimer's disease: potential role in disease pathogenesis. *Journal of Neurochemistry*, *82*(4), 809–18. Retrieved from http://www.ncbi.nlm.nih.gov/pubmed/12358786

Harauz, G., & Musse, A. A. (2007). A tale of two citrullines--structural and functional aspects of myelin basic protein deimination in health and disease. *Neurochemical Research*, *32*(2), 137–58. https://doi.org/10.1007/s11064-006-9108-9

Hardy, J. A., & Higgins, G. A. (1992). Alzheimer's disease: the amyloid cascade hypothesis. *Science (New York, N.Y.)*, *256*(5054), 184–5. Retrieved from http://www.ncbi.nlm.nih.gov/pubmed/1566067

Hardy, J., & Allsop, D. (1991). Amyloid deposition as the central event in the aetiology of Alzheimer's disease. *Trends in Pharmacological Sciences*, *12*(10), 383–8. Retrieved from http://www.ncbi.nlm.nih.gov/pubmed/1763432

Hardy, J., & Selkoe, D. J. (2002). The Amyloid Hypothesis of Alzheimer's Disease: Progress and Problems on the Road to Therapeutics. *Science*, *297*(5580), 353–356. https://doi.org/10.1126/science.1072994

Hartline, D. K. (2008). What is myelin? *Neuron Glia Biology*, *4*(2), 153–63. https://doi.org/10.1017/S1740925X09990263

Herms, J., Anliker, B., Heber, S., Ring, S., Fuhrmann, M., Kretzschmar, H., … Müller, U. (2004). Cortical dysplasia resembling human type 2 lissencephaly in mice lacking all three APP family members. *The EMBO Journal*, *23*(20), 4106–15.

https://doi.org/10.1038/sj.emboj.7600390

Higuchi, M., Ishihara, T., Zhang, B., Hong, M., Andreadis, A., Trojanowski, J., & Lee, V. M.-Y. (2002). Transgenic mouse model of tauopathies with glial pathology and nervous system degeneration. *Neuron*, *35*(3), 433–46. Retrieved from http://www.ncbi.nlm.nih.gov/pubmed/12165467

Hill, C. M. D., & Harauz, G. (2005). Charge effects modulate actin assembly by classic myelin basic protein isoforms. *Biochemical and Biophysical Research Communications*, *329*(1), 362–9. https://doi.org/10.1016/j.bbrc.2005.01.151

Hill, C. M. D., Libich, D. S., & Harauz, G. (2005). Assembly of tubulin by classic myelin basic protein isoforms and regulation by post-translational modification. *Biochemistry*, *44*(50), 16672–83. https://doi.org/10.1021/bi050646+

Hoos, M. D., Ahmed, M., Smith, S. O., & Van Nostrand, W. E. (2009). Myelin Basic Protein Binds to and Inhibits the Fibrillar Assembly of Aβ42 in Vitro. *Biochemistry*, *48*(22), 4720–4727. https://doi.org/10.1021/bi900037s

Horiuchi, M., Maezawa, I., Itoh, A., Wakayama, K., Jin, L.-W., Itoh, T., & Decarli, C. (2012). Amyloid β1-42 oligomer inhibits myelin sheet formation in vitro. *Neurobiology of Aging*, *33*(3), 499–509. https://doi.org/10.1016/j.neurobiolaging.2010.05.007

Hornig, J., Fröb, F., Vogl, M. R., Hermans-Borgmeyer, I., Tamm, E. R., & Wegner, M. (2013). The transcription factors Sox10 and Myrf define an essential regulatory network module in differentiating oligodendrocytes. *PLoS Genetics*, *9*(10), e1003907. https://doi.org/10.1371/journal.pgen.1003907

Hu, Q.-D., Ang, B.-T., Karsak, M., Hu, W.-P., Cui, X.-Y., Duka, T., … Xiao, Z.-C. (2003). F3/contactin acts as a functional ligand for Notch during oligodendrocyte maturation. *Cell*, *115*(2), 163–75. Retrieved from http://www.ncbi.nlm.nih.gov/pubmed/14567914

Huang, Y. (2006). Apolipoprotein E and Alzheimer disease. *Neurology*, *66*(Issue 1, Supplement 1), S79–S85. https://doi.org/10.1212/01.wnl.0000192102.41141.9e

Hutton, M., Lewis, J., McGowan, E., Rockwood, J., Melrose, H., Nacharaju, P., … Davies, P. (2000). Neurofibrillary tangles, amyotrophy and progressive motor disturbance in mice expressing mutant (P301L) tau protein. *Nature Genetics*, *25*(4), 402–405. https://doi.org/10.1038/78078

Inano, S., Takao, H., Hayashi, N., Abe, O., & Ohtomo, K. (2011). Effects of Age and Gender

on White Matter Integrity. *American Journal of Neuroradiology*, *32*(11), 2103–2109. https://doi.org/10.3174/ajnr.A2785

Jantaratnotai, N., Ryu, J. K., Kim, S. U., & McLarnon, J. G. (2003). Amyloid beta peptide-induced corpus callosum damage and glial activation in vivo. *Neuroreport*, *14*(11), 1429–33. https://doi.org/10.1097/01.wnr.0000086097.47480.a0

Kavcic, V., Ni, H., Zhu, T., Zhong, J., & Duffy, C. J. (2008). White matter integrity linked to functional impairments in aging and early Alzheimer's disease. *Alzheimer's & Dementia*, *4*(6), 381–389. https://doi.org/10.1016/j.jalz.2008.07.001

Kavroulakis, E., Simos, P. G., Kalaitzakis, G., Maris, T. G., Karageorgou, D., Zaganas, I., … Papadaki, E. (2017). Myelin content changes in probable Alzheimer's disease and mild cognitive impairment: Associations with age and severity of neuropsychiatric impairment. *Journal of Magnetic Resonance Imaging*. https://doi.org/10.1002/jmri.25849

Kimberly, W. T., Zheng, J. B., Guénette, S. Y., & Selkoe, D. J. (2001). The Intracellular Domain of the β-Amyloid Precursor Protein Is Stabilized by Fe65 and Translocates to the Nucleus in a Notch-like Manner. *Journal of Biological Chemistry*, *276*(43), 40288–40292. https://doi.org/10.1074/jbc.C100447200

Kitada, M., & Rowitch, D. H. (2006). Transcription factor co-expression patterns indicate heterogeneity of oligodendroglial subpopulations in adult spinal cord. *Glia*, *54*(1), 35–46. https://doi.org/10.1002/glia.20354

Klein, C., Kramer, E.-M., Cardine, A.-M., Schraven, B., Brandt, R., & Trotter, J. (2002). Process outgrowth of oligodendrocytes is promoted by interaction of fyn kinase with the cytoskeletal protein tau. *The Journal of Neuroscience : The Official Journal of the Society for Neuroscience*, *22*(3), 698–707. Retrieved from http://www.ncbi.nlm.nih.gov/pubmed/11826099

Klein, W. L. (2002). Abeta toxicity in Alzheimer's disease: globular oligomers (ADDLs) as new vaccine and drug targets. *Neurochemistry International*, *41*(5), 345–52. Retrieved from http://www.ncbi.nlm.nih.gov/pubmed/12176077

Koenning, M., Jackson, S., Hay, C. M., Faux, C., Kilpatrick, T. J., Willingham, M., & Emery, B. (2012). Myelin gene regulatory factor is required for maintenance of myelin and mature oligodendrocyte identity in the adult CNS. *The Journal of Neuroscience : The Official Journal of the Society for Neuroscience*, *32*(36), 12528–42.

https://doi.org/10.1523/JNEUROSCI.1069-12.2012

Krämer-Albers, E.-M., & White, R. (2011). From axon–glial signalling to myelination: the integrating role of oligodendroglial Fyn kinase. *Cellular and Molecular Life Sciences*, *68*(12), 2003–2012. https://doi.org/10.1007/s00018-010-0616-z

Lambert, M. P., Barlow, A. K., Chromy, B. A., Edwards, C., Freed, R., Liosatos, M., … Klein, W. L. (1998). Diffusible, nonfibrillar ligands derived from Abeta1-42 are potent central nervous system neurotoxins. *Proceedings of the National Academy of Sciences of the United States of America*, *95*(11), 6448–53. Retrieved from http://www.ncbi.nlm.nih.gov/pubmed/9600986

Laursen, L. S., Chan, C. W., & ffrench-Constant, C. (2009). An Integrin-Contactin Complex Regulates CNS Myelination by Differential Fyn Phosphorylation. *Journal of Neuroscience*, *29*(29), 9174–9185. https://doi.org/10.1523/JNEUROSCI.5942-08.2009

Laursen, L. S., Chan, C. W., & ffrench-Constant, C. (2009). An integrin-contactin complex regulates CNS myelination by differential Fyn phosphorylation. *The Journal of Neuroscience : The Official Journal of the Society for Neuroscience*, *29*(29), 9174–85. https://doi.org/10.1523/JNEUROSCI.5942-08.2009

Laursen, L. S., Chan, C. W., & ffrench-Constant, C. (2011). Translation of myelin basic protein mRNA in oligodendrocytes is regulated by integrin activation and hnRNP-K. *The Journal of Cell Biology*, *192*(5), 797–811. https://doi.org/10.1083/jcb.201007014

Lee, J.-T., Xu, J., Lee, J.-M., Ku, G., Han, X., Yang, D.-I., … Hsu, C. Y. (2004). Amyloid-β peptide induces oligodendrocyte death by activating the neutral sphingomyelinase–ceramide pathway. *The Journal of Cell Biology*, *164*(1), 123–131. https://doi.org/10.1083/jcb.200307017

Lee, K. K., de Repentigny, Y., Saulnier, R., Rippstein, P., Macklin, W. B., & Kothary, R. (2006). Dominant-negative beta1 integrin mice have region-specific myelin defects accompanied by alterations in MAPK activity. *Glia*, *53*(8), 836–44. https://doi.org/10.1002/glia.20343

Liang, X., Draghi, N. A., & Resh, M. D. (2004). Signaling from integrins to Fyn to Rho family GTPases regulates morphologic differentiation of oligodendrocytes. *The Journal of Neuroscience : The Official Journal of the Society for Neuroscience*, *24*(32), 7140–9. https://doi.org/10.1523/JNEUROSCI.5319-03.2004

Liao, M.-C., Ahmed, M., Smith, S. O., & Van Nostrand, W. E. (2009). Degradation of

Amyloid β Protein by Purified Myelin Basic Protein. *Journal of Biological Chemistry*, *284*(42), 28917–28925. https://doi.org/10.1074/jbc.M109.050856

Liu, A., Li, J., Marin-Husstege, M., Kageyama, R., Fan, Y., Gelinas, C., & Casaccia-Bonnefil, P. (2006). A molecular insight of Hes5-dependent inhibition of myelin gene expression: old partners and new players. *The EMBO Journal*, *25*(20), 4833–4842. https://doi.org/10.1038/sj.emboj.7601352

Lu, Z., Ku, L., Chen, Y., & Feng, Y. (2005). Developmental abnormalities of myelin basic protein expression in fyn knock-out brain reveal a role of Fyn in posttranscriptional regulation. *The Journal of Biological Chemistry*, *280*(1), 389–95. https://doi.org/10.1074/jbc.M405973200

Lyons, D. A., Naylor, S. G., Scholze, A., & Talbot, W. S. (2009). Kif1b is essential for mRNA localization in oligodendrocytes and development of myelinated axons. *Nature Genetics*, *41*(7), 854–858. https://doi.org/10.1038/ng.376

Makinodan, M., Rosen, K. M., Ito, S., & Corfas, G. (2012). A Critical Period for Social Experience-Dependent Oligodendrocyte Maturation and Myelination. *Science*, *337*(6100), 1357–1360. https://doi.org/10.1126/science.1220845

Malek-Hedayat, S., & Rome, L. H. (1994). Expression of a beta 1-related integrin by oligodendroglia in primary culture: evidence for a functional role in myelination. *The Journal of Cell Biology*, *124*(6), 1039–46. Retrieved from http://www.ncbi.nlm.nih.gov/pubmed/7510711

McKee, A. C., Kowall, N. W., Schumacher, J. S., & Beal, M. F. (1998). The neurotoxicity of amyloid beta protein in aged primates. *Amyloid : The International Journal of Experimental and Clinical Investigation : The Official Journal of the International Society of Amyloidosis*, *5*(1), 1–9. Retrieved from http://www.ncbi.nlm.nih.gov/pubmed/9546999

McKenzie, I. A., Ohayon, D., Li, H., Paes de Faria, J., Emery, B., Tohyama, K., & Richardson, W. D. (2014). Motor skill learning requires active central myelination. *Science*, *346*(6207), 318–322. https://doi.org/10.1126/science.1254960

Mei, F., Wang, H., Liu, S., Niu, J., Wang, L., He, Y., … Xiao, L. (2013). Stage-Specific Deletion of Olig2 Conveys Opposing Functions on Differentiation and Maturation of Oligodendrocytes. *Journal of Neuroscience*, *33*(19), 8454–8462. https://doi.org/10.1523/JNEUROSCI.2453-12.2013

Mi, S., Miller, R. H., Lee, X., Scott, M. L., Shulag-Morskaya, S., Shao, Z., … Pepinsky, R. B. (2005). LINGO-1 negatively regulates myelination by oligodendrocytes. *Nature Neuroscience*, *8*(6), 745–751. https://doi.org/10.1038/nn1460

Milner, R., & Ffrench-Constant, C. (1994). A developmental analysis of oligodendroglial integrins in primary cells: changes in alpha v-associated beta subunits during differentiation. *Development (Cambridge, England)*, *120*(12), 3497–506. Retrieved from http://www.ncbi.nlm.nih.gov/pubmed/7821217

Miron, V. E., Boyd, A., Zhao, J.-W., Yuen, T. J., Ruckh, J. M., Shadrach, J. L., … ffrench-Constant, C. (2013). M2 microglia and macrophages drive oligodendrocyte differentiation during CNS remyelination. *Nature Neuroscience*, *16*(9), 1211–1218. https://doi.org/10.1038/nn.3469

Mitew, S., Hay, C. M., Peckham, H., Xiao, J., Koenning, M., & Emery, B. (2014). Mechanisms regulating the development of oligodendrocytes and central nervous system myelin. *Neuroscience*, *276*, 29–47. https://doi.org/10.1016/j.neuroscience.2013.11.029

Mitew, S., Kirkcaldie, M. T. K., Halliday, G. M., Shepherd, C. E., Vickers, J. C., & Dickson, T. C. (2010). Focal demyelination in Alzheimer's disease and transgenic mouse models. *Acta Neuropathologica*, *119*(5), 567–577. https://doi.org/10.1007/s00401-010-0657-2

Müller, C., Bauer, N. M., Schäfer, I., & White, R. (2013). Making myelin basic protein -from mRNA transport to localized translation. *Frontiers in Cellular Neuroscience*, *7*, 169. https://doi.org/10.3389/fncel.2013.00169

Müller, U. C., Deller, T., & Korte, M. (2017). Not just amyloid: physiological functions of the amyloid precursor protein family. *Nature Reviews Neuroscience*, *18*(5), 281–298. https://doi.org/10.1038/nrn.2017.29

Musse, A. A., Gao, W., Homchaudhuri, L., Boggs, J. M., & Harauz, G. (2008). Myelin Basic Protein as a "PI(4,5)P_2-Modulin": A New Biological Function for a Major Central Nervous System Protein †. *Biochemistry*, *47*(39), 10372–10382. https://doi.org/10.1021/bi801302b

Naruse, M., Ishizaki, Y., Ikenaka, K., Tanaka, A., & Hitoshi, S. (2017, January 29). Origin of oligodendrocytes in mammalian forebrains: a revised perspective. *Journal of Physiological Sciences*. https://doi.org/10.1007/s12576-016-0479-7

Nave, K.-A., & Werner, H. B. (2014). Myelination of the Nervous System: Mechanisms and Functions. *Annual Review of Cell and Developmental Biology*, *30*(1), 503–533. https://doi.org/10.1146/annurev-cellbio-100913-013101

Nawaz, S., Kippert, A., Saab, A. S., Werner, H. B., Lang, T., Nave, K.-A., & Simons, M. (2009). Phosphatidylinositol 4,5-Bisphosphate-Dependent Interaction of Myelin Basic Protein with the Plasma Membrane in Oligodendroglial Cells and Its Rapid Perturbation by Elevated Calcium. *Journal of Neuroscience*, *29*(15), 4794–4807. https://doi.org/10.1523/JNEUROSCI.3955-08.2009

O'Meara, R. W., Michalski, J.-P., & Kothary, R. (2011). Integrin signaling in oligodendrocytes and its importance in CNS myelination. *Journal of Signal Transduction*, *2011*(354091), 1–11. https://doi.org/10.1155/2011/354091

Oddo, S., Caccamo, A., Shepherd, J. D., Murphy, M. P., Golde, T. E., Kayed, R., … LaFerla, F. M. (2003). Triple-Transgenic Model of Alzheimer's Disease with Plaques and Tangles. *Neuron*, *39*(3), 409–421. https://doi.org/10.1016/S0896-6273(03)00434-3

Osterhout, D. J., Wolven, A., Wolf, R. M., Resh, M. D., & Chao, M. V. (1999). Morphological Differentiation of Oligodendrocytes Requires Activation of. *Molecular Neurobiology*, *145*(6), 1209–1218. https://doi.org/10.1083/jcb.145.6.1209

Pernber, Z., Blennow, K., Bogdanovic, N., Månsson, J.-E., & Blomqvist, M. (2012). Altered Distribution of the Gangliosides GM1 and GM2 in Alzheimer's Disease. *Dementia and Geriatric Cognitive Disorders*, *33*(2–3), 174–188. https://doi.org/10.1159/000338181

Pike, C. J., Walencewicz, A. J., Glabe, C. G., & Cotman, C. W. (1991). In vitro aging of beta-amyloid protein causes peptide aggregation and neurotoxicity. *Brain Research*, *563*(1–2), 311–4. Retrieved from http://www.ncbi.nlm.nih.gov/pubmed/1786545

Pohl, H. B. F., Porcheri, C., Mueggler, T., Bachmann, L. C., Martino, G., Riethmacher, D., … Suter, U. (2011). Genetically Induced Adult Oligodendrocyte Cell Death Is Associated with Poor Myelin Clearance, Reduced Remyelination, and Axonal Damage. *Journal of Neuroscience*, *31*(3), 1069–1080. https://doi.org/10.1523/JNEUROSCI.5035-10.2011

Power, J., Mayer-Pröschel, M., Smith, J., & Noble, M. (2002). Oligodendrocyte Precursor Cells from Different Brain Regions Express Divergent Properties Consistent with the Differing Time Courses of Myelination in These Regions. *Developmental Biology*, *245*(2), 362–375. https://doi.org/10.1006/dbio.2002.0610

Price, J. L., Ko, A. I., Wade, M. J., Tsou, S. K., McKeel, D. W., & Morris, J. C. (2001). Neuron

number in the entorhinal cortex and CA1 in preclinical Alzheimer disease. *Archives of Neurology*, *58*(9), 1395–402. Retrieved from http://www.ncbi.nlm.nih.gov/pubmed/11559310

Raychaudhuri, M., & Mukhopadhyay, D. (2007). AICD and its adaptors - in search of new players. *Journal of Alzheimer's Disease : JAD*, *11*(3), 343–58. Retrieved from http://www.ncbi.nlm.nih.gov/pubmed/17851185

Readhead, C., Popko, B., Takahashi, N., Shine, H. D., Saavedra, R. A., Sidman, R. L., & Hood, L. (1987). Expression of a myelin basic protein gene in transgenic shiverer mice: correction of the dysmyelinating phenotype. *Cell*, *48*(4), 703–12. Retrieved from http://www.ncbi.nlm.nih.gov/pubmed/2434242

Roher, A. E., Weiss, N., Kokjohn, T. A., Kuo, Y.-M., Kalback, W., Anthony, J., … Beach, T. (2002a). Increased A beta peptides and reduced cholesterol and myelin proteins characterize white matter degeneration in Alzheimer's disease. *Biochemistry*, *41*(37), 11080–11090. https://doi.org/10.1021/bi026173d

Roher, A. E., Weiss, N., Kokjohn, T. A., Kuo, Y.-M., Kalback, W., Anthony, J., … Beach, T. (2002b). Increased A beta peptides and reduced cholesterol and myelin proteins characterize white matter degeneration in Alzheimer's disease. *Biochemistry*, *41*(37), 11080–90. Retrieved from http://www.ncbi.nlm.nih.gov/pubmed/12220172

Rosenberg, S. S., Kelland, E. E., Tokar, E., De La Torre, A. R., & Chan, J. R. (2008). The geometric and spatial constraints of the microenvironment induce oligodendrocyte differentiation. *Proceedings of the National Academy of Sciences*, *105*(38), 14662–14667. https://doi.org/10.1073/pnas.0805640105

Roy, K., Murtie, J. C., El-Khodor, B. F., Edgar, N., Sardi, S. P., Hooks, B. M., … Corfas, G. (2007). Loss of erbB signaling in oligodendrocytes alters myelin and dopaminergic function, a potential mechanism for neuropsychiatric disorders. *Proceedings of the National Academy of Sciences*, *104*(19), 8131–8136. https://doi.org/10.1073/pnas.0702157104

Ruckh, J. M., Zhao, J.-W., Shadrach, J. L., van Wijngaarden, P., Rao, T. N., Wagers, A. J., & Franklin, R. J. M. (2012). Rejuvenation of regeneration in the aging central nervous system. *Cell Stem Cell*, *10*(1), 96–103. https://doi.org/10.1016/j.stem.2011.11.019

Saab, A. S., Tzvetavona, I. D., Trevisiol, A., Baltan, S., Dibaj, P., Kusch, K., … Nave, K.-A. (2016). Oligodendroglial NMDA Receptors Regulate Glucose Import and Axonal

Energy Metabolism. *Neuron*, *91*(1), 119–132. https://doi.org/10.1016/j.neuron.2016.05.016

Salzer, J. L., Brophy, P. J., & Peles, E. (2008). Molecular domains of myelinated axons in the peripheral nervous system. *Glia*, *56*(14), 1532–1540. https://doi.org/10.1002/glia.20750

Samanta, J., & Kessler, J. A. (2004). Interactions between ID and OLIG proteins mediate the inhibitory effects of BMP4 on oligodendroglial differentiation. *Development*, *131*(17), 4131–4142. https://doi.org/10.1242/dev.01273

Santos, A. N., Ewers, M., Minthon, L., Simm, A., Silber, R.-E., Blennow, K., … Hampel, H. (2012). Amyloid-β oligomers in cerebrospinal fluid are associated with cognitive decline in patients with Alzheimer's disease. *Journal of Alzheimer's Disease : JAD*, *29*(1), 171–6. https://doi.org/10.3233/JAD-2012-111361

Schaeffer, E. L., Figueiro, M., & Gattaz, W. F. (2011). Insights into Alzheimer disease pathogenesis from studies in transgenic animal models. *Clinics (Sao Paulo, Brazil)*, *66 Suppl 1*(Suppl 1), 45–54. https://doi.org/10.1590/s1807-59322011001300006

Scholz, J., Klein, M. C., Behrens, T. E. J., & Johansen-Berg, H. (2009). Training induces changes in white-matter architecture. *Nature Neuroscience*, *12*(11), 1370–1371. https://doi.org/10.1038/nn.2412

Selkoe, D. J. (1991). The molecular pathology of Alzheimer's disease. *Neuron*, *6*(4), 487–98. Retrieved from http://www.ncbi.nlm.nih.gov/pubmed/1673054

Selkoe, D. J., Brown, B. A., Salazar, F. J., & Marchotta, C. A. (1981). Myelin basic protein in Alzheimer disease neuronal fractions and mammalian neurofilament preparations. *Annals of Neurology*, *10*(5), 429–436. https://doi.org/10.1002/ana.410100505

Selkoe, D. J., & Hardy, J. (2016). The amyloid hypothesis of Alzheimer's disease at 25 years. *EMBO Molecular Medicine*, *8*(6), 595–608. https://doi.org/10.15252/emmm.201606210

Simons, M., & Nave, K.-A. (2015). Oligodendrocytes: Myelination and Axonal Support. *Cold Spring Harbor Perspectives in Biology*. https://doi.org/10.1101/cshperspect.a020479

Simons, M., & Nave, K.-A. (2016). Oligodendrocytes: Myelination and Axonal Support. *Cold Spring Harbor Perspectives in Biology*, *8*(1), a020479. https://doi.org/10.1101/cshperspect.a020479

Simons, M., & Trotter, J. (2007). Wrapping it up: the cell biology of myelination. *Current Opinion in Neurobiology*, *17*(5), 533–540. https://doi.org/10.1016/j.conb.2007.08.003

Skaper, S. D., Evans, N. A., Soden, P. E., Rosin, C., Facci, L., & Richardson, J. C. (2009). Oligodendrocytes are a Novel Source of Amyloid Peptide Generation. *Neurochemical Research*, *34*(12), 2243–2250. https://doi.org/10.1007/s11064-009-0022-9

Snaidero, N., Möbius, W., Czopka, T., Hekking, L. H. P. H. P., Mathisen, C., Verkleij, D., … Simons, M. (2014). Myelin Membrane Wrapping of CNS Axons by PI(3,4,5)P3-Dependent Polarized Growth at the Inner Tongue. *Cell*, *156*(1–2), 277–290. https://doi.org/10.1016/j.cell.2013.11.044

Snaidero, N., & Simons, M. (2014a). Myelination at a glance, 2999–3004. https://doi.org/10.1242/jcs.151043

Snaidero, N., & Simons, M. (2014b). Myelination at a glance. *Journal of Cell Science*, *127*(Pt 14), 2999–3004. https://doi.org/10.1242/jcs.151043

Snaidero, N., Velte, C., Myllykoski, M., Raasakka, A., Ignatev, A., Werner, H. B., … Simons, M. (2017). Antagonistic Functions of MBP and CNP Establish Cytosolic Channels in CNS Myelin. *Cell Reports*, *18*(2), 314–323. https://doi.org/10.1016/j.celrep.2016.12.053

Sperber, B. R., Boyle-Walsh, E. A., Engleka, M. J., Gadue, P., Peterson, A. C., Stein, P. L., … McMorris, F. A. (2001). A unique role for Fyn in CNS myelination. *The Journal of Neuroscience : The Official Journal of the Society for Neuroscience*, *21*(6), 2039–47. Retrieved from http://www.ncbi.nlm.nih.gov/pubmed/11245687

Sperber, B. R., & McMorris, F. A. (2001). Fyn tyrosine kinase regulates oligodendroglial cell development but is not required for morphological differentiation of oligodendrocytes. *Journal of Neuroscience Research*, *63*(4), 303–312. https://doi.org/10.1002/1097-4547(20010215)63:4<303::AID-JNR1024>3.0.CO;2-A

Stricker, N. H., Schweinsburg, B. C., Delano-Wood, L., Wierenga, C. E., Bangen, K. J., Haaland, K. Y., … Bondi, M. W. (2009). Decreased white matter integrity in late-myelinating fiber pathways in Alzheimer's disease supports retrogenesis. *NeuroImage*, *45*(1), 10–6. https://doi.org/10.1016/j.neuroimage.2008.11.027

Sun, P., Enslen, H., Myung, P. S., & Maurer, R. A. (1994). Differential activation of CREB by Ca2+/calmodulin-dependent protein kinases type II and type IV involves

phosphorylation of a site that negatively regulates activity. *Genes & Development*, *8*(21), 2527–39. Retrieved from http://www.ncbi.nlm.nih.gov/pubmed/7958915

Takami, M., Nagashima, Y., Sano, Y., Ishihara, S., Morishima-Kawashima, M., Funamoto, S., & Ihara, Y. (2009). -Secretase: Successive Tripeptide and Tetrapeptide Release from the Transmembrane Domain of -Carboxyl Terminal Fragment. *Journal of Neuroscience*, *29*(41), 13042–13052. https://doi.org/10.1523/JNEUROSCI.2362-09.2009

Teipel, S. J., Bayer, W., Alexander, G. E., Zebuhr, Y., Teichberg, D., Kulic, L., … Hampel, H. (2002). Progression of corpus callosum atrophy in Alzheimer disease. *Archives of Neurology*, *59*(2), 243–8. Retrieved from http://www.ncbi.nlm.nih.gov/pubmed/11843695

Teipel, S. J., Stahl, R., Dietrich, O., Schoenberg, S. O., Perneczky, R., Bokde, A. L. W., … Hampel, H. (2007). Multivariate network analysis of fiber tract integrity in Alzheimer's disease. *NeuroImage*, *34*(3), 985–995. https://doi.org/10.1016/j.neuroimage.2006.07.047

Traka, M., Arasi, K., Avila, R. L., Podojil, J. R., Christakos, A., Miller, S. D., … Popko, B. (2010). A genetic mouse model of adult-onset, pervasive central nervous system demyelination with robust remyelination. *Brain*, *133*(10), 3017–3029. https://doi.org/10.1093/brain/awq247

Tyler, W. A., Gangoli, N., Gokina, P., Kim, H. A., Covey, M., Levison, S. W., & Wood, T. L. (2009). Activation of the Mammalian Target of Rapamycin (mTOR) Is Essential for Oligodendrocyte Differentiation. *Journal of Neuroscience*, *29*(19), 6367–6378. https://doi.org/10.1523/JNEUROSCI.0234-09.2009

Viola, K. L., & Klein, W. L. (2015). Amyloid β oligomers in Alzheimer's disease pathogenesis, treatment, and diagnosis. *Acta Neuropathologica*, *129*(2), 183–206. https://doi.org/10.1007/s00401-015-1386-3

von Rotz, R. C., Kohli, B. M., Bosset, J., Meier, M., Suzuki, T., Nitsch, R. M., & Konietzko, U. (2004). The APP intracellular domain forms nuclear multiprotein complexes and regulates the transcription of its own precursor. *Journal of Cell Science*, *117*(19), 4435–4448. https://doi.org/10.1242/jcs.01323

Wake, H., Lee, P. R., & Fields, R. D. (2011a). Control of Local Protein Synthesis and Initial Events in Myelination by Action Potentials. *Science*, *333*(6049), 1647–1651.

https://doi.org/10.1126/science.1206998

Wake, H., Lee, P. R., & Fields, R. D. (2011b). Control of Local Protein Synthesis and Initial Events in Myelination by Action Potentials. *Science*, *333*(6049), 1647–1651. https://doi.org/10.1126/science.1206998

Walsh, D. M., Lomakin, A., Benedek, G. B., Condron, M. M., & Teplow, D. B. (1997). Amyloid beta-protein fibrillogenesis. Detection of a protofibrillar intermediate. *The Journal of Biological Chemistry*, *272*(35), 22364–72. Retrieved from http://www.ncbi.nlm.nih.gov/pubmed/9268388

Wang, D.-S., Bennett, D. A., Mufson, E. J., Mattila, P., Cochran, E., & Dickson, D. W. (2004). Contribution of changes in ubiquitin and myelin basic protein to age-related cognitive decline. *Neuroscience Research*, *48*(1), 93–100. Retrieved from http://www.ncbi.nlm.nih.gov/pubmed/14687885

Wang, Q., Walsh, D. M., Rowan, M. J., Selkoe, D. J., & Anwyl, R. (2004). Block of Long-Term Potentiation by Naturally Secreted and Synthetic Amyloid -Peptide in Hippocampal Slices Is Mediated via Activation of the Kinases c-Jun N-Terminal Kinase, Cyclin-Dependent Kinase 5, and p38 Mitogen-Activated Protein Kinase as well as Metabotropic Glutamate Receptor Type 5. *Journal of Neuroscience*, *24*(13), 3370–3378. https://doi.org/10.1523/JNEUROSCI.1633-03.2004

Wang, S., Sdrulla, A. D., diSibio, G., Bush, G., Nofziger, D., Hicks, C., … Barres, B. A. (1998). Notch receptor activation inhibits oligodendrocyte differentiation. *Neuron*, *21*(1), 63–75. Retrieved from http://www.ncbi.nlm.nih.gov/pubmed/9697852

Waxman, S. G. (1997). Axon-glia interactions: building a smart nerve fiber. *Current Biology : CB*, *7*(7), R406-10. Retrieved from http://www.ncbi.nlm.nih.gov/pubmed/9210363

Waxman, S. G., & Ritchie, J. M. (1993). Molecular dissection of the myelinated axon. *Annals of Neurology*, *33*(2), 121–136. https://doi.org/10.1002/ana.410330202

Weidemann, A., Eggert, S., Reinhard, F. B. M., Vogel, M., Paliga, K., Baier, G., … Evin, G. (2002). A novel epsilon-cleavage within the transmembrane domain of the Alzheimer amyloid precursor protein demonstrates homology with Notch processing. *Biochemistry*, *41*(8), 2825–35. Retrieved from http://www.ncbi.nlm.nih.gov/pubmed/11851430

White, R., Gonsior, C., Bauer, N. M., Krämer-Albers, E.-M., Luhmann, H. J., & Trotter, J.

(2012). Heterogeneous Nuclear Ribonucleoprotein (hnRNP) F Is a Novel Component of Oligodendroglial RNA Transport Granules Contributing to Regulation of Myelin Basic Protein (MBP) Synthesis. *Journal of Biological Chemistry*, *287*(3), 1742–1754. https://doi.org/10.1074/jbc.M111.235010

White, R., Gonsior, C., Krämer-Albers, E.-M., Stöhr, N., Hüttelmaier, S., & Trotter, J. (2008). Activation of oligodendroglial Fyn kinase enhances translation of mRNAs transported in hnRNP A2-dependent RNA granules. *The Journal of Cell Biology*, *181*(4), 579–86. https://doi.org/10.1083/jcb.200706164

White, R., & Krämer-Albers, E.-M. (2014). Axon-glia interaction and membrane traffic in myelin formation. *Frontiers in Cellular Neuroscience*, *7*, 284. https://doi.org/10.3389/fncel.2013.00284

Xie, H., & Rothstein, T. L. (1995). Protein kinase C mediates activation of nuclear cAMP response element-binding protein (CREB) in B lymphocytes stimulated through surface Ig. *Journal of Immunology (Baltimore, Md. : 1950)*, *154*(4), 1717–23. Retrieved from http://www.ncbi.nlm.nih.gov/pubmed/7836756

Xing, J., Ginty, D. D., & Greenberg, M. E. (1996). Coupling of the RAS-MAPK pathway to gene activation by RSK2, a growth factor-regulated CREB kinase. *Science (New York, N.Y.)*, *273*(5277), 959–63. Retrieved from http://www.ncbi.nlm.nih.gov/pubmed/8688081

Xu, J., Chen, S., Ahmed, S. H., Chen, H., Ku, G., Goldberg, M. P., & Hsu, C. Y. (2001). Amyloid-beta peptides are cytotoxic to oligodendrocytes. *The Journal of Neuroscience : The Official Journal of the Society for Neuroscience*, *21*(1), RC118. https://doi.org/20014845 [pii]

Yin, X., Peterson, J., Gravel, M., Braun, P. E., & Trapp, B. D. (1997). CNP overexpression induces aberrant oligodendrocyte membranes and inhibits MBP accumulation and myelin compaction. *Journal of Neuroscience Research*, *50*(2), 238–247. https://doi.org/10.1002/(SICI)1097-4547(19971015)50:2<238::AID-JNR12>3.0.CO;2-4

Young, K. M., Psachoulia, K., Tripathi, R. B., Dunn, S.-J., Cossell, L., Attwell, D., … Richardson, W. D. (2013). Oligodendrocyte dynamics in the healthy adult CNS: evidence for myelin remodeling. *Neuron*, *77*(5), 873–85. https://doi.org/10.1016/j.neuron.2013.01.006

Zeger, M., Popken, G., Zhang, J., Xuan, S., Lu, Q. R., Schwab, M. H., … Ye, P. (2007). Insulin-like growth factor type 1 receptor signaling in the cells of oligodendrocyte lineage is required for normalin vivo oligodendrocyte development and myelination. *Glia*, *55*(4), 400–411. https://doi.org/10.1002/glia.20469

Zhan, X., Jickling, G. C., Ander, B. P., Liu, D., Stamova, B., Cox, C., … Sharp, F. R. (2014). Myelin injury and degraded myelin vesicles in Alzheimer's disease. *Current Alzheimer Research*, *11*(3), 232–8. Retrieved from http://www.ncbi.nlm.nih.gov/pubmed/24484278

Zhan, X., Jickling, G. C., Ander, B. P., Stamova, B., Liu, D., Kao, P. F., … Sharp, F. R. (2015a). Myelin basic protein associates with AβPP, Aβ1-42, and amyloid plaques in cortex of Alzheimer's disease brain. *Journal of Alzheimer's Disease : JAD*, *44*(4), 1213–29. https://doi.org/10.3233/JAD-142013

Zhan, X., Jickling, G. C., Ander, B. P., Stamova, B., Liu, D., Kao, P. F., … Sharp, F. R. (2015b). Myelin basic protein associates with AβPP, Aβ1-42, and amyloid plaques in cortex of Alzheimer's disease brain. *Journal of Alzheimer's Disease : JAD*, *44*(4), 1213–29. https://doi.org/10.3233/JAD-142013